University of Natural Resources and Life Science, Vienna

Characterization and optimization of filtration unit operations for GFP purification

Matthias Müller, B. Sc.

Master Thesis

in partial fulfilment of requirements for the degree of

Diplom - Ingenieur

Department of Biotechnology

University of Natural Resources and Life Science, Vienna

Department Head: Univ. Prof. Dipl.-Ing. Dr. rer. nat. Reingard Grabherr

Supervisor: Assoc. Prof. Dipl.-Ing. Dr. Rainer Hahn

Vienna, December 2020

Acknowledgement

I want to express special thanks to my supervisor Prof. Rainer Hahn who supported me whenever I needed factual advice or motivational words. I also want to address special thanks to all members of my working group, who helped me solving my questions about practical work in laboratory. Additionally, I want to thank the whole department of biotechnology for offering me all the required technical equipment that was necessary for my experiments.

Moreover, special thanks may be directed to my family and friends whose encouragements kept my “mental disposition” on a constant level when working on my master thesis.

Abstract

In this work, clarification of high pressure homogenates from *E. coli* was investigated. Cell suspensions of *E. coli* comprising recombinant green fluorescence (GFP) protein were subjected to high pressure homogenization at different operating conditions and obtained homogenates were clarified by standardized centrifugation at low to moderate G-forces in a benchtop centrifuge. Examination of supernatants by nanoparticle tracking analysis revealed the presence of cell debris predominantly in the range of 100 nm. Surprisingly, cell debris size was largely independent of homogenization pressure. Flocculation of cell debris particles by addition of the cationic polymer polyethylenimine (PEI) prior to centrifugation analysis resulted in even smaller particles in the supernatant. A variety of dead-end depth- and sterile filters were applied for removal of debris particles. As could already be expected from the particle size measurement, none of the tested filters could significantly retain the particles and clarify the homogenates to an acceptable turbidity of 5-10 NTU (nephelometric turbidity units). Following, micro- and ultrafiltration membranes with high molecular weight cut-off were tested in tangential flow filtration mode. Best results were obtained with a 750 kDa ultrafiltration membrane when operated at low transmembrane pressure of 0.5 bar and high crossflow rates. At these conditions, debris particles were completely retained, and filtrates comprised a turbidity below 5 NTU. The loss of GFP as around 6%. Overall, flux decline during a 20-fold concentration of the process solution was low; an average flux of 50 LMH (liter per square meter per hour) could be achieved. Further processing of filtrate was performed by ultra/diafiltration. It could be shown that GFP can be concentrated up to 14 g/L (or higher) without observing any fouling effects or product losses. Membranes based on regenerated cellulose achieved permeate fluxes that were twice as high compared to polyethersulfone (PES) membrane. Residual PEI, especially 10 kDa PEI, significantly reduced permeate flux. Generally, linear pressure-flux relationships were observed up to 1.5-2.0 bars. The received knowledge about filtration techniques will help to set up biotechnological product streams more properly and avoid vast product losses or material costs.

Zusammenfassung

In dieser Arbeit wurde die verfahrenstechnische Klärung von hochdruckbehandelten *E. coli* Homogenaten untersucht. *E. coli* Zellsuspensionen, welche das rekombinante Protein „Green Fluorescence Protein“ (GFP) enthalten, wurden verschiedenen Hochdruckhomogenisationsbedingungen ausgesetzt. Die daraus erhaltenen Homogenate erfuhren daraufhin eine milde Klärung mittels Zentrifugation, um eine akkurate Partikelanalyse der Lösung durchführen zu können. Die angewandte Partikelmessmethode „Nanoparticle Tracking Analysis“ (NTA) wies im Bereich von 100 nm die größten Mengen an Zellbruchstückpartikel auf. Interessanterweise beeinflusste eine Änderung der Hochdruckhomogenisationsbedingungen die Partikelzusammensetzung der Homogenate nicht signifikant. Eine zusätzliche Behandlung mit dem kationischen Flockulationsmittel „Polyethylenimine“ (PEI) vor der Zentrifugation führte sogar zu einer noch kleineren Partikelzusammensetzung im Überstand. Mehrere Mikro- und Sterilfiltrationsexperimente wurden ausgeführt, um die Anwendbarkeit im biotechnologischen Verfahren zu überprüfen. Wie aufgrund der Ergebnisse der Partikelanalyse zu erwarten war, konnte keiner der verfügbaren Filter eine vollständige Klärung der Zellbruchstückpartikel erwirken. Jedenfalls konnte die erforderliche Reduktion des Trübungswerts auf 5-10 NTU (Nephelometric Turbidtiy Units) in keinen der Fälle erreicht werden. Daraufhin wurden Mikro- und Ultrafiltrationsmembranen mit einem hohen molekularen Porenausschluss in tangentialer Flussströmung ausgetestet. Dabei wies die Ultrafiltrationsmembran mit Porenausschluss von 750 kDa bei hohen Flüssen und geringem Transmembrandruck von 0.5 bar, die optimalsten Ergebnisse auf. Bei diesen Bedingungen werden die Zellbruchstücke vollständig zurückgehalten was zu einem Trübungswert von 5 NTU führte. Auch die NTA Messanalyse zeigte keinerlei nennenswerte Restpartikelaktivität auf. Dabei lag der Verlust an GFP bei ungefähr 6%, wobei eine weitere Retentantvolumsreduktion den Verlust nochmals minimieren würde. Die Permeatflussabnahme während tangentialer Filtration war sehr gering und erzielte einen durchschnittlichen Wert von 50 LMH (Liter pro Quadratmeter und Stunde). Darauffolgende Behandlung des partikelfreien Filtrats beinhaltete eine Aufkonzentrierung und Pufferwechsel mithilfe von Ultra- und Diafiltration. Es konnte beobachtet werden, dass eine GFP-Aufkonzentrierung auf 14 g/L zu keinem Membranfouling, beziehungsweise geringen Produktverlusten führte. Membranen, bestehend aus regenerierter Zellulose, erzielten dabei doppelt so große Permeatflusswerte, verglichen mit jenen aus Polyethersulfon. In Homogenaten verbliebenes PEI, speziell höhermolekulare Variante (10 kDa), führte zu verminderten Permeatflüssen während Ultra- und Diafiltration. Im Allgemeinen war ein linearer TMP-Flux Zusammenhang bis 1.5 bis 2 bar zu bemerken. Die gewonnenen Erkenntnisse erleichtern die Handhabung und Verständnis der Filtrationsaufreinigungsprozessen, was zukünftig biotechnologische Produktaufreiningungen im großen Maßstab erleichtern sollte.

Table of Content

Abbreviations

HPH	High pressure homogenization
MF	Microfiltration
PEI	Polyethylenimine
CF	Cross flow
TMP	Transmembrane pressure
E. coli	*Escherichia coli*
GFP	Green fluorescence protein
wt	wild-type
pDADMAC	Polydiallyldimethylammoniumchloride
PEI	Polyethylenimine
HCP	Host cell protein
POI	Protein of interest
PA	Polyamides
PSU	Polysulfone
PTFE	Polytetrafluorethylen
MWCO	Molecular weight cut-off
NF	Nanofiltration
pI	Isoelectric point
RO	Reverse osmosis
NTA	Nanoparticle tracking analysis
DLS	Dynamic light scattering
CDM	Cell dry mass
PES	Polyethersulfone
CIP	Cleaning in place
PBS	Phosphate buffer system
LOD	Limit of detection
LOQ	Limit of quantification
PP	Polypropylene
GF	Glass fiber

Annotations

(Brackets reveal the chapter, where annotation is found)

Å	Amströng (1 Å ≙ 0.1 nm)
Da	Dalton (1 da ≙ 1 g/mol)
LMH	$L \cdot m^{-2} \cdot h^{-1}$
R_{max}	Maximum amount of available protein (HPH)
N	Number of passages (HPH)
R	Protein release after N passages (HPH)
k	Rate constant (HPH)
p	Applied pressure (HPH)
α	Cell's disruption resistance parameter (HPH)
b	Cell concentration parameter (HPH)
q_n	Net charge (flocculation)
ε_τ	Substance related specific permittivity (flocculation)
ε_0	Permittivity of vacuum (7.85×10^{-2} $C^2\,N^{-1}\,m^2$) (flocculation)
r	Distance between charges (flocculation)
r_n	Radius of particle n (flocculation)
x	Distance between particle centres (flocculation)
A	Hamaker constant (flocculation)
ψ_E	Repulsive double layer potential (flocculation)
ψ_L	Attractive potential (flocculation)
ψ	Total potential (flocculation)
N	Fraction of native protein (heat precipitation)
D	Fraction of denaturated protein (heat precipitation)
Ag	Fraction of irreversibly aggregated protein (heat precipitation)
u_g	Particle settling velocity by gravitation (centrifugation)
ρ_P	Particle density (centrifugation)
ρ_L	Liquid density (centrifugation)
d_P	Particle diameter (centrifugation)

g	Gravitational force (centrifugation)
μ	Liquid viscosity (centrifugation)
u_c	Particle settling velocity by centrifugational force (centrifugation)
ω	Angular velocity (centrifugation)
r	Distance between particle and centre of rotor (centrifugation)
TMP	Transmembrane pressure (filtration)
p_F	Feed pressure (filtration)
p_R	Retentate pressure (filtration)
p_P	Permeate pressure (filtration)
J_P	Permeate flux (filtration)
A	Membrane area (filtration)
t	Time (filtration)
$\dot{V}$	Volumetric flow (filtration)
k	Darcy coefficient (filtration)
α	Cake resistance (filtration)
ω	Solid mass content (filtration)
V	Feed volume (filtration)
β	Filter resistance (filtration)
ε	Portion of pore area (filtration)
d	Pore diameter (filtration)
L	Membrane thickness (filtration)
R_M	Membrane resistance (filtration)
R_F	Membrane fouling resistance (filtration)
R_δ	Gel layer resistance (filtration)
R'_M	$R_M + R_F$
c_B	Concentration of solute in bulk (filtration)
c_P	Concentration of solute in permeate (filtration)
D	Diffusion coefficient (filtration)
x	Path (filtration)
c_G	Concentration of solute in gel layer (filtration)

k	Mass transfer coefficient (filtration)
Re	Reynold's number (filtration)
Sh	Sherwood number (filtration)
Sc	Schmidt number (filtration)
d_h	Hydraulic diameter (filtration)
L	Channel length (ultrafiltration)
u	Linear velocity (filtration)
ν	Kinematic viscosity (filtration)
P_π	Osmotic pressure (filtration)
i	Number of ionise molecules (filtration)
M	Molecular weight (filtration)
R	Ideal gas constant (filtration)
T	Temperature (filtration)
A_n	Virial coefficient (filtration)
A	Membrane permeability constant (ultrafiltration)
c_R	Concentration of solute in retentate (filtration)
λ	Wavelength (methods for detection)
c	Light velocity (methods for detection)
ν	Frequency (methods for detection)
E	Energy (methods for detection)
h	Planck's quantum of action (methods for detection)
$\overline{(x,y)^2}$	Mean-squared speed of particle (methods for detection)
k_B	Boltzmann constant (methods for detection)
r_h	Stoke's radius (methods for detection)
r	Lumen radius (methods for detection)
E	Extinction (GFP measurement)
ε_m	Mass extinction coefficient (GFP measurement)
c	Concentration (GFP measurement)
d	Cuvette's path length (GFP measurement)

k	Slope of calibration curve (GFP measurement)
$\bar{\sigma}_{Res}$	Average of residual standard deviations (GFP measurement)
Y_{Est}	Estimated value from calibration curve (GFP measurement)
Y_{Res}	Real measurement signals (GFP measurement)
n	Number of measurements (GFP measurement)
P	Backpressure (depth filtration)
$k_{Ca}, k_{In}, k_{St}, k_{Co}$	Rate constants for used filtration model (depth filtration)
V	Filtrate volume (depth filtration)
q_0	Volumetric flow rate (depth filtration)

1 Introduction

Well-established genetic and physiological characterization, ease of handling, broad fermentation know-how and short generation time are only few of many benefits which make gram-negative bacteria *Escherichia coli* (*E. coli*) to an ideal production host for many heterologous proteins and biopharmaceuticals. Especially high production yields of mentioned proteins nominate *E. coli* often to the first-choice organism for many biotechnological applications (1). However, the limited secretion of such proteins beyond the outer membrane of the Gram-negative bacteria is a major disadvantage and often the reason for a switch of production host. Recombinantly produced proteins mainly remain in cytoplasm of the cell and lead to high protein concentrations (2). Therefore, a robust downstream operation process called high-pressure-homogenization (HPH) is necessary to disrupt the cell wall mechanically which leads to a release of proteins out of cell. During HPH the biological material is fed through an adjustable discharge valve that generates pressures of about 300-1500 bar, which stimulate mechanical cell disruption (3). The operation parameters impact the quantity of product recovery and the formation of cellular debris particles whose small size interfere with further downstream purification processes, such as microfiltration (MF) (4). For that reason, particle size distributions of different operation methods of HPH have to be identified to receive knowledge about the optimal balance between product recovery and cell debris formation. Most of the cell debris' particular matter in solution could be then removed by heat precipitation technique in combination with the flocculation aid Polyethylenimine (PEI), followed by batch centrifugation. The type of PEI as well as the concentration in solution affect the effectiveness of cell debris particles accumulation, which in consequence influence the efficiency of batch centrifugation. Due to remaining small sized cell wall particles, MF would remove the rest of small particular matter out of product solution. Hence, an optimal filter medium and pore size has to be identified to get the product solution completely particle-free. Ultrafiltration (UF) would be the next filtration step and operation unit. UF is a well established and widely used sieving procedure with the aim to reduce the product volume by retaining the biomolecule and passing through liquid buffer and molecules of low molecular weight. (5) The type as well as the concentration of product and solution matrix affect the UF performance. Consequently, the optimal parameters such as crossflow (CF) and transmembrane pressure (TMP) have to be identified, avoiding filter blocking and product membrane fouling effects. The last filtration unit operation is the so-called diafiltration (DF). It uses the same technical equipment as UF and follows therefore similar parameter choices. Thus, the final goal of this work is to describe the influence of filter material and operation parameters for DF, avoiding product and operational time losses.

2 Descriptions and properties of relevant biological material

2.1 *Escherichia coli*

E. coli is a harmless gram-negative prokaryotic bacterium and exist as part of human microflora in gastrointestinal system. According to its natural shape, *E. coli* is approximately 2 µm long and has a diameter of approximately 1 µm. It is a chemoheterotrophic bacterium which uses organic carbon as energy source and is able to cover its nitrogen demand with inorganic salts, such as ammonium.

The bacterium's membrane consists of an outer membrane and an inner plasma membrane which both enclose a thin but robust peptidoglycan layer. The inner plasma membrane is responsible for the encapsulation of the cytoplasm and inner cell components. Figure 1 illustrates a typical prokaryotic bacterium and its major cell wall components. (6)

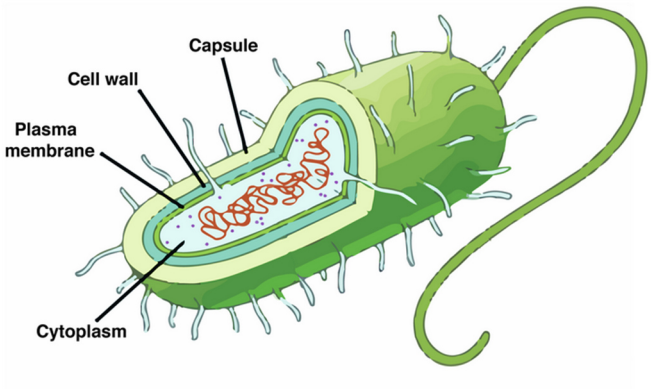

Figure 1 Prokaryotic cell and its cell wall components (7).

The peptidoglycan layer itself consists of sugar polymers, which are interconnected with covalently bound amino acids. Figure 2 depicts a schematic drawing of a typical gram-negative cell wall.

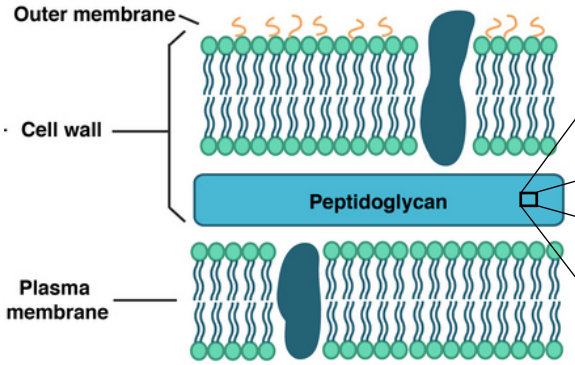

Figure 2 Schematic drawing of a gram-negative bacterial cell wall.

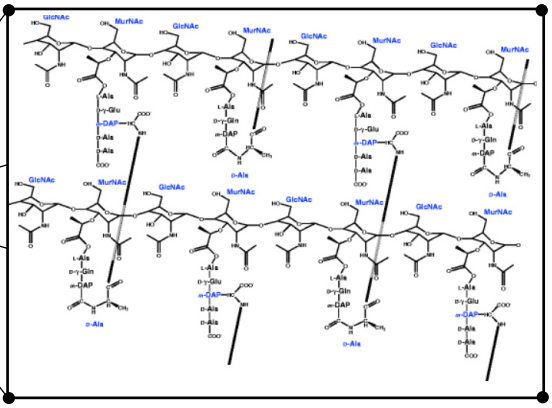

Figure 3 Typical peptidoglycan layer of a gram-negative bacteria. Peptidoglycan consists of disaccharide polymers comprised of N-acetylglucosamine (GlcNAc) and N-acetylmuraminacid (MurNAc) moieties. The sugar layers are covalently interconnected with an amino acid of existing pentapeptides (8).

Figure 3 shows a typical molecular structure of a peptidoglycan layer. The sugar polymer layers consist of alternant N-acetylglucosamin and N-acetylmuraminacid monomers. Sugar polymers itself are covalently interconnected with the amino acid meso-diaminopimelic of existing pentapeptides (8). The presence of the outer membrane makes the overall bacterial cell wall more flexible, which cause a higher resistance against cell disruption techniques such as HPH. High pressure and multiple homogenization passages are widely used ways to overcome this property. Additionally, a high number of phospholipids in the cell wall of *E. coli*, make disrupted cell debris highly negatively charged. This characteristic can be taken as a benefit by using positively charged PEI molecules as flocculation aid. (9)

2.2 Polyethyleneimine

Polythylenimine is an organic linear or branched polymer. It is highly basic and positively charged, containing primary, secondary and tertiary amino groups in an approximate ratio of 1:2:1. Every third atom of the polymer backbone is a nitrogen that may undergo protonation. At neutral pH it has a high positive net charge, which makes the molecule water-soluble (10). PEI molecules are commercially available in both linear and branched forms and molecular weights range from 600 Da to 270,000 Da (11). Figure 4 shows molecular structures of branched and linear type of PEI.

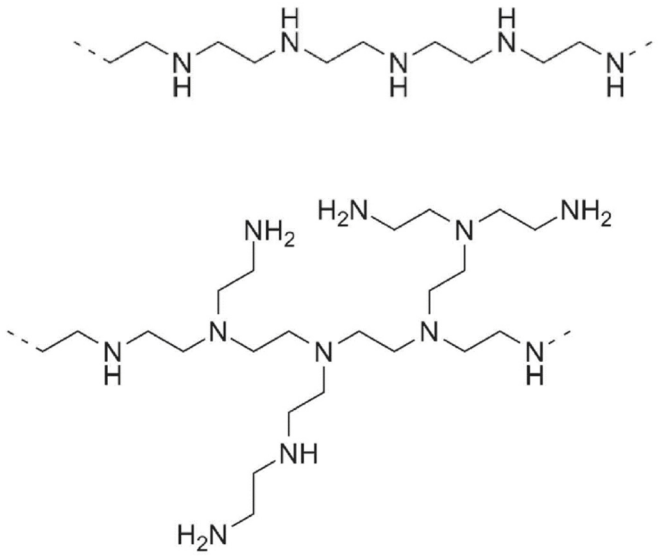

Figure 4 Linear (top) and branched (bottom) form of polyethylenimine (12).

PEI, as a chemical, is used in many different fields, such as in research or industrial sectors. Its main application is the use as drug and antimicrobial coating agent, whereat non pharmaceutical processes, including water purification, paper bulk and shampoo manufacturing also use the advantages of the polymer. It was proven that PEI is relatively safe for internal use in animals and humans, so the pharmaceutical industry often uses it to facilitate the flocculation of cellular contaminants, nucleic acids and lipids for improved purifications of biopharmaceuticals. Immobilizing agent and soluble carrier of enzymes or chelation of metal ions are other applications that are often used (10). This work focus on PEI's property of cell debris accumulation and attempts to figure out which parameter favours effective flocculation performance.

2.3 Green fluorescence protein

Green fluorescence protein (GFP) was originally extracted and purified from the jellyfish, *Aequorea* sp.. According to x-ray crystallographic analysis, it has a barrel-shaped form and consists of 239 amino acids, which result in a molecular weight of 26.9 kDa. The quantitative form is given by a diameter and length of 24 Å and 42 Å, respectively. Figure 5 shows a three-dimensional structure of a wild-type (wt) GFP molecule (13).

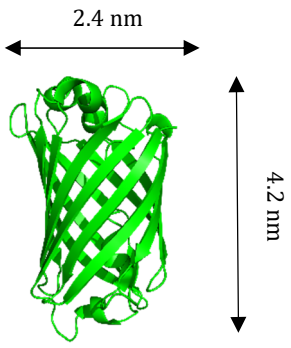

Figure 5 Three-dimensional model of the wild-type GFP protein (14).

The peptide sequence Ser–Tyr–Gly on positions 65, 66 and 67, which are located inside the β-barrel, is responsible for autooxidation and consequently excites at a wavelength of 396 nm and emits at 508 nm. The tripeptide, also called chromophore, is no longer fluorescent, if it is isolated from β-barrel (13).

GFP has a low toxicity and shows a high resistance against denaturising factors and is simple to detect or quantify. These properties make GFP to an optimal reporter molecule, as fluorescing indicator or fusion tag, due to no affection on its fusion partner and vice versa. Hence, GFP and its genetically modified variants are used as non-invasive biosensors for protein expression, protein-protein interactions, protein dynamics and protein infrastructure research of living cells (15). Due to many disadvantages of the wtGFP of *Aequorea* sp., many genetically modified variants have been developed with increased stability, fluorescent intensity and shift of light excitation range (16).

In this work the genetically variant GFPmut3.1 is used. It has the same amino acid number but two amino acid exchanges at position 65 and 72. Serin-65 and Serin-72 are substituted by Glycine and Alanine, respectively. This modification leads to a shift of excitation maxima from 395 nm to 501 nm and an emission maximum from 508 nm to 511 nm. Additionally, the mutation offers a higher fluorescence intensity and chromophore formation at 37 °C, which improves the visual *E. coli* detection during fermentations (16).

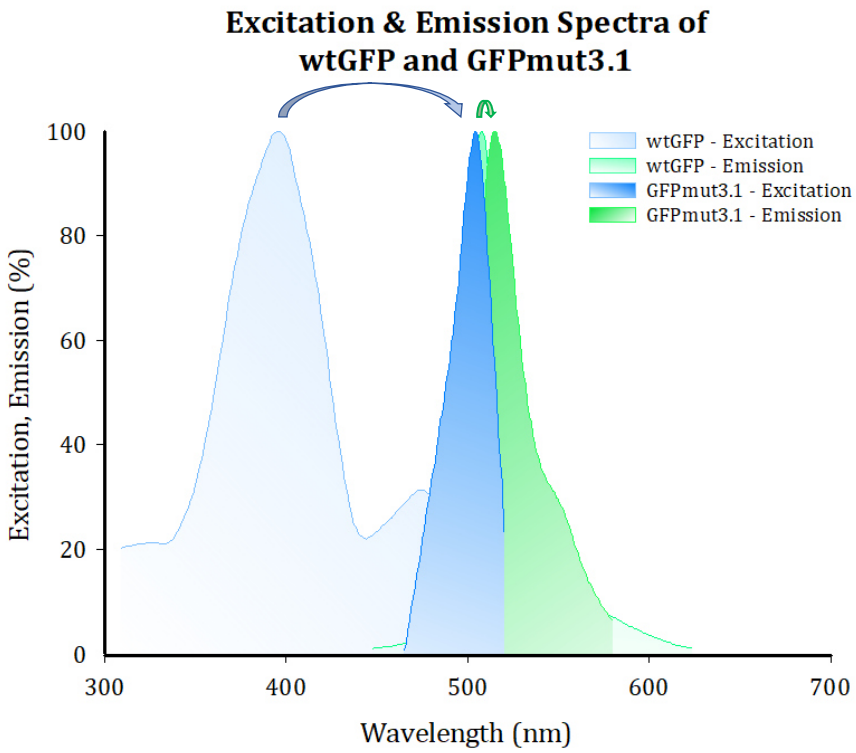

Figure 6 Excitation and Emission chromatograms of wtGFP and GFPmut3.1. Light blue and dark blue graphs show the excitation range of wtGFP and GFPmut3.1, respectively. Light green and dark green areas illustrate the emission spectra of wtGFP and GFPmut3.1, correspondingly. Mutation of wtGFP to GFPmut3.1 leads a shift of excitation maximum from 395 to 501 nm, whereas emission maximum displaces from 508 to 511 nm.

Figure 6 shows the change of excitation and emission maxima that result from the genetical modification of wtGFP. Especially the excitation maximum shifts more than 100 nm to infrared direction. Data for illustration of excitation and emission chromatograms were received from internet database “FPbase” (17).

3 GFP recovery and purification units

The biological material, frozen *E. coli* pellets, had to be processed to receive the required GFP homogenate.

3.1 High pressure homogenization

Homogenization was firstly introduced in food industry and is nowadays a common process step in diary industry. The “milk standardization process” is a famous example whose aim is to reduce the volumes of fat droplets in an oil-water emulsion, preventing an early separation of milk fat and water. This is done by forcing the emulsion through a narrow inlet at high velocity, transforming emulsion into a more stable standardized solution (18).

Main components of an HPH are essentially a homogenizing valve and a high-pressure pump. The valve offers an adjustable gap of few hundred millimetres. The feed emulsion is pumped through the gap, where the fat droplets shear against each other. Finally, they get deformed and disrupted. Many valves offer a hard surface, set normal to the flow direction, which promotes disruption of weak fat droplets. Additionally, a sudden drop in pressure after the valve gap leads often to a collapse of oil bubbles, due to cavitation (18).

An oil-water emulsion shows high similarities with a bacteria-water suspension. Moreover, the flexibility and formation characteristics of oil droplet and a bacterial cell are nearly the same. Hence, HPH is also in the biotechnological field a widely used application, especially in recombinant protein production, where recombinant proteins are often contained in the bacterial cytoplasm. It refers to the type of mechanical cell disruption processes and can be used for all cell types. Figure 7 shows the principle and the way of cell suspension passing through the adjustable gap (19).

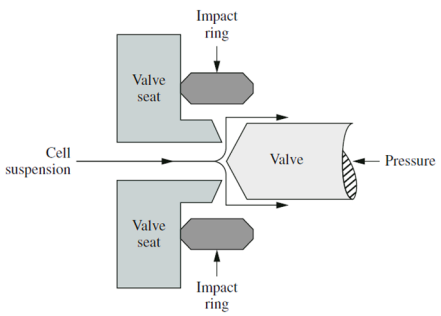

Figure 7 Principle and main elements of high-pressure homogenization apparatus (19).

Commercial homogenizers are normally available as single and two-stage devices, where the first stage generates the required inlet pressure and the second stage is responsible for the pressure drop and the reduction of the outlet pipe's vibration (20). Most of biotechnological homogenizers operate in two-stage mode, due to an increased protein release out of bacterial cell. It is demonstrated that a fully opened second valve reduces the protein release content by about 20%, dependent on the amount of applied pressure. In addition, the disruption efficiency is affected by the number of homogenization cycles. About 2 cycles of homogenization have to be fulfilled to guarantee a complete protein release out of the cell (21). Moreover, gram-negative bacteria are disrupted more efficiently, due to a lower amount of stabilizing peptidoglycan in the cell wall. Thus, HPH is a frequently used method for extracting cytoplasmatic protein out of *E. coli* cells (22).

There are several parameters that influence the homogenization performance. Middleberg et al. claimed that an increase of bacteria concentration decreases the cell disruption capacity. They showed that the specific protein release of a 145 g/L Wet Cell Weight (WCW) solution is of a higher amount than disrupting 330 g/L WCW cell suspension. Additionally, a lower temperature leads to a poorer cell disruption. A variation in pH shows only low protein release effects, whereas the presence of inclusion bodies or accumulated proteins in cytoplasm improve the cell lysis effectiveness, drastically. Interestingly, a recombinant protein containing *E. coli* was disrupted more efficiently compared to *E. coli* without any genetic modifications (23).

As mentioned above, to guarantee a desired degree of cell disruption and product release multiple passes through homogenizer are required. It is shown that the release after *N* passes could be expressed by following equation (19):

$$ln\left(\frac{R_{max}}{R_{max}-R}\right) = kNp^{\alpha} \quad (1)$$

R_{max} is the maximum amount of protein available for release, R is the amount of protein released after N passes through a homogenizer, k is a temperature dependent rate constant of feed suspension and p is the operating pressure. Exponent α is a measure of cell's disruption resistance. Values vary from 0.9 to 2.9 for bacteria and yeast (19). However, the efficiency of homogenizers has been found to decrease slightly with suspensions of high cell concentration (19). Hence, Sauer et al. suggested to modify equation 1 with the additional exponent b that varied linearly with feed's cell concentration, giving following equation (24):

$$ln\left(\frac{R_{max}}{R_{max}-R}\right) = kN^b p^\alpha \quad (2)$$

The newly introduced value was found to be in between 0.28 and 0.94, depending on specific growth rate of cells, the type of cell (e.g. wild-type or recombinant strain) and predominantly the concentration of cell suspension passed through the homogenizer (24).

In practice, it is recommended to operate with multiple passes for a full release of the desired protein. However, many passes can lead to negative side effects, such as thermal protein degradation inside the homogenizer, due to emerged process heat. One way to overcome this problem is to refrigerate the homogenized cell suspension directly after the last valve outlet via cooling jacket. Additionally, multiple homogenizing cycles lead to the formation of very fine cell debris, which restrict subsequent clarification process units (19).

3.2 Flocculation

Cell disruption leads to a tremendous amount of bioparticles in solution. The particles mainly consist of agglomerations of former cell plasma lipids and parts of peptidoglycan layer. In aqueous solutions cell debris has a negative net charge that normally conducts an electrostatic repulsive force between colloid particles (25). Figure 8 depicts an illustration of cell debris suspension in aqueous solution.

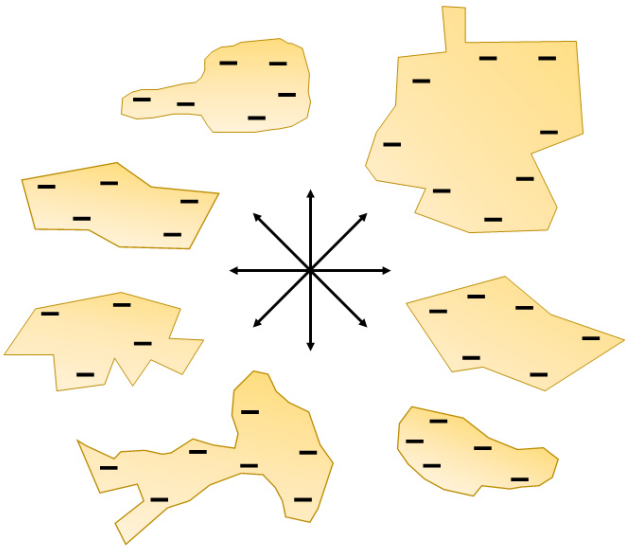

Figure 8 Illustration of cell debris suspension. Arrow-formed double cross stands for electrostatic repulsion forces between particles.

Flocculation is a bioprocess unit operation that depends on the approach and attraction of objects of similar charge. The electrostatic repulsion force between particles can be overcome by Van-der-Waals forces. The Coulomb's law (3) defines the electrostatic repulsion force between particles (26):

$$F = \frac{q_1\, q_2}{4\pi\, \varepsilon_\tau\, \varepsilon_0^2\, r^2} \tag{3}$$

q_1 and q_2 are the charges of particles, ε_τ is the substance related specific permittivity, ε_0 is the permittivity of vacuum (7.85x10^{-2} C^2 N^{-1} m^2) and r quantifies the distance between the two net charges. Electrostatic interaction is a long-range effect because the force decreases relatively slowly with distance r (26). The electric repulsion is highly influenced by the relative permittivity, which again is affected by the type of liquid and its temperature. For example, at 20 °C distilled water has a relative permittivity of approximately 80, whereas the more apolar substance acetone has a value of 21.30. At 10 °C, distilled water and acetone have a slightly higher relative permittivity of 85.85 and 22.30, respectively (27). Moreover, the presence of salt in solution also influence the value of relative permittivity. Midi et al. (28) exposed that water with a conductivity of 5 S/m has 90% of the relative permittivity of distilled water without any dissolved salts (28). This phenomenon proves the hypothesis of shielding charges, which leads to a decrease of repulsive force.

So, for a successful particle coagulation, a strong attraction energy is required that is able to overcome strong electrostatic repulsion. Van der Waals Forces, also called London dispersion forces, are such attraction forces that originate from dipole generation in atoms by random movement of negatively charged electrons around positively charged protons. However, if two atoms come close together, the repulsion of their electron clouds can become very strong and finally counterbalance the attraction force (29).

One way to determine the strength of Van der Waals forces is the Hamaker model. This model tries to extend the Van der Waals force theory to macro-scale objects, summing up all of the forces between the molecules in each of macro-scale objects involved. Equation 4 describes the force between two particles in consideration of newly introduced Hamaker constant A (30):

$$F\,(x) = \frac{A\, r_1\, r_2}{(r_1 + r_2)\, 6x^2} \tag{4}$$

where r_1 and r_2 are the radii of particle 1 and particle 2, respectively and x is the distance between particle centres. The Hamaker constant A can be derived from the surface tension of particle, which is in range of 10^{-19} to 10^{-20} Joule (31).

The so-called **DLVO** (**D**erjagui, **L**andau, **V**erwey, **O**verbeek) theory is an opportunity to sum up the repulsion as well as the attraction force, ending up in a total potential energy. Figure 9

illustrates the repulsion and attraction forces of two similarly charged particles, resulting in a total potential that defines required distances for effective accumulation (25).

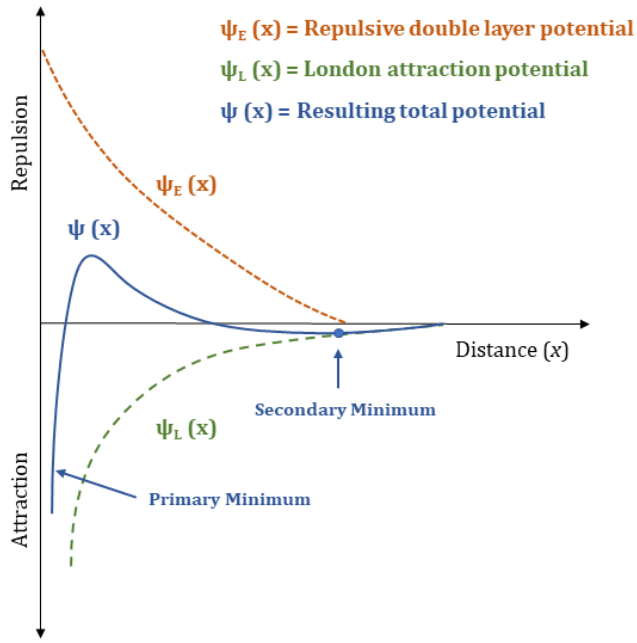

Figure 9 Potential energies of two similarly charged particles (adapted from Trefal and Brokovec (25)).

Figure 9 depicts the potential energy between similarly charged particles as a function of distance x. $\psi_E\,(x)$ stands for repulsive double layer potential, $\psi_L\,(x)$ demonstrates attractive potential, due Van der Waals forces. The summation of both functions results in the total potential $\psi\,(x)$ that reveals the optimal binding distance (25).

Substance dependent flocculation is a common way forcing particles together, reaching the optimal binding distance (x). Several so-called flocculants are commercially available. Salts, such as $CaCl_2$ or $AlCl_3$ are used to shield the repulsive double layer potential between particles, whereas polyelectrolytes build bridges between particles and neutralize the particle's charge. Cationic Polydiallyldimethylammoniumchloride (pDADMAC), DEAE-Dextran, Chitosan, Polyethylenimine (PEI) and anionic polyacrylates are flocculation aids that support the particle agglomeration process (32) (33). Cationic polyelectrolytes neutralize negative charges of bio-particles, causing a decrease of long-distance repulsion forces. Consequently, the short-distance Van der Waals forces can overcome the weakened repulse forces that lead to an improved particle precipitation. Additionally, long cationic polymers can occupy more than one bio-particle, building bridges between particles that again create bigger flocs of particles. The efficiency of polymers is influenced by molecular weight, molecular structure (linear, branched) and solubility, whereas particle interactions are affected by pH, ionic strength, temperature and particle concentration (34). Moreover, bacterial host cell proteins (HCPs) can be also the target of flocculation aids. Hence, it is crucial to find a combination of polymer affecting parameters,

preventing a high degree of protein of interest (POI) attachment (33). Figure 10 shows the polymeric bridging effect between negatively charged bio-particles and affecting factors.

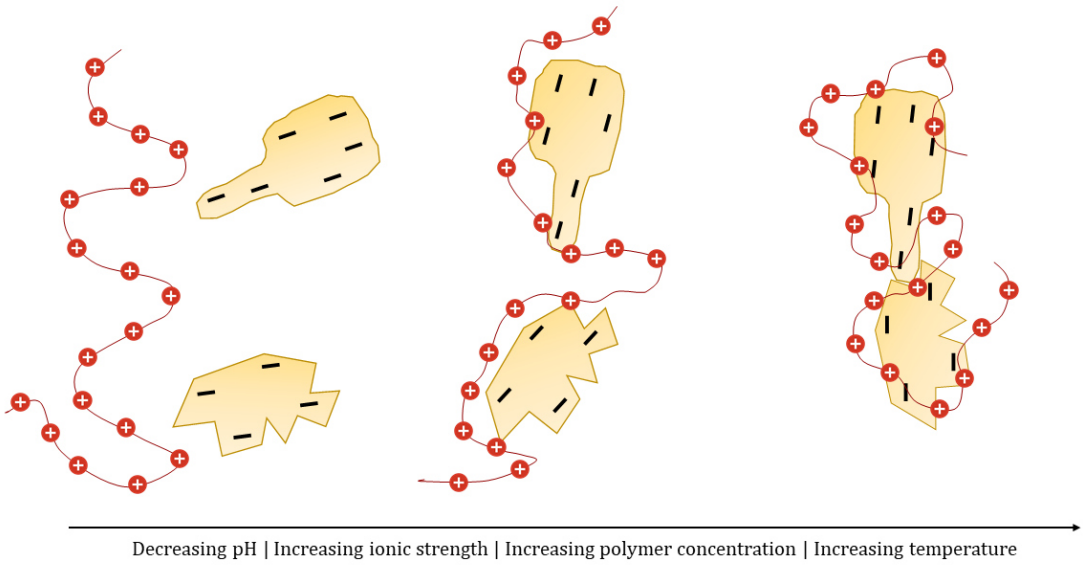

Figure 10 Electrolytic polymer bridging between two similarly charged bio-particles and factors influencing flocculation efficiency (modified and adapted from Harrison et al. (34)).

3.3 Heat Precipitation

Heat precipitation is an important method in purification of proteins and normally comes early in a purification process. It has several advantages, such as low costs, cheap equipment and it can be operated continuously. Overall, heat precipitation can be used for two different modes of operation. On the one hand precipitation is used for the agglomeration and concentration of a product in solution. It is used if the product (e.g. POI) is in high concentration and easy to precipitate, while contaminants (e.g. HCPs) are left in solution. On the other hand, a common approach is to use precipitation for removal of contaminants out of solution. Latter mode is normally applied, if the product is of low content (34).

In general, there are several operational practices of protein precipitations. Batch mixing, varying temperature or pH (isoelectric precipitation), increase (salting in) or decrease (salting out) of salt concentration or adding organic solvents are only few of many process operations that lead to protein precipitates (19).

In this study a combination of batch mixing method and thermal energy induced precipitation is performed. Due to low concentration of POI (GFP) in solution compared to *E. coli*'s HCPs, the operational mode design focus on retention of GFP in solution. During temperature increase undesired proteins are unfolded and distort at some point of thermic denaturation. A simple way of describing denaturation is the two-state model of protein denaturation (29):

$$N \leftrightarrow D \tag{5}$$

N stands for the percentage of native protein, whereas D is the denatured fraction of protein. The double arrow implies a reversible reaction. Hence, the denaturated form can return to the native state. For most proteins, especially for intracellular proteins a modified version of equation 5 has to be introduced (35):

$$N \leftrightarrow D \rightarrow Ag \tag{6}$$

Ag stands for the fraction of aggregated proteins that cannot be transformed back into previous states. Usually, for proteins that denature at temperatures below 60 °C, aggregation is responsible for the irreversibility of the third state (35). Figure 11 depicts example proteins in their native, unfolded and aggregated state.

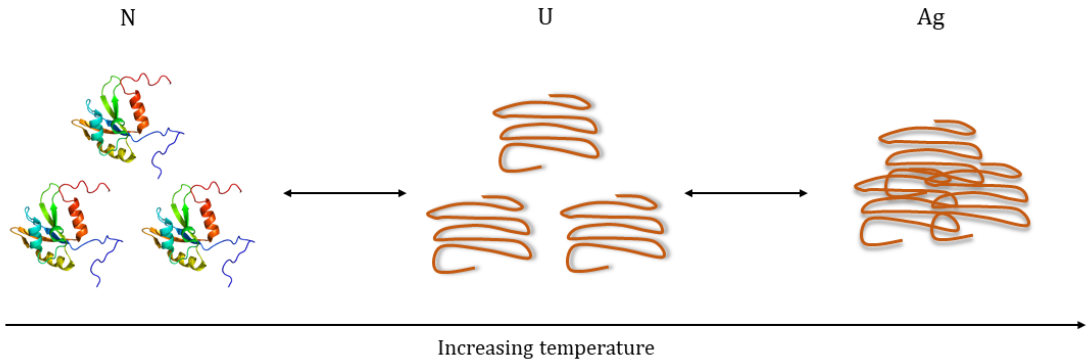

Figure 11 Protein structure illustration of a three-state unfolding model.

The process of unfolding and subsequent aggregate formation is accelerated by an temperature increase. Nevertheless, the chosen temperature should not affect the stabilty of POI. At melting temperature (T_m), 50% of protein are in the unfolded state, whereas the rest remains in native form. Nicholls and Hardy showed that GFP begins to denaturate at a temperature of approximately 69 °C and measured a T_m of 76 °C. Therefore, all temperatures under 69 °C are acceptable, preventing a GFP denaturation and subsequent yield reduction (36).

Regarding clearence efficiency, purification and GFP yield, Fink M. discovered that heat precipitation is most effective if the homogenate was treated for 2 hours at 50 °C followed by centrifugal clarification (37).

3.4 Centrifugation

Centrifugation is a widely used unit operation in downstream processing. It separates materials of different density, applying a force greater than earth's gravity. The unit operation is used to remove cells from fermentation broths or cell debris fragments, to collect precipitates and separate liquid phases after extraction processes. Depending on the centrifuge, the clarification under force can be operated in batch or continuous mode. For small-scale operations, the batch mode is first choice, whereas, especially in industry, continuous centrifugation designs are often preferred, due to higher product throughputs per time (19). The efficiency of centrifugation is improved if the density difference of particle and liquid is significant, the particle diameter is big, and the viscosity of liquid is low (34). The comparison of particle velocity reached in a specific centrifuge and settling velocity under gravity defines the effectiveness of centrifugation. The velocity during gravity settling of a small sphere-shaped particle in suspensions is expressed by Stoke's law (34):

$$u_g = \frac{\rho_P - \rho_L \, d_P^2 \, g}{18\mu} \tag{7}$$

u_{g} describes the settling velocity of a particle, ρ_P and ρ_L are densities of particle and surrounding liquid, respectively, d_P is the particle diameter, g the gravitational force (9.81 m/s^2) and μ is the viscosity of liquid. In a centrifuge, the equivalent particle velocity is defined by following equation (19):

$$u_c = \frac{\rho_P - \rho_L \, D_P^2 \, \omega^2 \, r}{18\mu} \tag{8}$$

Here the gravitational force g is replaced by $\omega^2 \, r$, where ω is the angular velocity and r represents the particle distance from the centre of rotor.

A common way of characterizing the effectiveness of centrifuges is the so-called centrifuge effect, g-number or relative centrifugal force (RCF) and is normally symbolized with z, introducing next equation (38) (19):

$$g - \mathrm{number} = RCF = z = \frac{\omega^2 \, r}{g} \tag{9}$$

Industrial centrifuges have Z factors up to 16,000, whereas small laboratory centrifuges can reach g-numbers of about 500,000 (19).

3.5 Filtration

Filtration is defined as the separation of two or more constituents from a fluid stream, based on size differences. Usually, it refers to separation of non-dissolved solid particles from liquid or gaseous streams. Typically, filter materials are non-woven, natural or synthetic fibres or other inorganic or organic materials. Depending on the product of interest, either fluid stream or particles, the separation process can be performed as cake filtration (particles as product) or depth filtration (fluid as product). Normally, applied pressure can go up to 10^6 Pascal, when size of particular matter is bigger than 1 µm (5).

3.5.1 Membrane filtration

Membrane filtration is a filtration type and extends filtration application to include dissolved solutes (<1 µm) in liquid or gaseous streams. The membrane itself act as a selective barrier, permitting passage of certain components, while other components of different properties are retained (39). Reasons for choosing membrane separation processes are numerous. If, for instance, the treated product is temperature sensitive or charges or dimensions play a role, a membrane process would be an excellent choice. Besides the most frequently used pressure-dependent membrane processes, also more separation forms, such as electrodialysis, gas separation or pervaporation, are in use. Table 1 lists the most common pressure-driven membrane processes:

Table 1 Pressure-driven membrane processes (adapted from Cheryan (39) and Belafi-Bako et al. (5)).

Process (Abbreviation)	Driving force	Membrane type	Mechanism	Dimension of rejected solutes
Microfiltration (MF)	Δp (1-3 bar)	Symmetric or asymmetric	Sieving	0.1 - 5 µm
Ultrafiltration (UF)	Δp (3-10 bar)	Asymmetric	Sieving	0.01 - 0.1 µm
Nanofiltration (NF)	Δp (10-30 bar)	Charged film	Sieving, ion transport	10 - 100 nm
Reverse Osmosis (RO)	Δp (100 bar)	Dense film	Solution diffusion	10 - 100 nm

The application of hydraulic pressure difference distinguishes the pressure-driven membrane processes. Nevertheless, membrane property controls, which components are permeated through or retained, and is specific for distinct membrane process. Ideally, RO retain all components beside solvent, while NF mainly let pass uncharged molecules or monovalent salts. Ultrafiltration reject only molecules above 0.1 µm, whereas MF permeate molecules beneath 0.1 µm. Figure 12 shows a schematic drawing of most common pressure-driven membrane filtration processes:

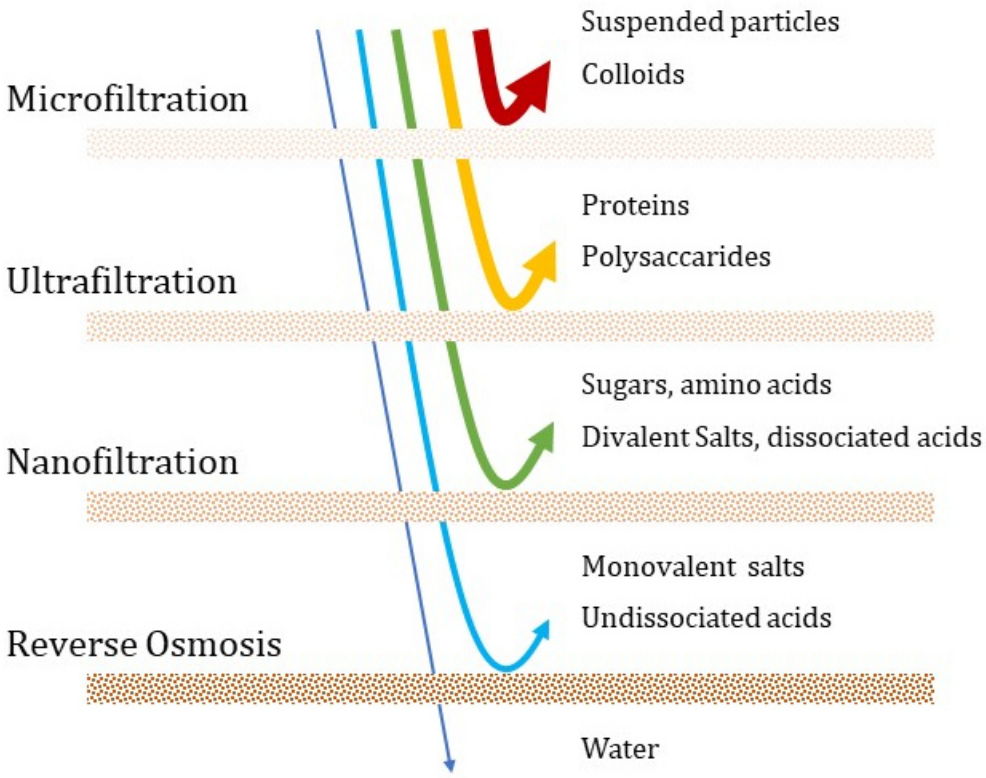

Figure 12 Pressure-driven membrane processes and their separation properties (adapted from Cheryan (39)).

3.5.2 Microfiltration

MF is a filtration process of relatively low applied pressure. It normally operates at pressure of 1-3 bar and is used for removal of suspended particles or whole cells out of fermentation broth. Treatment of dairy products or clarification of corn syrup are other application fields (40). Generally, the molar masses are > 500,000 g/mol that justifies the term “micro”. Retention of micro-scale matter occurs either by size exclusion (sieving effect or filter cake formation) or adsorption (depth filtration) inside the membrane matrix. Additionally, NF can be supported by charge sensitive membrane modules (5).

In general, two different modes are used for MF. Figure 13 shows the mostly used dead-end (static filtration) as well as the more seldom crossflow mode (dynamic filtration) (5).

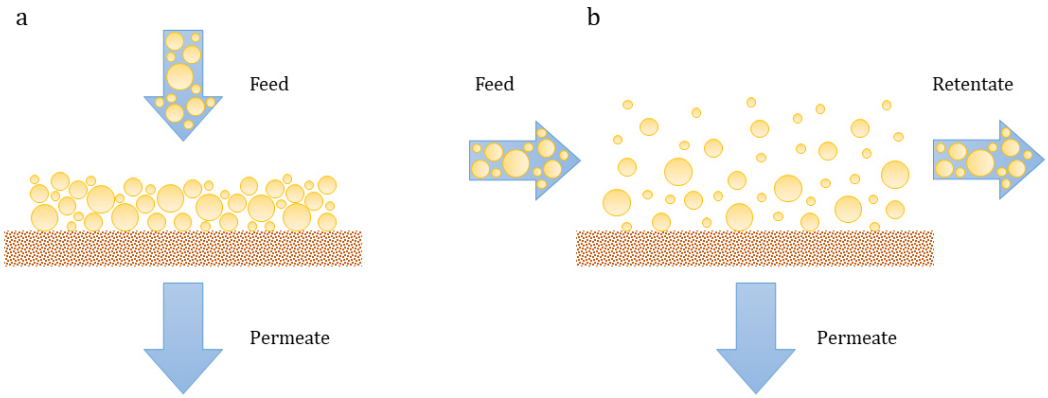

Figure 13 Typical microfiltration modes: a dead-end filtration, b crossflow filtration (adapted by Belafi-Bako et al. (5))

The driving force and crucial parameter for filtration processes is the so-called transmembrane pressure (TMP). It can be defined as the difference of the average of feed pressure p_F and retentate pressure p_R and permeate pressure p_P (39):

$$TMP = \frac{p_F - p_R}{2} - p_P \tag{10}$$

For dead-end filtration the TMP is the difference of p_F and p_P, due to missing retentate flow. Nevertheless, TMP is not distributed equally on the membrane module. It is, more or less, the average of all TMPs that are present across the membrane. Figure 14 depicts the TMP and the existence of unique pressure locations on membrane during crossflow filtration:

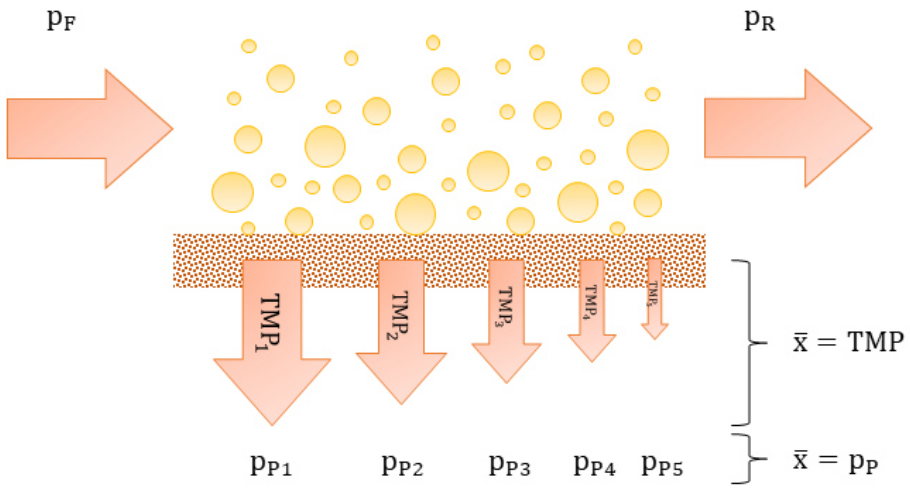

Figure 14 The transmembrane pressure theory and allocation of different pressure values.

Another filtration key parameter is the specific volumetric permeate flow, also called flux. It is defined as the volume that passes through the filter per area and time. Mostly, its unit is given

in L/m²·h (LMH) and it is a widely used parameter for scaling approaches. Following equation represents the flux definition (39):

$$J_P = \frac{V_P}{A \cdot t} \tag{11}$$

where V_P is the permeate volume in L, A is the membrane area in m² and t is the time in h.

Normally, the longer the filtration, the higher the concentration of solids above the top layer of filter. Due to increase of solid content and the resulting resistance, the permeate flux declines over time. Figure 15 shows the thickness of solid layer and permeate flux as a function of filtration time.

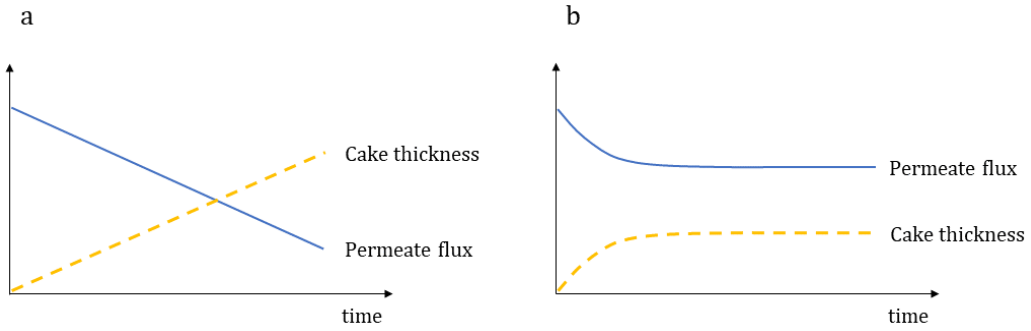

Figure 15 Specific flux and solid cake formation as a function of time for dead-end (a) and crossflow (b) filtration.

Dead-end mode is preferred if suspensions have a high load of solid matter. Ideally solids get attached at the surface of the membrane (cake filtration). At low content of solid matter crossflow filtration is normally preferred (5).

Generally, the transport of filtered stream can be described by Darcy's Law (5):

$$\dot{V} = \frac{dV}{dt} = \frac{A\,(p_F - p_P)}{\eta}\,k \tag{12}$$

where $\dot{V}$ is the volumetric flow in m³/s, A is the filter area in m², p_F and p_P are feed pressure and permeate pressure in Pa, respectively, η is the viscosity in Pa·s and k is the Darcy coefficient. The Darcy coefficient depends on cake and filter resistance and can be expressed as follows (5):

$$k = \frac{1}{\frac{\alpha\ \omega\ V}{A} + \beta} \tag{13}$$

α describes the cake resistance in m·kg^{-1}, ω is the solid mass content in kg/m^3, V is the feed volume in m^3, A is the filter area in m^2 and β is the membrane resistance.

Combination of equation 10 and 11 gives:

$$\frac{dV}{dt} = \frac{A\ (p_F - p_P)}{\eta} \left(\frac{1}{\frac{\alpha\ \omega\ V}{A} + \beta} \right) \tag{14}$$

Integration of equation 14 yields:

$$\frac{t}{V} = \frac{\eta\ \alpha\ \omega}{2\ \Delta p\ F^2} V + \frac{\eta\ \beta}{F\ \Delta p} \tag{15}$$

which facilitate the determination of α and β. Next figure shows a fictive crossflow microfiltration process. First part of the curve represents the formation of a solid layer on the top of membrane, whereas second part depicts pore blocking inside the membrane module (5):

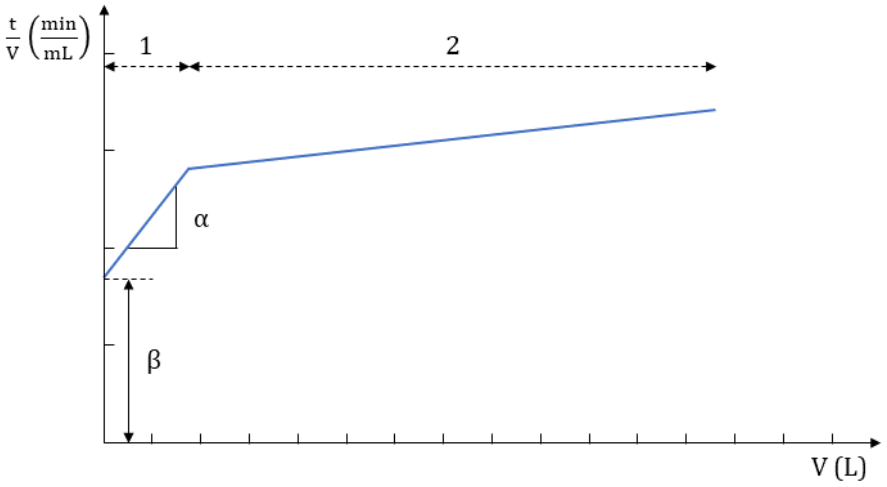

Figure 16 Time feed volume ratio as a function of feed volume of fictive crossflow MF process. The curve is split into the cake formation part (1) and the membrane pore blocking part (2) (adapted from Belafi-Bako et al. (5)).

The curve's slope originates on the one hand from the deposition of particles upon the filter membrane and on the other hand from blocking of smaller particles inside the membrane.

Normally, during cake filtration the volumetric flow reduces as a function of time. In contrast, crossflow mode prevents the cake formation process by transmembrane shear stress effect (40). Backwashing is applied when filtration lasts for a longer period of time or hydrophilic

membranes are used. Preventing hydrophobic interactions between membrane and substrate is another counter act (5).

Typical modules have plate forms, capillaries or are filter cartridges. Module materials are normally made of celluloses, polyamides (PA), polytetrafluorethylene (PTFE) and polysulfone (PSU). Most commercially available filters are symmetric (one particular substance) and have pore diameters between 0.1 µm and 0.45 µm (41).

3.5.3 Ultrafiltration

UF is a membrane separation process that aims at concentration or removal of high molecular substances, such as proteins, enzymes or oligosaccharides. Typical application fields are concentration of whey and pharmaceutical proteins and desalting of product solutions. Due to higher density and lower pore diameter of the membrane in contrast to MF, the operation pressure is in a range of 3-10 bar (39). The word "ultra*"* is Latin and stands for "beyond", due to retained solutes that are beyond those separated by MF. UF is, as microfiltration, a sieving procedure. The pores of membranes are normally smaller than 10 nm, whereupon pore dimension exclusion takes place. Usually, a gel layer is built up during filtration process that promotes additional rejection. The gel layer can be compared with cake formation of MF. Besides molecules that can be retained, special organic solvent-resistant membranes allow filtration treatments of organic solutions (5).

According to solution transport mechanics, the Hagen-Poiseuille equation gives a satisfying description of the permeate flux behaviour (5) (39):

$$J_P = \frac{V}{A \cdot t} = \frac{\varepsilon \, d^2 \, TMP}{32 \, \eta \, L} \tag{16}$$

where V is the permeate volume in m^3, A is the membrane area in m^2, t is the filtration time s, ε is the pore area, d is the pore diameter in m, η is the dynamic viscosity in Pa·s and L is the membrane thickness in m.

Due to low dimensions and high concentrations of rejected molecules during UF processes, many physical influences come into play, which make the whole process less predictable, compared to MF. One important phenomenon that comes into play is the so-called concentration polarization (membrane surface gel layer formation). Concentration polarization occurs, if hydrocolloids, macromolecules or other relatively large solutes are filtered. These components tend to form viscous or gelatinous layers on the membrane's surface. Hence, additional resistance for permeate flow is encountered. To eliminate such misunderstanding, concentration polarization should not be confused with membrane fouling. In contrast to membrane fouling effect, the solutes of gel layer can be fully brought back to solution (39).

Concentration polarization can have a big impact on the performance of UF and its flux behaviour. In general, two effects influence the flux during filtration. On the one hand, the increased concentration of retained small molecules lead significantly to osmotic pressure conditions. Hence, not only the membrane is responsible for flux decline. The layer's local molecule accumulation lead to a hold of solvent, due to concentration compensation. Thus, the applied pressure would be reduced (TMP – Δπ), which decreases the overall flux. The other effect comes into play, due to hydrodynamic resistance of the boundary layer. The convective transport of solutes to the membrane results in a steep concentration gradient within the layer. This phenomenon causes a back-transport into bulk solution due to diffusion. Steady-state conditions are reached, if both effects balance each other. However, there is a maximum of solute concentration if no molecule is able to travel to the membrane's surface, due to steric motion hindrances. A high gel layer concentration (C_G) could cause irreversible precipitations, by building membrane fouling agglomerates. Several factors, such as size and dimension of solute, ionic strength or pH influence the gel layer's characteristics. Nevertheless, the most important one is the material of the filter membrane. The grade of hydrophilicity may affect the flux performance, drastically (41).

The formed gel layer is usually responsible for the so-called pressure independent region of flux. Figure 17 shows flux behaviour as a function of TMP, according to a typical UF filtration process:

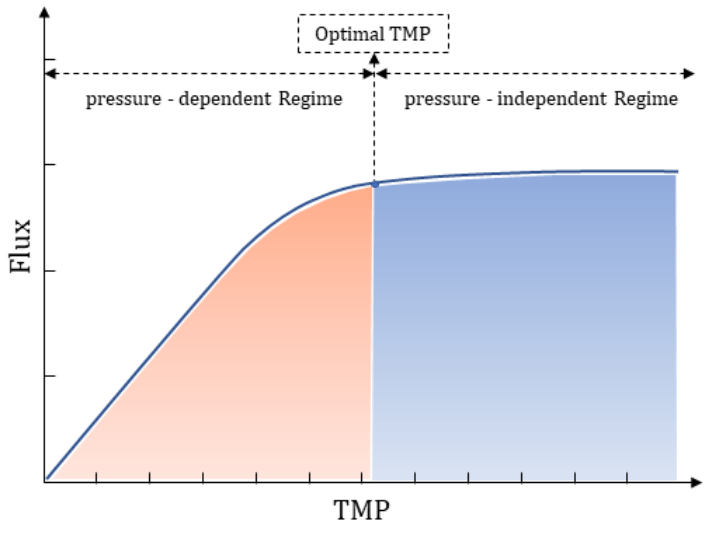

Figure 17 TMP controlled flux behaviour of a typical UF process. The optimal TMP split the curve into pressure - dependent and pressure - independent regimes. It is recommended to operate till optimal TMP, preventing membrane fouling effects.

An increase in pressure leads to a thicker and more dense gel layer that inhibits the solvent to permeate. After an abrupt flux rise it will drop back to the previous state. In principle, the solute gel layer is dynamic and theoretically returns the flux to the pressure-dependent region after

changing operating conditions, such as lowering the TMP or increasing feed velocity. In practice, it lasts some time till solutes resettle from the membrane's surface after lowering the TMP, which is due to micromolecular steric hindrances. A combination of feed velocity and TMP reduction can facilitate the removal gel layer from the membrane's surface (39).

Different engineering models have been developed that aim to predict the overall process performance. Practice shows that a combination of UF models would give the best results. The next chapters will give information about the most important ones that are provided at present.

3.5.3.1 Resistance model

Three resistance factors are responsible for the drop of permeate flow: the membrane, the gel layer and the membrane fouling resistance (39):

$$J_P = \frac{TMP}{R_M + R_F + R_\delta} \tag{17}$$

where R_M is the membrane resistance in $m^2 \cdot h^{-1} \cdot bar \cdot m^{-3}$, R_F is resistance due to membrane fouling and R_δ is the gel layer resistance in $m^2 \cdot h^{-1} \cdot bar \cdot m^{-3}$. Since the fouling layer is assumed to be irreversible because of physicochemical interactions between membrane and attached molecule, R_F remains relatively unaffected by changing operating parameters and is integrated into the intrinsic membrane resistance defined as $R'_M = R_M + R_F$. On the other hand, R_δ is a function of operating parameters, such as tangential flow or TMP, being influenced by the permeability of gel layer and its thickness (discussed in next chapter), which is then a function of applied TMP (39):

$$R_\delta = \phi \, TMP \tag{18}$$

Hence, the resistance model becomes:

$$J_P = \frac{TMP}{R'_M + \phi \, TMP} \tag{19}$$

Due to lower compression at low pressure the term R_δ is small compared to R'_M. Thus, flux will be a function of applied TMP. On the other hand, at high pressure R_δ becomes relatively large. Flux is then less dependent on applied TMP and approaches the value $1/\phi$. The newly introduced term ϕ, which accounts for mass transfer effects, is affected by feed stream's

viscosity, velocity and temperature. The optimal operating TMP is, when R'_M and R_δ are equal (39):

$$TMP_{Optimum} = R'_M/\phi \quad (20)$$

Filtration studies showed that the fouling resistance term R_F should be kept in focus because it is often the limiting factor during filtration process. Especially protein fouling can be reduced, holding the temperature constant and using moderate TMPs during UF. The gel layer thickness and resistance (R_δ) can be easily influenced by varying the recirculation flow velocity. Jiraratananon and Chanachai, for instance, showed that during passion fruit juice treatment, R_δ was decreased from 6.4 to 1.9 kPa/LMH when recirculation flow rate was increased from 600 mL/min to 1200 mL/min (42).

All in all, the resistance model is a relatively simple model that offers rapid solutions for operational issues. However, its simplicity is also its main disadvantage, since the parameters do not offer any information about the gel layer's properties, such as type of components or concentrations.

3.5.3.2 Mass transfer model or film theory

Another simple and widely used model for modelling the flux is the film theory that also includes the concentration of formed gel layer. For better understanding figure 18 illustrates a scheme about concentration polarization during UF with building up the gel layer and an associated boundary layer (41):

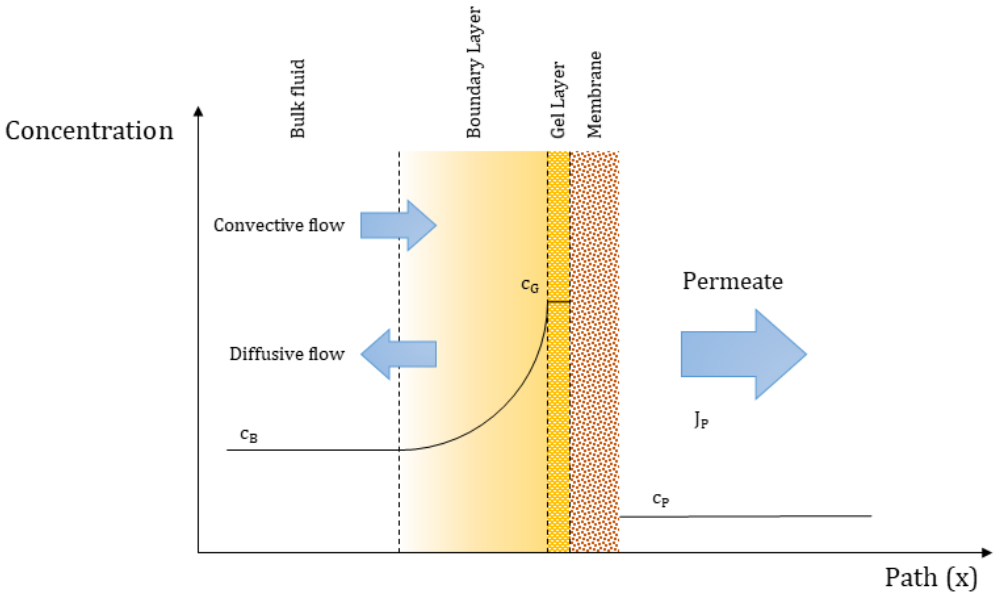

Figure 18 Gel layer formation of a typical UF process. At steady-state conditions, all concentrations remain constant (Adapted from Cheryan (39)).

As already mentioned in previous chapters, the steep concentration gradient near the membrane leads to a back-transport of retained solute into the bulk liquid. The mass balance for steady-state conditions of solute is as follows (39):

$$c_B J_P - D \frac{dc}{dx} - J_P c_P = 0 \tag{21}$$

where c_B is the concentration of solute in the bulk fluid, J_P is the permeate flow, D is the diffusion coefficient of solute, x is the path length, and c_P is the permeate concentration of solute.

Integration with boundary conditions $x = 0$, $c = c_G$ and $x = \delta =$ thickness of boundary layer, $c_i = c_B$ of equation 21 leads to (40):

$$J_P = \frac{D_i}{\delta} ln \left(\frac{c_G - c_P}{c_G - c_P} \right) \tag{22}$$

In case of full retention of solute ($c_P = 0$) and introducing the mass transfer coefficient k ($k = D/\delta$), a shorter form of permeate flux description can be derived (40):

$$J_P = k \, ln \frac{c_G}{c_B} \tag{23}$$

It has to be pointed out that in this model no pressure term is used. In this case it is assumed that pressure does not have any impact on flux. Thus, the diffusion model can only be applied in the pressure-independent region. The flux is controlled by the rate at which solutes are transferred back from the membrane's surface to the bulk fluid. In most operation modes the terms c_G and c_B are fixed values. Hence, the only way to improve the flux is to increase the value of k by reducing the gel layer thickness or improving the diffusion coefficient (39).

The mass transfer coefficient can be determined either empirically or mathematically. Regarding the empirical way, the permeate flux values are plotted against solute's bulk concentration. Then the intercept and the slope represent gel layer concentration and mass transfer coefficient, respectively (5).

Assuming a laminar flow ($Re < 1800$) in filter module, the following general relationship can be used to determine the mass transfer coefficient (39):

$$Sh = 1.62\ Re^{0.33}\ Sc^{0.33}\left(\frac{d_h}{L}\right)^{0.33} \tag{24}$$

where Sh is the Sherwood number $(k\ (d_h/D))$, Re is the Reynold's number $(u\ d_h/\nu)$, Sc is the Schmidt number (υ/D), d_h is the equivalent hydraulic diameter in cm, L is the channel length, u is the mean linear velocity in $\mathrm{cm/s}$ and ν is the kinematic velocity in $\mathrm{cm^2/s}$.

Solving and rearranging newly introduced dimensionless numbers would lead to the equation for mass transfer coefficient (5):

$$k = 1.62\ D^{0.66}\left(\frac{u}{d_h\ L}\right)^{0.33} \tag{25}$$

Turbulent flow $(Re > 4000)$ mainly occur in tubular modules, such as hollow fiber membranes and change the general relationship into:

$$Sh = 0.023\ Re^{0.8}\ Sc^{0.33} \tag{26}$$

Experiments showed that the film theory is only valid for MF and UF processes with solutes of low molecular weight. For big macromolecules nearly no diffusion takes place and therefore the permeate flux cannot be explained by a model based on convective-diffusion ratio. Moreover, UF processes show often a slight pressure dependency also above the optimal TMP point. Thus, the so-called osmotic pressure model has been established (41).

3.5.3.3 Osmotic pressure model

For macromolecular substances involved in UF processes, osmotic pressure often plays a crucial role. The osmotic pressure can be described by van't Hoff relation:

$$P_\pi = i\ \frac{c}{M}\ R\ T \tag{27}$$

where i is the number of ionized solutes (e.g. sugars $= 1$, proteins $= 1$, NaCl $= 2$, $MgCl_2 = 3$ c is the concentration of solute in $\mathrm{g/L}$, M is the molecular weight in $\mathrm{g/mol}$, R is the ideal gas constant $(8.3145\ \mathrm{L{\cdot}kPa{\cdot}mol^{-1}K^{-1}})$ and T is the temperature in $\mathrm{K^{-1}}$.

At higher solute concentrations, the osmotic pressure is calculated by so-called virial coefficients as follows:

$$P_\pi = A_1\, c + A_2\, c^2 + A_3\, c^3 \qquad (28)$$

where A_n are experimentally derived virial coefficients. At higher concentrations of macromolecules, the second and the third coefficient become much more sufficient. Virial coefficients are molecule specific and depend on temperature and pH of solution. Table 2 list virial coefficients of variously selected molecules:

Table 2 Virial coefficients of variously selected molecules, able to calculate osmotic pressure (kPa), using equation (25) (adapted from Cheryan (39))

Molecule	Range of concentration	Unit of c	A_1	A_2	A_3
Bovine Serum Albumin					
pH 7.4	0-450 g/L	g/L	3.787×10^{-1}	-2.980×10^{-3}	1.000×10^{-5}
pH 5.5	0-450 g/L	g/L	5.633×10^{-2}	-2.800×10^{-4}	2.604×10^{-6}
pH 4.5	0-450 g/L	g/L	7.539×10^{-2}	-4.900×10^{-4}	1.852×10^{-6}
Fibrinogen (bovine)	0-80 g/L	g/L	9.948×10^{-3}	-2.104×10^{-4}	2.833×10^{-6}
Glycerol	0-35%	% w/w	262.06	2.669	0.0481
NaCl (aq)	0-25%	% w/w	869.50	-5.1105	1.0403
Polyethylene glycol					
PEG 6	14-40%	% w/w	15.72	-0.5738	0.0787
PEG 20	0-60%	% w/w	9.65	-0.177	0.04964
β-lactoglobulin	0-250 g/L	g/L	2.699×10^{-2}	1.311×10^{-3}	7.277×10^{-8}

As table 2 shows, the strength of osmotic pressure highly depends on the size of molecule, isoelectric point and surrounded matrix conditions, such as pH. It can be stated that a big difference between pI and pH and a low molecular size leads to higher osmotic pressures. Bovine serum albumin, for instance, which has an isoelectric point of 4.7 (43), shows higher preferences for building up osmotic pressure conditions. Additionally, smaller molecular sizes normally lead to higher osmotic pressures, which can be recognized from virial coefficients of PEG 6 and PEG 20. Both molecules only differ in size and show that the smaller version (PEG 6) build up much bigger osmotic pressure conditions. According to membrane processing to overcome the osmotic pressure phenomenon, the applied external pressure must be higher than the osmotic pressure of solution. According to the model, the flux can be calculated as follows (5):

$$J_P = A\,(TMP - P_\pi) \tag{29}$$

where A is the membrane permeability constant (also the reciprocal of membrane resistance constant).

3.5.3.4 Technical considerations

Ultrafiltration is commonly run in crossflow mode, due to efficient reduction of possible membrane fouling effects. Next figure shows a sketch of a basic ultrafiltration process with all its essential elements:

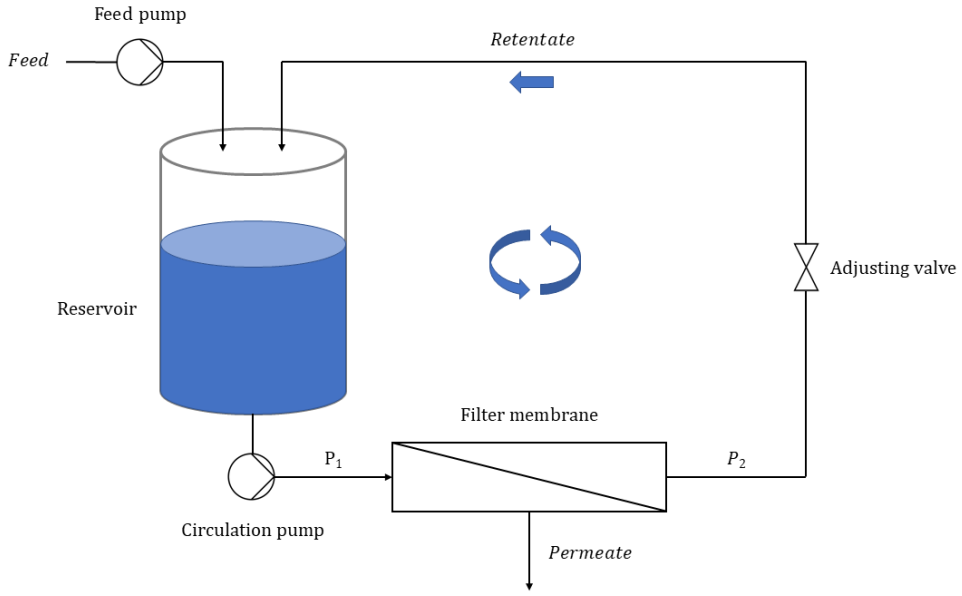

Figure 19 Scheme of an ultrafiltration process and its main elements.

At beginning of UF, the product solution is pumped into a previously installed reservoir. The circulation pump forces the solution through the filter which let pass liquid and small molecular compounds through the filter (permeate). A fraction of the repelled solution (retentate) is transferred back into the reservoir. The number of rejected solutes in feed solution remains the same, whereas the volume is reduced. Hence, a reduction in product volume leads to an increase of solute concentration (40).

The so-called diafiltration process uses the same principle but aims at buffer exchange. In continuous diafiltration a constant amount of new buffer is added to the product solution via feed pump. Often the amount of added buffer is equal to the removed permeate volume, which holds the solute concentration constant. Conductivity sensors often measure the salt content of the retentate stream. The information is then used to estimate when the retained solute is fully rebuffered into the new solution matrix (39).

For UF membranes a broad spectrum of materials is used. Besides different types of cellulose derivates, chemically more resistant PA, PSU and PES membranes are frequently used. There are several methods to characterize the quality of UF membranes. The flux is determined by measuring the permeate volume at a distinct TMP and temperature with distilled clean water per time unit. The rejection *R* is determined by using a solute of known molecular size. Measuring the permeate and retentate concentrations after a distinct UF process time, reveals the amount of rejected solute:

$$R = 1 - \frac{c_P}{c_R} \tag{30}$$

Moreover, molar mass of solute has to be taken into consideration. With a mixture of polydisperse substances the molecular weight cut-off (MWCO) can be estimated. For instance, an ultrafiltration membrane with a MWCO of 100 kDa rejects 90% of a solute of same size. Therefore, the MWCO of a membrane is chosen at least 10 times lower than the size of the treated solute. Next figure shows examples of membranes with different MWCOs:

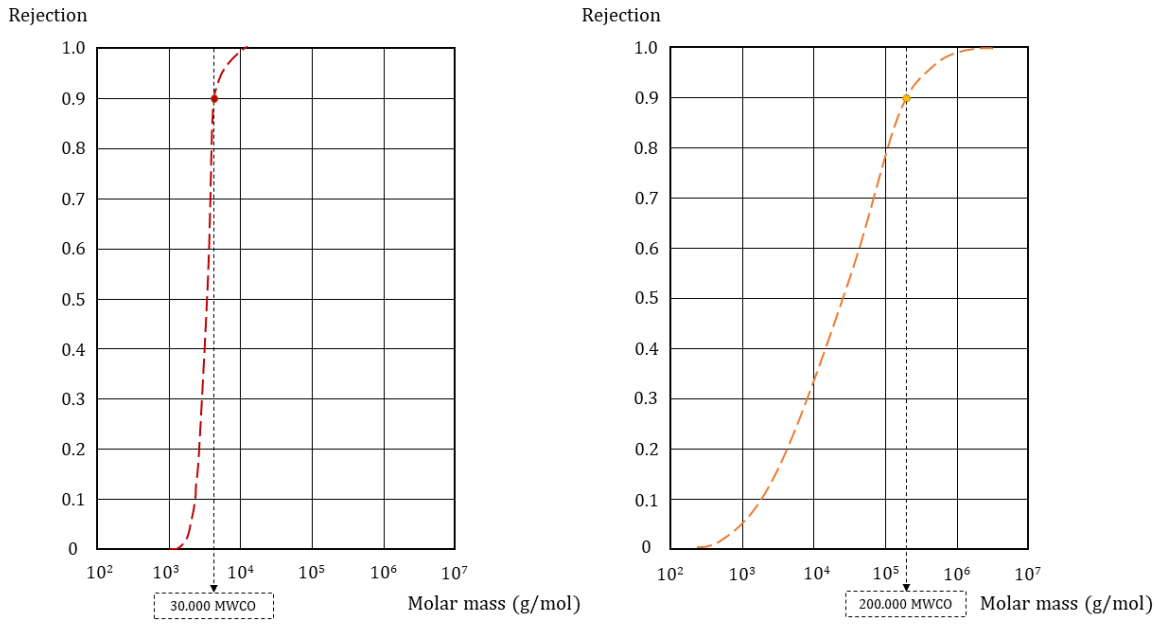

Figure 20 Examples of two different MWCO profiles. The left profile shows a 30 kDa ultrafilter with narrow pore size distribution, whereas the right profile depicts a 200 kDa ultrafilter with broad pore size distribution (adapted by Cheryan (39)).

The dashed lines represent the pore size distribution of membranes. The higher the slope of the sigmoidal curve, the bigger is the deviation from the pore size average. Filter membrane producers often uses mixtures of PEG or dextran molecules of different sizes to determine the distribution (39).

3.5.4 Nanofiltration

Nanofiltration (NF) is a membrane filtration process in the intermediate range of UF and RO (see chapter 3.5.5). Only molecules above a molecular weight of approximately 200 g/mol are retained. That includes sugar monomers, amino acids and most of divalent salts. Typical application fields are desalting of dairy products, virus removal, extraction of hydrolysed proteins, concentration of sugar solutions and purification of dissolvable pigment molecules. Due to its relatively simple separation mechanism, NF is and will be an essential part of drinking water supplies all over the world. It normally operates at pressure ranges between 10 and 30 bar and the membranes are the same type as used for reversed osmosis. Therefore, this membrane process is also called low pressure reverse osmosis, especially in older literature (5).

Basically, two mechanisms are in separation processes. Membrane's pore size is essential for sieving mechanisms, prior to repulsion of molecules that have the same charge as the membrane material. Figure 21 shows a schematic drawing of NF's separation principle.

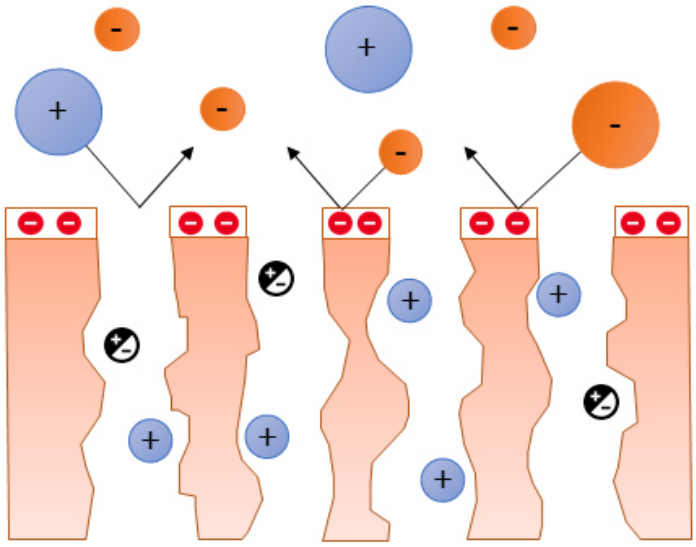

Figure 21 Schematic drawing of a nanofiltration separation process (adapted by Belafi-Bako et al. (5)).

Depending on the membrane's surface charge, only counter ions smaller than the pore size are able to travel through the filter material. This charge separation technique is often used to separate certain amino acids. Every amino acid has a distinct isoelectric point (pI), at which the amino acid appears neutral. Hence, an amino acid's charge can be adjusted to neutrality with a buffer system at particular pH, preventing a repulsion against charged membrane surface (39).

The membranes of NF are mainly of asymmetric nature and comparable to those as for reverse osmosis (RO).

3.5.5 Reversed Osmosis

Reversed Osmosis is a high-pressure filtration process with pressure of ~100 bar. It is similar to NF separation technique except the high pressure. Due to high density of membrane material, all substances except solvents are retained. Typical applications are concentration of low-weight molecules, reduction of water from process liquids and producing drinking water out of sea water (39).

4 Detection methods

4.1 GFP Quantification

Absorption measurement is a quick and frequently used tool to determine the concentration of proteins and nucleic acids. Additionally, the purity of a protein can be estimated within few seconds. Absorption of photons of a distinct wavelength is based on (valence) electron transition (excitation) phenomena of measured macromolecule. The molecule remains only few nanoseconds in the excited state, before its electrons jump back to ground state (44).

The UV/VIS spectroscopy is a measurement technique that utilises the absorption effects at UV and visible light spectrum. Next figure illustrates the range and distinct sections of the electromagnetic light spectrum:

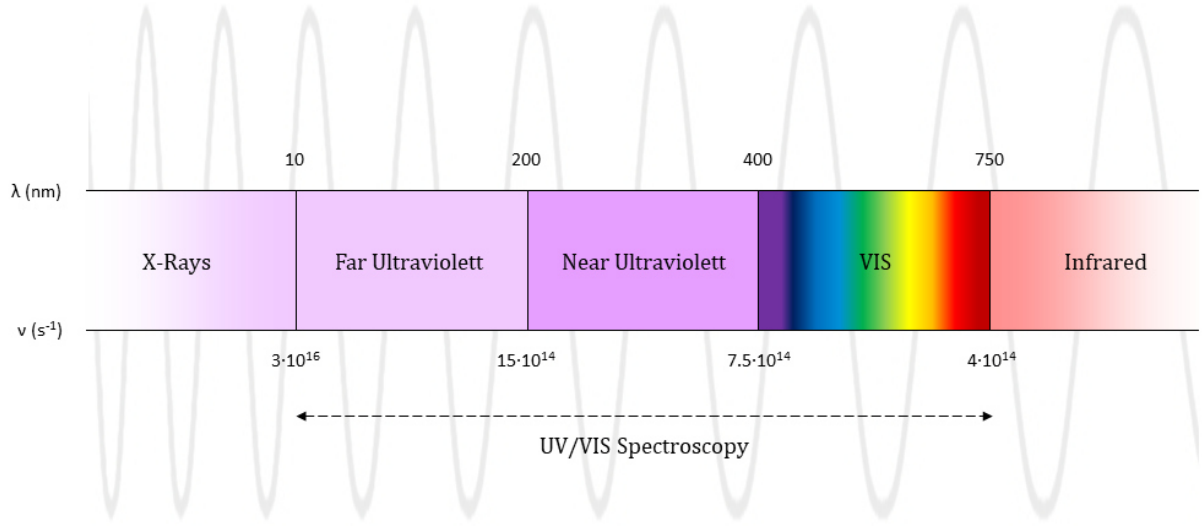

Figure 22 Section of electromagnetic spectrum used for UV/VIS spectroscopy (adapted by Hesse et al. (45)).

As figure 22 shows, electromagnetic waves are characterized by their wavelength λ and the frequency ν, which have following relationship (45):

$$\lambda = \frac{c}{\nu} \tag{31}$$

whereas c is the light velocity (in vacuum $\approx 2.99 \cdot 10^{10}$ cm/s)

According to Einstein, a photon has the energy of:

$$E = h\nu \tag{32}$$

where h is the Planck's quantum of action with $\approx 6.63 \cdot 10^{-34}$ Js.

Whereas proteins and nucleic acids are detected at near UV (280 nm and 260 nm, respectively), only substances with chromophores can be only detected at VIS spectra. So-called fluorophores are molecules that can be detected via fluorescence spectroscopy.

Fluorescence spectroscopy is a special form of emission spectroscopy. Some organic molecules (e.g. GFP) absorb light of higher energy than they emit. For example, excitation occurs at the near UV region, while light emission appears in the middle VIS region. Figure 23 depicts the absorption and emission phenomena for proper understanding:

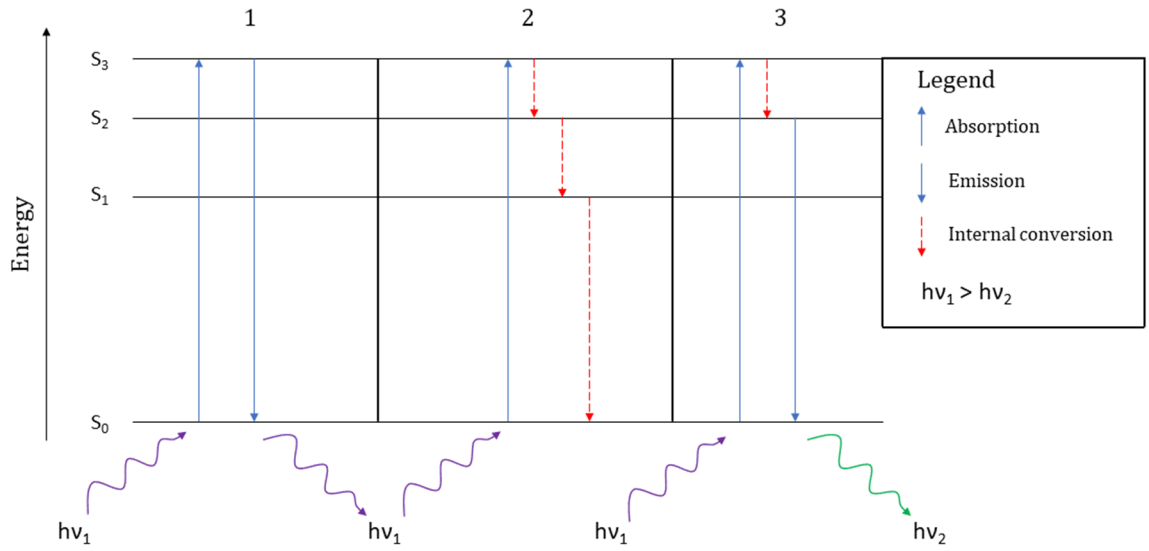

Figure 23 Light absorption and emissions of three different example molecules (adapted by Hesse et al. (45))

Figure 23 shows absorption mechanisms of three different example molecules. Example 1 absorbs light and transfers an electron from ground state S_0 to more energized state S_3. After transition, the electron goes back to ground state S_0, while emitting light of same energy.

Example 2 depicts a molecule absorbing at same light frequency. Due to so-called molecular internal conversion, no light emission occurs. Absorption spectroscopy takes advantage of this phenomena, quantifying absorbing molecule.

Example 3 shows a fluorophore that emits light of a different wavelength than it absorbs. In this case electrons are excited to the more energized S_3 level, before molecular internal conversions bring them to a state of lower energy (S_2). After that, the electrons are transferred back to the ground state (S_0) while emitting light of lower energy.

GFP is a molecule that emits light of lower energy than it absorbs. In this thesis the special GFP mutant GFPmut3.1, whose absorption maximum is at 501 nm and emission maximum at 511 nm, was used. The fluorescence properties of GFP can be used to determine its concentration, while other molecules in solution do not interfere at this absorption wavelength.

4.2 Nephelometry

Nephelometry is based on comparison of light intensity scattered by a sample under defined conditions with the light intensity scattered by a reference suspension. The higher the intensity of reflected light, the more turbid is the measured sample. In contrast to turbidimetry, which detects the remaining light after the sample barrier, nephelometric devices count the light photons that are scattered by solutes being in sample. Nephelometry is used to determine concentrations of various solute types. Besides the determination of cell number in solution at wavelength 600 nm (OD_{600}), which is a well-established and frequently used method in biotechnology, also the amount of particular matter or biomolecules (e.g. antibodies, antigens) can be measured (44). Figure 24 illustrates the measurement principle of nephelometry.

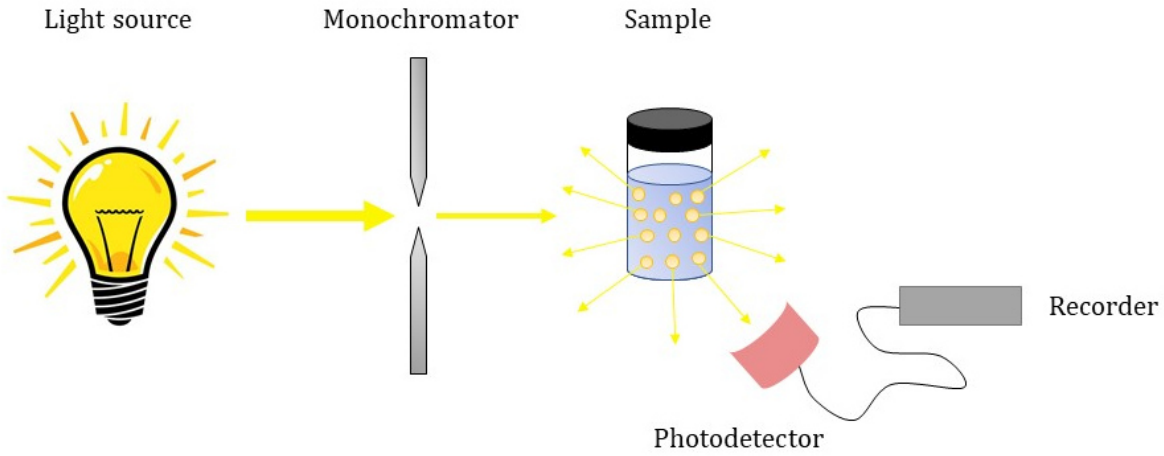

Figure 24 Principle of nephelometry (adapted by Marmer et al. (46)).

The intensity of the scattered light is given in nephelometric turbidity unit (NTU) and follows a linear relationship to scattering solutes in solution. Thus, suspensions of high particle content can be diluted prior to measurement (47).

This work uses nephelometry to determine the content of cell particular matter. It is an accurate method that quantifies the particle content within seconds. Nevertheless, it gives no information of particle size distribution. Hence, another method, called nanoparticle tracking analysis, comes into play.

4.3 Nanoparticle tracking analysis

Nanoparticle tracking analysis (NTA) is a method for detecting, visualizing and analysing particles in liquid suspensions. It is an innovative system for sizing particles from 30 to 1000 nm. NTA combines laser light scattering microscopy with an integrated camera which enables visualization and recording of particles in solution. Figure 25 gives a schematic overview of NTA.

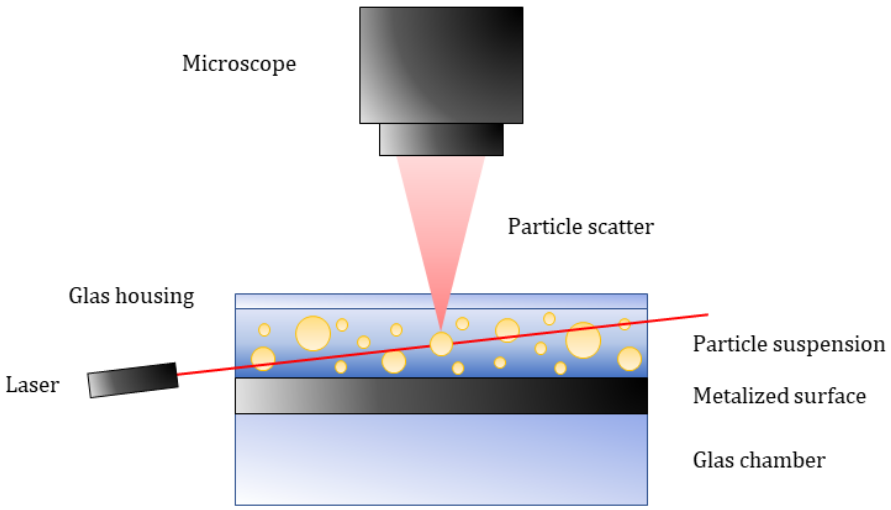

Figure 25 Principle of Nanoparticle tracking analysis.

A highly developed NTA software analyses recorded videos, identifies and tracks nanoparticles moving under Brownian motion, which can be related to a distinct particle size. The particle diameter can be derived by calculating the radius from the Stokes-Einstein equation (48):

$$\overline{(x,y)^2} = \frac{2k_B T}{3r_h \pi \eta} \tag{33}$$

where $\overline{(x,y)^2}$ is the mean-squared speed of particle, k_B is the Boltzmann constant ($\approx 1.38\text{x}10^{-23}\text{m}^2\text{kgs}^{-2}\text{K}^{-1}$), T is the temperature, r_h is the hydrodynamic radius or Stokes radius

of the particle and η is the viscosity in medium. Hydrodynamic radius and Stokes radius follow the same idea; however, the hydrodynamic radius is more related to biophysics describing biomolecules in solutions. The equation is only valid for liquids of low Reynold numbers.

The Brownian motion is the random motion of particles in a fluid (i.e. gas or liquid) that results from their collisions with fast-moving molecules in the fluid. This property can be used to determine radii of small particles (49).

The Stokes radius of a particle is defined as the radius of a hard sphere that diffuses in the same way as the solute. Besides the real radius of particle, the theory also takes solvent effects into consideration. A smaller ion, for instance, with stronger hydration and more surrounded counter ions may have a greater radius than a hydrophobic particle. This work uses NTA to determine the size distributions of cell debris particles, which are aggregates of cell membrane's negatively charged phospholipids and amino acids. Hence, the motion of particles also depends on buffer compositions and surrounding effects (50).

Figure 26 illustrates a cell debris agglomeration particle and its hydrodynamic radius:

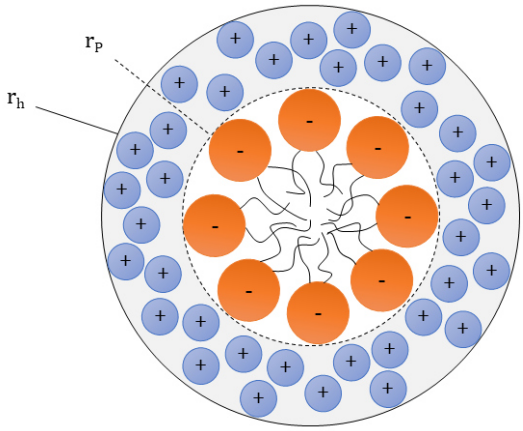

Figure 26 Schematic drawing of agglomerated phospholipids surrounded by negatively charged counter molecules.

The figure shows the real particle radius (dashed circle) and the mentioned hydrodynamic radius (solid circle). The application of PEI as agglomeration agent has to be considered, in so far as PEI has numerous positive charges that neutralize phospholipid agglomerations. As a consequence, the hydrodynamic radius can be hardly estimated as the real particle radius, which is due to PEI induced neutralisation event.

In contrast to older particle size determination methods, such as dynamic light scattering (DLS), NTA measures every single particle in solution which leads to much higher resolution and enables to analyse also complex suspension matrices. Additionally, samples need only minimal preparation before the measurement, provided that they are within the narrow concentration range of 10^7 to 10^9 particles/mL (48).

Despite the overall advantages of this powerful method, some critical drawbacks may come into play and influence the particle evaluation. The technique is very sensitive and the computational evaluation settings highly influence the outcome. Hence NTA requires a minimum of operation experience to maintain the reproducibility and makes analytic experiments comparable (48).

Summing up, NTA is a powerful particle analysing tool that gives highly realistic estimations of suspensions' particle size distributions.

5 Materials and methods

5.1 Host Strain

Escherichia coli strain HMS 174(DE3), carrying the plasmid pet11a_GFP_mut3.1 was used as primary biological material for upcoming studies.

5.2 High Pressure Homogenisation

5.2.1 Equipment

- Balance – Sartorius GL3202i-1CEU – Sartorius, Göttingen, Germany
- Stirrer – IKA C-MAG IKAMAG HS 10 – IKA, Staufen, Germany
- 2 stage homogeniser – Panda NS 1001 L2K – GEA Niro Soavi, Düsseldorf, Germany

5.2.2 Material

- Chemicals from Merck, Darmstadt, Germany
- Homogenisation buffer:
    - 20 mM Tris(hydroxymethyl)-aminomethan
    - 50 mM NaCl
    - pH 7.5
- Flushing solution: RO – H_2O
- Cleaning solution: 0.1 M NaOH
- Storing solution: 20% (v/v) Ethanol in RO – H_2O

5.2.3 Method

Frozen *E. coli* cells (-24°C) were suspended with homogenisation buffer to a final cell dry mass concentration (CDM) of 25 g/L. The cell suspension was stirred with an inert magnetic bar until no cell clumps were visible and a homogeneous suspension was reached. The homogeniser which was stored in 20% (v/v) ethanol was turned on and flushed with RO – H_2O several times to remove the ethanol from the entire system. Afterwards, a clean water flow test with 700 bar in the first stage and 70 bar in the second stage was performed. A flow rate of approximately 180 mL/min was achieved before each homogenisation run, which meets the equipment specific requirements of 160 – 200 mL/min range. After removal of RO – H_2O from device's cone, homogenisations of the homogeneous cell suspensions were started. Table 3 shows the number of passages and applied pressures used for homogenisation runs.

Table 3 Number of passages and applied pressures used for homogenisation experiments.

Number of passages	1. Stage	2. Stage
1	300	30
2	300	30
1	700	70
2	700	70

After homogenisation, all samples were shortly centrifuged (2575xg, 10 min) to remove crude particles that lay above a detectable range of 0 – 1000 nm. Afterwards, samples of each homogenate were taken, and the particle size distributions were determined via NTA.

5.3 Treatment of homogenates with PEI of different concentrations

5.3.1 Equipment

- Balance – Sartorius GL3202i-1CEU – Sartorius, Göttingen, Germany
- Stirrer – IKA C-MAG IKAMAG HS 10 – IKA, Staufen, Germany
- Water bath – GFL type 1083 – GFL, Burgwedel, Germany
- Vortexer – IKA Vortex Genius 3 – Merck, Darmstadt, Germany
- Centrifuge – Sigma 2-16P – ThermoFisher, Waltham, Massachusetts, USA

5.3.2 Material

- *E. coli* homogenate 1 treated with:
    - Resuspended in 20 mM Tris, 50 mM NaCl, pH 7.5
    - High pressure homogenisation (300/30 bar | 1 passage)
- *E. coli* homogenate 2 treated with:
    - Resuspended in 20 mM Tris, 50 mM NaCl, pH 7.5
    - High pressure homogenisation (300/30 bar | 2 passages)
- *E. coli* homogenate 3 treated with:
    - Resuspended in 20 mM Tris, 50 mM NaCl, pH 7.5
    - High pressure homogenisation (700/70 bar | 1 passage)
- *E. coli* homogenate 4 treated with:
    - Resuspended in 20 mM Tris, 50 mM NaCl, pH 7.5
    - High pressure homogenisation (700/70 bar | 2 passages)
- Polyethylenimine, branched, 10,000 Da – Polyscience, Warrington, USA
- RO – H_2O
- Greiner centrifuge tubes, 15 mL, 17x120 mm, conical bottom – Merck, Darmstadt, Germany

5.3.3 Method

At first, 4 homogenates were prepared under the same conditions as shown in table 3. A 10% (w/v) solution of Polyethylenimine (PEI) was made with RO – H_2O.

Prior to heat precipitation, the water bath was filled with RO – H_2O and preheated to 52°C. 15 mL Greiner centrifuge tubes, each filled with 10 mL of differently treated homogenates, were heated for 45 minutes to reach the desired homogenate temperature of 50°C. Then, 10% PEI solution was added to 10 mL of *E. coli* homogenates into the preheated Greiner tubes, before they were properly mixed with vortexer. Table 4 lists all final PEI concentrations and added volumes of 10% PEI solution:

Table 4 In 10 mL Greiner centrifuge tubes final PEI concentrations and added volumes of 10% (w/v) PEI solution.

Final PEI concentration (% w/v)	Added PEI solution (µL)
0.10	100
0.15	150
0.20	200
0.25	250
0.30	300

After mixing, PEI treated homogenates were again placed into the water bath to hold the homogenate's temperature of 50°C for 2 hours. After 2 hours of incubation Greiner tubes were centrifuged at 2575xg for 10 minutes to remove biggest cell debris precipitates that normally disturb the NTA detection method. After centrifugation, supernatants of each sample were analysed by nephelometry and NTA.

5.4 Centrifugation of homogenates treated with different PEI types

5.4.1 Equipment

- Balance – Sartorius GL3202i-1CEU – Sartorius, Göttingen, Germany
- Stirrer – IKA C-MAG IKAMAG HS 10 – IKA, Staufen, Germany
- Water bath – GFL type 1083 – GFL, Burgwedel, Germany
- Vortexer – IKA Vortex Genius 3 – Merck, Darmstadt, Germany
- Centrifuge – Sigma 2-16P – ThermoFischer, Waltham, Massachusetts, USA

5.4.2 Material

- *E. coli* homogenate treated with:
    - High pressure homogenisation (700/70 bar | 2 passages)
- Polyethylenimine, branched, 10,000 Da – Polyscience, Warrington, USA
- Polyethylenimine, branched, 1,200 Da – Polyscience, Warrington, USA

- RO – H_2O
- Greiner centrifuge tubes, 15 mL, 17x120 mm, conical bottom – Merck, Darmstadt, Germany

5.4.3 Method

Two 10% (w/v) solutions of both PEI types (1.2 kDa & 10 kDa) were prepared with RO – H_2O. Prior to heat precipitation, the water bath was filled with RO – H_2O and preheated to 52°C. 15 mL Greiner centrifuge tubes each filled with 10 mL of homogenate (700/70 bar | 2 passages) were prewarmed for 45 minutes to reach the desired homogenate temperature of 50°C. Then, different volumes of both PEI types were added to the homogenates, obtaining same PEI concentrations as shown in table 4.

After mixing, the PEI treated homogenates were again placed into the water bath to hold the homogenate's temperature of 50°C for 2 hours. After 2 hours of incubation the Greiner tubes with PEI treated homogenates were centrifuged at 3280xg for 0, 1, 2, 4, 8, 12, 15, 20 and 30 minutes. After each centrifugation run the turbidites of the supernatants were determined via nephelometry.

5.5 Centrifugational cell debris reduction

5.5.1 Equipment

- Balance – ENTRIS5201-1S – Sartorius, Göttingen, Germany
- Centrifuge – Avanti JXN-26 Centrifuge with fixed angle rotor (JLA-10.500, max 10,000 rpm) and metal centrifuge buckets – Beckman Coulter, Brea, USA

5.5.2 Material

- *E. coli* homogenate 1 treated with:
    - Resuspended in 20 mM Tris, 50 mM NaCl, pH 7.5
    - High pressure homogenisation (700/70 bar | 1 passage)
- *E. coli* homogenate 2 treated with:
    - Resuspended in 20 mM Tris, 50 mM NaCl, pH 7.5
    - High pressure homogenisation (700/70 bar | 2 passages)
- *E. coli* homogenate 3 treated with:
    - Resuspended in 20 mM Tris, 50 mM NaCl, pH 7.5
    - High pressure homogenisation (700/70 bar | 2 passages)
    - 0.2% (w/v) PEI (10 kDa)
    - Heat precipitation (2 hours)
- Centrifugal bottles – Type 3141, 500 mL – Roth, Karlsruhe, Germany

5.5.3 Method

Samples for depth and sterile filtration experiments were prepared. Hence, particles of two different *E. coli* homogenates were removed in two different ways.

500 mL of *E. coli* homogenate 1 was filled into two 500 mL centrifugal bottles. The bottles were balanced to a weight difference of 0.1 g and sealed, properly. The homogenate was centrifuged at 10,000xg for 30 minutes. The turbidity of supernatant was measured (107 NTU) and collected in a clean 500 mL flask.

1000 mL of *E. coli* homogenate 2 was separated into 4 centrifugal bottles. They were balanced to a weight difference of 0.1 g and closed, properly. The homogenate was centrifuged at 10,000xg for 15 minutes. The turbidity of the supernatant was measured (480 NTU) and collected in a clean 1000 mL flask.

1000 mL of *E. coli* homogenate 3 was filled into 4 separate centrifugal bottles. They were balanced to a weight difference of 0.1 g and sealed, properly. The homogenate was centrifuged at 500xg for 15 minutes, reaching a final supernatant's turbidity of 167 NTU. The supernatant was collected in a clean 1000 mL bottle, whereas the cell pellets were disposed.

5.6 Depth and sterile filtration

5.6.1 Equipment

- Pump and sensor system – ÄKTA Explorer – GE healthcare, Uppsala, Sweden
- Stirrer – VWR VS-C1 – VWR, Darmstadt, Germany

5.6.2 Material

- *E. coli* homogenate 1 (107 NTU) treated with:
    - Resuspended in 20 mM Tris, 50 mM NaCl, pH 7.5
    - High pressure homogenisation (700/70 bar | 1 passage)
    - Centrifuged (10,000xg | 30 minutes)
- *E. coli* homogenate 2 (480 NTU) treated with:
    - Resuspended in 20 mM Tris, 50 mM NaCl, pH 7.5
    - High pressure homogenisation (700/70 bar | 2 passages)
    - Centrifuged (10,000xg | 15 minutes)
- *E. coli* homogenate 3 (167 NTU) treated with:
    - Resuspended in 20 mM Tris, 50 mM NaCl, pH 7.5
    - High pressure homogenisation (700/70 bar | 2 passages)
    - 0.2% (w/v) PEI (10 kDa)
    - Centrifuged (500xg | 15 minutes)

- Depth filter:
    - Millistak +µpod, PES + Glassfiber (GF), 23 cm^2, 0.1 µm – Merck, Darmstadt, Germany
    - Sartoclear®, S010 Cap, Cellulose, 17.5 cm^2, 0.1 µm – Sartorius, Göttingen, Germany
    - 2 Sartoscale 25, Sartoguard GF, PES + GF, 4.5 cm^2, 0.1 µm – Sartorius, Göttingen, Germany
    - 2 Sartoguard GF, PES + GF, 17.3 cm^2, 0.1 µm – Sartorius, Göttingen, Germany
    - Sartoscale 25, Sartoguard GF, PES + GF, 4.5 cm^2, 0.2 µm – Sartorius, Göttingen, Germany
    - 3 Sartoscale 25, Sartoguard PES, PES, 4.5 cm^2, 0.1 µm – Sartorius, Göttingen, Germany
    - Sartoguard GF, PES + GF, 17.3 cm^2, 0.2 µm – Sartorius, Göttingen, Germany
- Sterile filter:
    - 2 Sartopore 2 XLM, Polyethersulfone (PES), 17.3 cm^2, 0.1 µm – Sartorius, Göttingen, Germany
    - 2 Sartopore 2 XLG, PES, 17.3 cm^2, 0.2 µm – Sartorius, Göttingen, Germany
- Prefilter:
    - Sartopure PP2, Polypropylen (PP), 17.3 cm^2, 0.65 µm – Sartorius, Göttingen, Germany
    - Sartoscale 25 Sartoguard PP3, PP, 4.5 cm^2, 0.45 µm – Sartorius, Göttingen, Germany
    - Sartoscale Sartoguard GF+, PES + GF, 4.5 cm^2, 0.65 µm – Sartorius, Göttingen, Germany
    - Sartopure GF+, PES + GF, 17.3 cm^2, 1.2 µm – Sartorius, Göttingen, Germany

5.6.3 Method

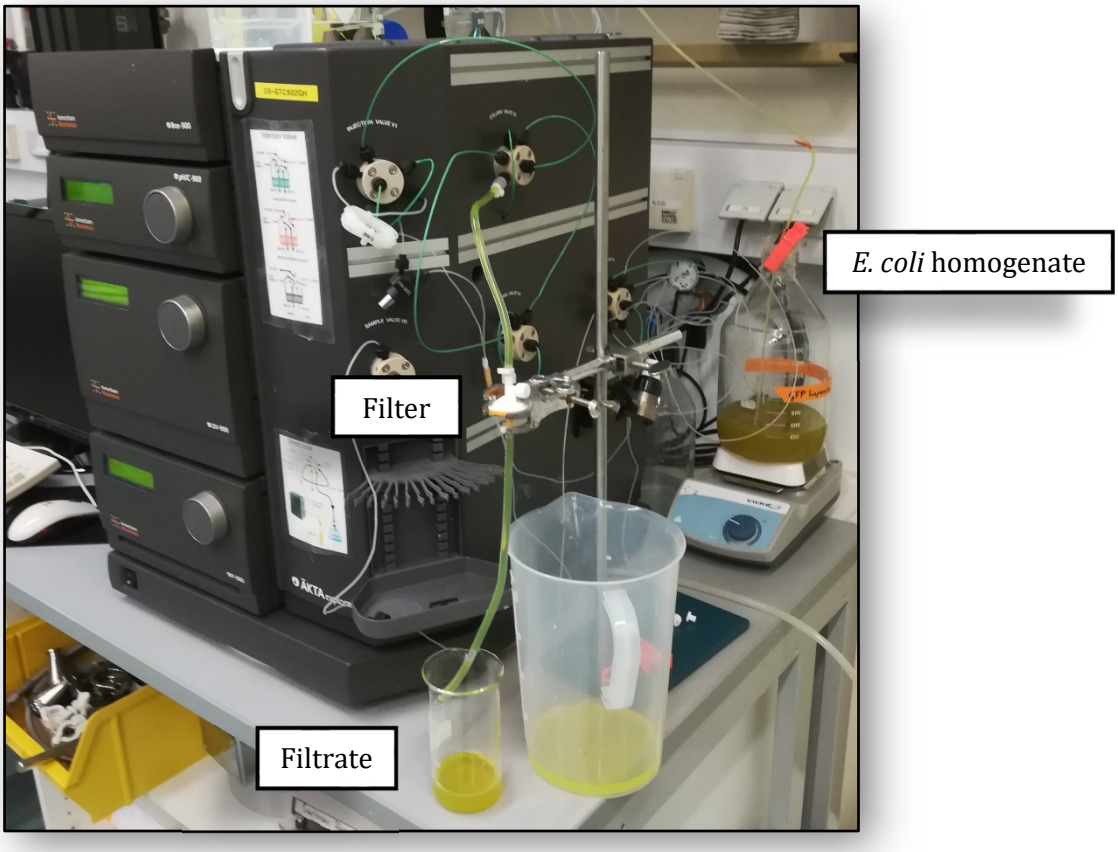

Figure 27 Set-up of depth and sterile filtration method.

Figure 27 shows the main set-up for depth and sterile filtration experiments. ÄKTA explorer is used for pumping the *E. coli* homogenate through the filter and measuring the back pressure built up by filter and cell debris particles.

All prepared homogenates were pumped through chosen filters with a constant flux of 200 LMH, while simultaneously measuring the back pressure. The filtrate was collected until the pressure sensor detected a back pressure of 3 bar, or no pressure increase occurred. The amount of filtrate was determined, receiving the filter dependent maximal filtrate volume (v_{max}). Moreover, the turbidity of each filtrate was measured with nephelometer.

5.7 TFF cell debris particle reduction

5.7.1 Equipment

- Ultrafiltration apparatus – Cogent µScale TFF System – Merck, Darmstadt, Germany

5.7.2 Material

- *E. coli* homogenate 1 (32.5 NTU) treated with:
    - Resuspended in 20 mM Tris, 50 mM NaCl, pH 7.5

    - High pressure homogenisation (700/70 bar | 1 passage)
    - 0.2% (w/v) PEI (10 kDa)
    - 2 h heat precipitation
    - Centrifugation at 4780xg for 40 minutes
- *E. Coli* homogenate 1 (36.5 NTU) treated with:
    - Resuspended in 20 mM Tris, 50 mM NaCl, pH 7.5
    - High pressure homogenisation (700/70 bar | 2 passage)
    - 0.2% (w/v) PEI (10 kDa)
    - 2 h heat precipitation
    - Centrifugation at 4780xg for 40 minutes
- Filter – Hollow fiber cartridge, UFP-500-E-3MA, 110 cm^2, 500,000 NMWC – GE healthcare, Uppsala, Sweden
- Filter – Hollow fiber cartridge, UFP-750-E-3MA, 110 cm^2, 750,000 NMWC – GE healthcare, Uppsala, Sweden
- Filter – Hollow fiber cartridge, CFP-1-D-3MA, 120 cm^2, 0.1 µm – GE healthcare, Uppsala, Sweden
- Pure GFP solution in PBS (16.31 g/L) [prepared by members (inclusive author of thesis) of bioprocess engineering laboratory course (in Engl.) - 790359 in November 2018]
- Filter cleaning in place (CIP) solutions:
    - RO – H_2O
    - CIP – solution (0.4 M NaOH + 300 ppm NaOCl)
- Storage solution:
    - 20% Ethanol

5.7.3 Method

At first, homogenate 1 turbidity was determined via nephelometry. After evaluating the 500,000 NMWC filter, 300 mL of homogenate 1 was filled into the reservoir of the ultrafiltration device. The tangential flow of feed was set to 250 mL/min, avoiding a cake formation of cell debris particles. The permeate was collected until the retentate had a volume of approximately 50 mL. After stopping ultrafiltration 10 mL of the collected permeate was taken to measure the remaining turbidity by nephelometer.

The same procedure was performed with two other filters (750,000 MWCO, 0.1 µm).

Afterwards a filter cleaning step for each used filter was performed to re-establish the original permeate flux of the filters: The filter was flushed with clean RO – H_2O with a maximum tangential flow rate of 300 mL/min for 10 minutes. After removing RO – H_2O from the system, 300 mL of the CIP-solution was filled into reservoir tank. The tangential flow was set to 250 mL/min and the permeate was recirculated back into the reservoir tank, maintaining a constant

volume inside the system. The TMP was set to 1 bar After chemical treatment, the CIP-solution was completely removed, and the filter was again flushed two times with a tangential flow rate of 300 mL/min. After removing the remaining RO – H_2O, the filters were ready for the next ultrafiltration method.

The same procedure, as described in paragraph one and two of this chapter, was performed with homogenate 2 to evaluate the filter performances, using a solution containing particles of lower diameter. Hence, the turbidities of all collected permeate solutions were once more determined via nephelometry.

Filters were cleaned with the same CIP method as described in paragraph 3 and stored in 20% ethanol, by flushing the filter with 20% Ethanol solution two times. After deinstalling the filters from the ultrafiltration device, the filters were sealed with dummy plugs, properly for an optimum of conservation.

5.8 GFP shear stress stability

5.8.1 Equipment

- Filtration system – ÄKTAcrossflow tangential flow filtration system – GE healthcare, Uppsala, Sweden
- Stirrer – VWR VS-C1 – VWR, Darmstadt, Germany

5.8.2 Material

- Filter – Hollow fiber cartridge, UFP-750-E-3MA, 110 cm^2, 750,000 NMWC – GE healthcare, Uppsala, Sweden
- 500 mL Phosphate buffer system (PBS):
    - 137 mM NaCl
    - 2.7 mM KCl
    - 10 mM Na_2HPO_4 * 2 H_2O
    - 2 mM KH_2PO_4
- GFP in PBS – 16.7 g/L
- Flushing solution:
    - RO – H_2O
- Filter cleaning in place (CIP) solutions:
    - RO – H_2O
    - CIP – Solution (0.4 M NaOH + 300 ppm NaOCl)
- Storage solution:
    - 20% Ethanol

5.8.3 Method

At first, a solution of 7.5 g/L pure GFP was prepared by dilution of GFP solution (16.7 g/L) with PBS. Before the stability test could start a method was written with the programme UNICORN 5 that includes commands guaranteeing a flow rate of 600 mL/min over 70 minutes. The programme calculated a shear rate of 8000 s^{-1} by using following relationship:

$$\tau = \frac{4\,\dot{V}}{\pi\,r^3} \tag{34}$$

where $\dot{V}$ is volumetric flow rate in cm^3/s, and r is the lumen radius in cm.

Prior to ultrafiltration start the ÄKTA system was pre-flushed with PBS and the reservoir tank was filled with 1000 mL of diluted GFP solution (7.5 g/L). The permeate outlet of filtration was closed to prevent any permeate flow. During the recirculation of solution through hollow fiber membrane back to the reservoir tank, every 10 minutes a sample of 1 mL was taken out of the reservoir for determining the GFP concentration.

After 70 minutes the GFP solution was removed from the whole system. Afterwards a CIP procedure was started, followed by a storage process with 20% ethanol for an optimal filter conservation.

5.9 Flux behaviours of TFF cell debris particle removal

5.9.1 Equipment

- Filtration system – ÄKTAcrossflow tangential flow filtration system – GE healthcare, Uppsala, Sweden
- Stirrer – VWR VS-C1 – VWR, Darmstadt, Germany

5.9.2 Material

- Filter – Hollow Fiber Cartridge, UFP-750-E-3MA, 110 cm^2, 750,000 NMWC – GE healthcare, Uppsala, Sweden
- *E. coli* homogenate (30 NTU) treated with:
    - Resuspended in 20 mM Tris, 50 mM NaCl, pH 7.5
    - High pressure homogenisation (700/70 bar | 2 passage)
    - 0.2% (w/v) PEI (10 kDa)
    - 2 h heat precipitation
    - Centrifugation at 4780xg for 45 minutes
- Flushing solution:
    - RO – H_2O

- Filter cleaning in place (CIP) solutions:
    - RO – H_2O
    - CIP – Solution (0.4 M NaOH + 300 ppm NaOCl)
- Storage solution:
    - 20% Ethanol

5.9.3 Method

At the beginning, the system as well as the filter was flushed with RO – H_2O to remove all storage ethanol. Next, UNICORN 5 was used to write a method that includes a feed flow rate of 400 mL/min and a TMP of 0.5 bar. Moreover, a programmed command would stop the filtration process when retentate volume reaches 50 mL, avoiding a too high particle concentration in the remaining retentate. Before filtration was started, system and filter were pre-flushed with homogenisation buffer (20 mM Tris, 50 mM NaCl | pH 7.5), followed by the filling of 1000 mL *E. coli* homogenate into a reservoir tank. 1 mL samples were taken from permeate in 100 mL steps as well as 500 µL from the reservoir at the beginning, in the middle and in the end of filtration. GFP concentrations of permeate samples were measured, whereas GFP concentrations and turbidities of retentate samples were determined. Permeate flow data of each filtration were used to identify maximum specific permeate volume.

After filtration the GFP solution was removed from the whole system. Afterwards, a CIP procedure, including two RO – H_2O flushes and CIP – solution treatment, was started, followed by a storage process with 20% ethanol for an optimal filter conservation.

The previously described method was also applied for volumetric flow rates of 500 mL/min and 600 mL/min in combination with TMPs of 0.5, 1 and 2 bars each. Hence, the whole experimental method was applied 3x3 =9 times.

5.10 Influence of buffer on TFF filtration

5.10.1 Equipment

- Filtration system – ÄKTAcrossflow tangential flow filtration system – GE healthcare, Uppsala, Sweden
- Stirrer – VWR VS-C1 – VWR, Darmstadt, Germany

5.10.2 Material

- Filter – Hollow Fiber Cartridge, UFP-750-E-3MA, 110 cm^2, 750,000 NMWC – GE healthcare, Uppsala, Sweden
- *E. coli* homogenate 1 (30 NTU) treated with:
    - Resuspended in 50 mM Tris, 50 mM NaCl, pH 7.5
    - High pressure homogenisation (700/70 bar | 2 passage)
    - 0.2% (w/v) PEI (10 kDa)

    - 2 h heat precipitation
    - Centrifugation at 4780xg for 45 minutes
- *E. Coli* homogenate 2 (30 NTU) treated with:
    - Resuspended in 80 mM Tris, 50 mM NaCl, pH 7.5
    - Rest same as homogenate 1
- Flushing solution:
    - RO – H_2O
- Filter Cleaning In Place (CIP) solutions:
    - RO – H_2O
    - CIP – Solution (0.4 M NaOH + 300 ppm NaOCl)
- Storage solution:
    - 20% Ethanol

5.10.3 Method

Prior to use, the hollow fiber filter was flushed to remove the ethanol storage solution. Afterwards the already written method that includes a tangential flow rate of 400 mL/min and a TMP of 2 bar was set by controlling programme.

The TFF filtration with homogenate 1 was initiated and the permeate was collected in a clean bottle. As described in chapter 8.9.3, 1 mL permeate was taken every time when 100 mL of permeate was collected. Additionally, 500 µL at the beginning, in the middle and in the end were taken for the determination of rejected GFP molecules in retentate. All taken samples were used to measure their GFP content. Finally, the turbidites of the collected permeate and the rest of retentate in reservoir were measured by nephelometry. As well as in the previous chapter, the permeate flow rate data were used to determine the maximum specific permeate volume.

After filtration retentate was removed from system and the CIP procedure as described in chapter 8.9.3 paragraph 2 was applied.

The same described method was used for a TFF filtration of homogenate 2. The collected data were used to compare the GFP rejections of different buffer solutions during filtration process.

5.11 Comparison of flux behaviours under different ultrafiltration conditions

5.11.1 Equipment

- Filtration system – ÄKTAcrossflow tangential flow filtration system – GE healthcare, Uppsala, Sweden
- Stirrer – VWR VS-C1 – VWR, Darmstadt, Germany
- Filter holder – Sartocon® Slice 200 Stainless Steel Holder – Sartorius, Göttingen, Germany

5.11.2 Material

- Filter – Sartocon® Slice PESU Cassette, 0.02 m^2, 10 kDa – Sartorius, Göttingen, Germany
- Filter – Sartocon® Slice 200 Hydrosart® Cassette, 0.02 m^2, 10 kDa – Sartorius, Göttingen, Germany
- Filter – Hollow Fiber Cartridge, UFP-10-C-2U, 50 cm^2, 10 kDa MWCO – GE healthcare, Uppsala, Sweden
- *E. coli* homogenate 1 (2 g/L GFP) treated with:
    - Resuspended in 50 mM Tris, 50 mM NaCl, pH 7.5
    - High pressure homogenisation (700/70 bar | 2 passage)
    - 0.2% (w/v) PEI (10 kDa)
    - 2 h heat precipitation
    - Centrifugation at 4780xg for 45 minutes
    - TFF filtrated (600 mL/min, 0.5 bar)
- *E. coli* homogenate 2 (2 g/L GFP) treated with:
    - 0.2% (w/v) PEI (1.2 kDa)
    - Rest same as homogenate 1
- Flushing solution:
    - RO – H_2O
- Filter cleaning in place (CIP) solutions:
    - RO – H_2O
    - CIP – Solution (0.4 M NaOH + 300 ppm NaOCl)
- Storage solution:
    - 20% Ethanol

5.11.3 Method

Prior to ultrafiltration a method was written in UNICORN 5 including tangential flow rates of 111.11 mL/min, 222.22 mL/min and 333.33 mL/min in combination with TMPs of 0.5, 1.0, 1.5, 2.0, 2.5, 3.0 bar. It was programmed that for each different pressure a mark was set that recorded the permeate flow rate. After this method another method followed that would concentrate the homogenate to a GFP concentration of 4 g/L. This newly concentrated homogenate would be then treated in the way of the first written method, by recording different permeate flows affected by chosen parameters. Other concentration methods, containing GFP concentrations of 7.5 g/L, 10.5 g/L and 13.5 g/L were treated the same way. All written methods are combined into a method queue that would last about 8 hours. The method queue also included a RO – H_2O flush, CIP – solution treatment and ethanol storage method that would clean and conserve used filters.

The filter was installed to a filter holder and connected to ÄKTAcrossflow, excepting the second permeate outlet which was closed with a dummy plug.

Before the filtration procedure was started, homogenate 1 was filled into the ultrafiltration device's reservoir tank. The UNICORN's method queue was started to record every permeate flow of every single parameter variant. Additionally, 500 µL sample was taken before and after each method to monitor GFP concentration and to carry out mass balance control.

For homogenate 2 the same filter and procedures were used accordingly.

Furthermore, the same experiment with homogenate 1 was performed, but a cellulose based Hydrosart® filter was used.

After the runs all relevant permeate flow rate data were assembled, generating filtration flux behaviour curves at different parameters. Relevant graphs were designed, using graphic evaluation programme SigmaPlot 13.

5.12 Comparison of flux behaviours under different diafiltration conditions

5.12.1 Equipment

- Filtration system – ÄKTAcrossflow tangential flow filtration system – GE healthcare, Uppsala, Sweden
- Stirrer – VWR VS-C1 – VWR, Darmstadt, Germany
- Filter holder – Sartocon® Slice 200 Stainless Steel Holder – Sartorius, Göttingen, Germany

5.12.2 Material

- *E. coli* homogenate 1 (4 g/L GFP) treated with:
    - Resuspended in 50 mM Tris, 50 mM NaCl, pH 7.5
    - High pressure homogenisation (700/70 bar | 2 passage)
    - 0.2% (w/v) PEI (10 kDa)
    - 2 h heat precipitation
    - Centrifugation at 4780xg for 45 minutes
    - TFF filtrated (600 mL/min | 0.5 bar)
- *E. coli* homogenate 2 (4 g/L GFP) treated with:
    - 0.2% (w/v) PEI (1.2 kDa)
    - Rest same as homogenate 1
- *E. coli* homogenate 3 (4 g/L GFP) treated with:
    - Without PEI treatment
    - Centrifugation at 18,600xg for 45 minutes
    - Rest same as homogenate 1

- Flushing solution:
  - RO – H_2O
- Homogenisation buffer:
  - 10 mM Tris(hydroxymethyl)-aminomethan
  - pH 7.5
- Filter Cleaning In Place (CIP) solutions:
  - RO – H_2O
  - CIP – Solution (0.4 M NaOH + 300 ppm NaOCl)
- Storage solution:
  - 20% Ethanol

5.12.3 Method

Before diafiltration experiments could be started, homogenate 1 was treated as follows to remove approximately half of residual PEI in the homogenate:

Concentrated sample of homogenate 1 of chapter 8.13 (13.5 g/L) was diluted with RO – H_2O to a concentration of 4 g/L. This led to a drastic conductivity decrease (15 mM, 15 mM NaCl) which facilitated precipitation of dissolved PEI. The precipitates were removed by centrifugation (18,600xg, 30 minutes). After centrifugation, 1,27 g Tris and 0,61 g NaCl were dissolved in 300 mL supernatant, creating the same buffer conditions as in other homogenates.

Prior to diafiltration experiments, a diafiltration method was written with UNICORN 5 that included a tangential flow of 400 mL/min and a TMP of 1 bar. The method would stop at a diavolume (V_D) of 5. Following equation shows the determination of diavolume:

$$V_D = \frac{V_P}{V_0} \tag{35}$$

where V_P is the permeate volume and V_0 is the initial feed volume.

The diafiltration process started with filling 140 mL of homogenate 1 into the reservoir tank of ÄKTAcrossflow device. During diafiltration the volume of homogenate was balanced by transferring the same amount of diafiltration buffer as removed permeate. Consequently, the conductivity decreased until it reached a certain plateau. During diafiltration the permeate volume rate was recorded to determine the flux behaviour over diafiltration time. After 5 volume exchanges the process was stopped and a 1 mL sample was taken from the reservoir, for measuring GFP concentration after diafiltration.

Finally, filter cassette was flushed by RO – H_2O, followed by a CIP procedure. For optimal conservation, the filter cassette was flushed with 20% ethanol.

The same diafiltration process was applied with homogenate 2 and 3, identifying the influences of homogenate compositions on the flux behaviours. Collected data were evaluated and plotted with the programme SigmaPlot 13®.

5.13 Nephelometry

5.13.1 Equipment

- Nephelometer – Hach 2100Q – Hach-Lange, Düsseldorf, Germany

5.13.2 Material

- 20 NTU Hach STABLCAL Formazin
- 100 NTU Hach STABLCAL Formazin
- 800 NTU Hach STABLCAL Formazin
- 10 mL Sample cuvette with screw cap

5.13.3 Method

For accurate turbidity measurement the device was calibrated with 20 NTU, 100 NTU and 800 NTU standards. After calibration, 10 – 15 mL of sample of interest was filled into a special cuvette and placed into the device. After closing the sample cap of the device, measurement was initiated by pressing the “Measure” button. After a few seconds device’s display showed the measured turbidity of sample.

5.14 GFP photometric measurement

5.14.1 Equipment

- UV/Vis Spectrometer – Cary 60 UV/Vis – Agilent, Santa Clara, California, USA

5.14.2 Material

- Pure GFP solution in PBS of unknown concentration [prepared by members (inclusive the author of this thesis) of bioprocess engineering laboratory course (in Engl.) - 790359 in November 2018]
- 100 mL PBS
- 1.5 mL cuvettes – BRAND® standard disposable cuvettes – (Merck, Darmstadt, Germany)

5.14.3 Method

First, the molar extinction coefficient was determined by using the bioinformatics resource platform ExPASy (51). The platform offers a tool, called ProtPara (52), that calculates and determines several chemical characteristics of proteins such as molecular weight, theoretical pI and extinction coefficient. The amino acid sequence of GFPmut3.1 was taken from the database FPbase (17) and was inserted into the ProtPara tool. Besides several basic protein

information, the molar extinction coefficient of 0.817 $L \cdot g^{-1} \cdot cm^{-1}$ was taken for photometric protein quantification. The GFP solution was diluted 1:20 to meet the optimal absorbance range of 0.2 – 2. Ten dilutions of 1:20 were prepared to find an appropriate estimation and an elimination of dilution errors. Each sample was filled into plastic cuvette and placed into the sample holder of photometer. The measurement was controlled and recorded by connected computer. Table 5 shows measured extinctions at 280 nm of all prepared samples and their mean value.

Table 5 GFP solution samples and their extinctions at 280 nm.

Sample number	Extinction at 280 nm
1	0.6578
2	0.6679
3	0.6646
4	0.6690
5	0.6672
6	0.6665
7	0.6663
8	0.6709
9	0.6658
10	0.6670
Mean	0.6663

The mean extinction was used to determine average concentration in solution, using the Beer-Lambert Law:

$$E = \varepsilon_m \, c \;\; d \tag{36}$$

where E is the extinction of sample, ε_m is the mass extinction coefficient in $L \cdot g^{-1} \cdot cm^{-1}$, c is the concentration of solute in sample in $g \cdot L^{-1}$ and d is the sample path length in cm.

In this case the sample pathlength is 1 cm. Hence, sample concentration is the quotient of extinction and extinction coefficient. Considering the applied dilution, the concentration of the GFP solution is 16.31 g/L. Due to several bioengineering polishing steps, the solution can be seen as totally pure. The same solution is used to set up a calibration curve for fluorescence measurement.

5.15 GFP fluorescence measurement

5.15.1 Equipment

- Plate reader spectrometer – Tecan Infinite® M200 Pro – Tecan, Männedorf, Schweiz

5.15.2 Material

- Pure GFP solution in PBS (16.31 g/L) [prepared by members (inclusive author of this thesis) of bioprocess engineering laboratory course (in Engl.) - 790359 in November 2018]
- 96 well plate – Nunc™ F96 MicroWell™ Polysterene plate, black – ThermoFisher, Waltham, Massachusetts, USA
- 200 mL PBS dilution buffer

5.15.3 Method

GFP was quantified by measuring the fluorescence signal of samples which have to be in a linear range of a GFP calibration curve. Hence, a GFP regression curve had to be developed:

At first, 15 different dilutions of GFP solution were prepared for identifying the linear range of fluorescence measurement. Each dilution was made five times, and each was measured four times. The detected values were used to generate their averages, whereas the received averages were used to form one major mean value which eliminated the measurement deviations as well as dilution errors. The parameters for the measurements in plate reader spectrometer are shown in table 6.

Table 6 Measurement parameter settings of plate reader for GFP determination.

Parameter	Value
Temperature	25 °C
Excitation Wavelength	485 nm
Emission Wavelength	520 nm
Excitation Bandwidth	9 nm
Emission Bandwidth	20 nm
Gain	53
Number of Flashes	40
Integration Time	20 µs
Lag Time	0 µs
Settle Time	0 ms
Z-Position	18811 µm

Table 7 shows prepared solutions, their GFP concentrations and obtained major mean.

Table 7 Prepared dilutions and their concentrations for creating GFP calibration curve

Dilution	GFP (mg/L)	Major Average (RFU)
1:5000	3.26	149.2
1:2000	8.16	900.9
1:1000	16.31	1075.5
1:800	20.39	1881.7
1:500	32.62	2211.0
1:200	81.54	4793.1
1:100	163.11	9421.6
1:80	203.89	11670.9
1:50	326.22	17892.2
1:40	407.77	21200.8
1:20	815.54	34654.9
1:10	1631.09	50150.7
1:8	2038.86	53035.7
1:5	3262.18	60732.3
1:4	4077.72	62753.0

The received measurement data were used to create a diagram plotting Relative Fluorescence Unit (RFU) in correlation with GFP concentration. Visually, a section was identified where a linear relationship between measurement signal and GFP concentration exists. Figure 29 depicts 2 diagrams that present the received calibration curve.

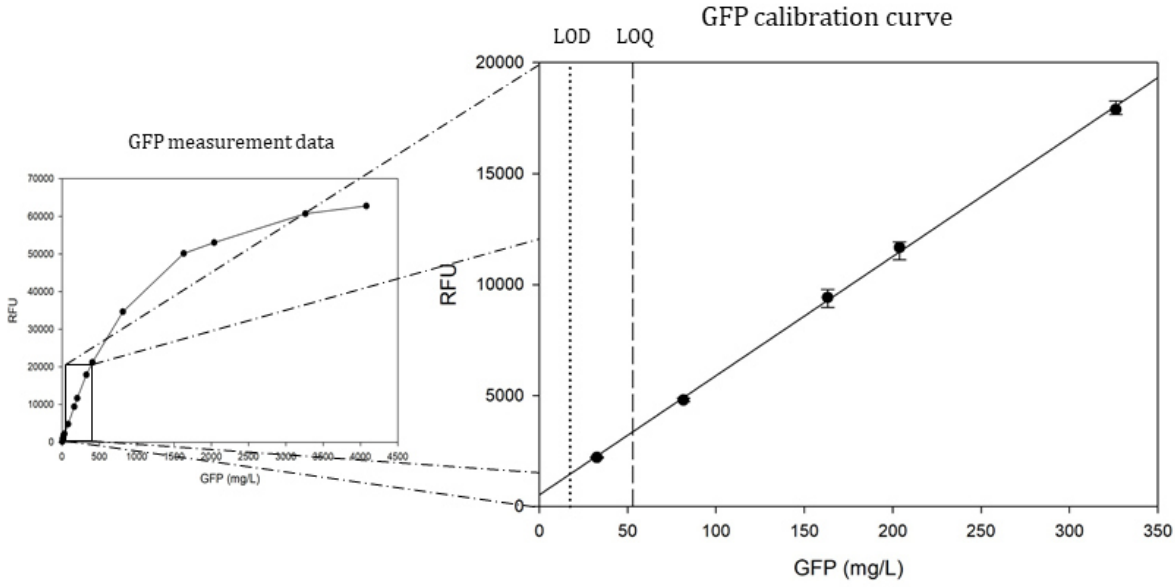

Figure 28 GFP measurements of prepared solutions and received signals (left plot) and its section of linear relationship (right plot).

Left diagram represents obtained fluorescence signal averages of all prepared dilutions, whereas the right diagram emphasizes the section which can be used as a valid calibration curve, due to its linear relationship. The general equation of the regression line was defined as:

$$\mathrm{Y} = 53.722\,\mathrm{x} + 522.84 \tag{37}$$

Dots of right diagram include error bars which contain all residues that scatter around their mean value. The thresholds of the bars represent the lowest and highest residue. However, the dotted and dashed line stand for the Limit of detection (LOD) and Limit of quantification (LOQ), respectively. Hence, each analysed sample should be in the so-called working range which lays within LOQ and the point with the highest signal value. The scattering residues around the mean values are key for the determination of LOD and LOQ. According to validation guideline of International Council of Harmonisation (ICH) Q2 (R1), the LOD is the quotient of 3.3 times the mean standard deviation of residues and slope, whereas LOQ is the quotient of 10 times the mean standard deviation of residues and slope.

$$LOD = \frac{3.3 * \bar{\sigma}_{Res}}{k} \tag{38}$$

$$LOQ = \frac{10 * \bar{\sigma}_{Res}}{k} \tag{39}$$

where k is the slope of regression curve, $\bar{\sigma}_{Res}$ is the average of residual standard deviations around the calibration curve:

$$\sigma_{Res} = \sqrt{\frac{Y_{Est} - Y_{Res}}{n - 1}} \tag{40}$$

where Y_{Est} estimated signal value received from calibration curve, Y_{Res} are real signals of the measurements and n is the number of measurements.

In this case, LOD resulted in 17.46 mg/L and equation of LOQ yielded 52.92 mg/L. According to the results it is highly recommended to quantify GFP solutions, which are in the working range of 52.92 mg/L and 326.22 mg/L. All GFP solutions of higher concentrations have to be diluted to fulfil the requirements.

5.16 Nanoparticle Tracking Analysis

5.16.1 Equipment

- Nanoparticle tracking system – NanoSight NS300 – Malvern Panalytical, Kassel, Germany
- Syringe pump – NanoSight syringe pump – Malvern Panalytical, Kassel, Germany

5.16.2 Material

- 1 mL syringes – OMNIFIX®-F Solo Syringe – B. Braun Melsungen AG, Melsungen, Germany

5.16.3 Method

To assure optimal analytical conditions, each sample should be in a range of 10^6 - 10^9 particles/mL. In case of a cell debris suspension of, for instance, a turbidity of 30 NTU, the sample should be diluted 1:1000, obtaining a particle concentration of approximately 10^8 particles/mL. Unfortunately, it highly depends on the suspension's matrix and its compositions. Hence, each suspension's concentration had to be tested, prior to perform an accurate NTA. After finding a sophisticated dilution, 1 mL sample was sucked up by 1 mL syringe, which was then coupled with a tube connecting the sample with a special sample chamber. The sample chamber had been flushed with 800 µL sample before the syringe with the remaining sample was installed to the NanoSight syringe pump. The whole sample compartment was placed into the NanoSight device, assuring that all metal connectors were in touch, properly. The NanoSight operating software was started via connected PC and capture as well as analysis adjustments were set. Table 8 shows the operating conditions, which were used during particle analysis.

Table 8 Capture and analysis adjustments for particle tracking analysis.

Capture Setting	Value
Camera type	sCMOS
Laser type	Blue488
Camera level	16
Slide shutter	1300
Slider gain	512
Frames per second	25.0
Number of frames	749
Temperature	25.0 °C
Viscosity	0.9 cP (Water)
Dilution factor	10^3 – 10^5 (variable)
Syringe pump speed	30
Analysis Setting	**Value**
Detect threshold	3
Blur size	Auto
Max jump distance	Auto: 18.1 – 20.3 pix

After setting the parameters, the system tracked particles of each sample 5 times. In the end, an average was taken, guaranteeing appropriate results and eliminating outlying tracking periods.

6 Results and discussion

6.1 High pressure homogenisation

Goal of high pressure homogenisation (HPH) experiments was to study the influence of applied pressures and number of passages on the number and particle size distribution of cell debris. The experiments can be also seen as extension experiments of Jurjevec (53) and Zartler (21), where the authors investigated DNA, endotoxin and GFP content of homogenate after homogenisation. Additionally, Zartler (21) showed that a higher applied pressure led to a reduction in particle size. These experiments had to be repeated to illustrate the particle size distribution between 0 and 200 nm with the NTA in a more precisely way, identifying the most appropriate homogenisation mode to enhance the followed depth filter performances. For this, frozen *E. coli* cell pellet was resuspended with Tris buffer (20 mM Tris + 50 mM NaCl), obtaining 25 g/L CDW. The cell suspension was homogenized in 4 different ways. Before NTA analysis, the homogenates were centrifuged at 2757xg for 10 minutes to remove larger particles that would disturb the particle size distribution measurement. Figure 29 depicts particle size distribution of 4 different HPH modes.

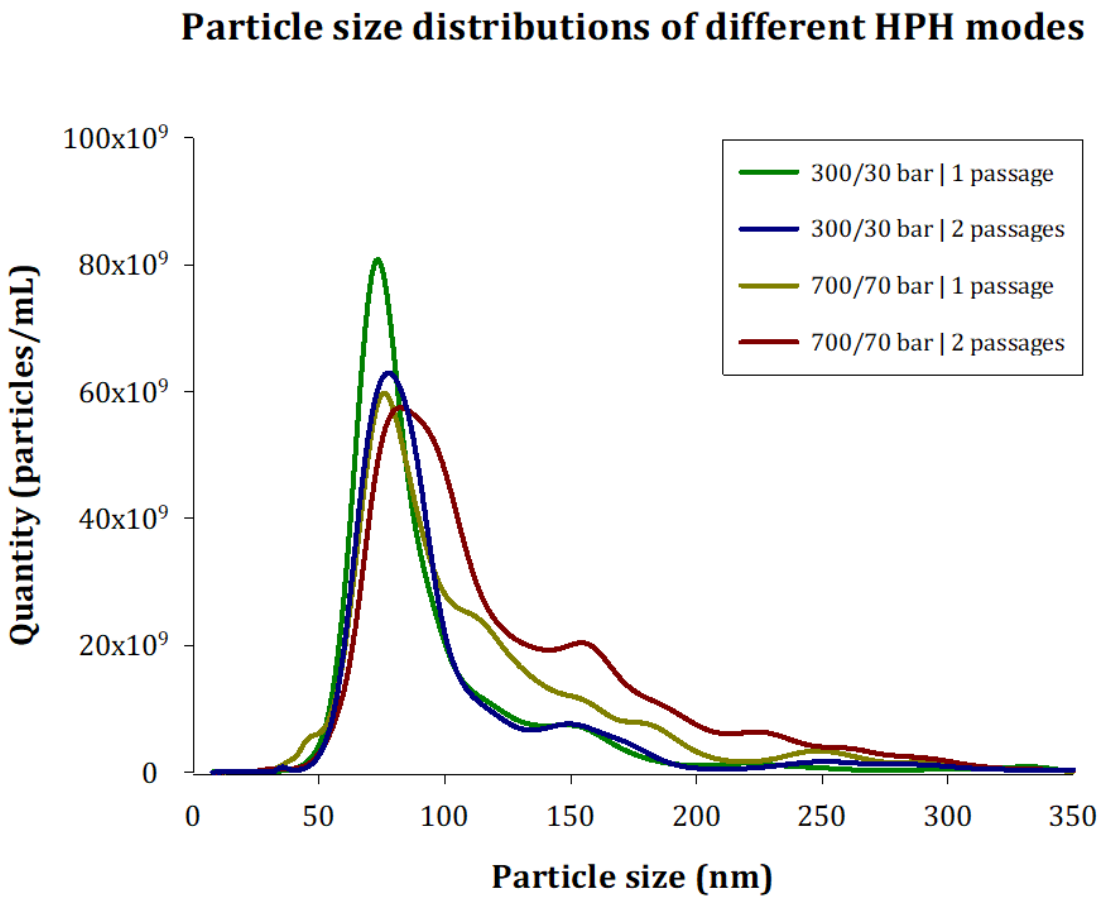

Figure 29 Particle size distribution of 4 different HPH modes. Green, blue, yellow and red lines represent the different HPH modes that are defined in legend.

The graph shows that all HPH variants comprise very similar particle size distributions. Most particle size fractions were around 100 nm and below. Surprisingly, homogenates, processed by mild HPH conditions, contained less particles above 100 nm than particle suspensions, treated with high pressure (700 bar). One explanation would be that higher pressure leads to more particles below 350 nm, disrupted from bigger ones that were normally removed by previously applied centrifugation. Table 9 shows most important properties of obtained homogenates.

Table 9 Extracted GFP, total number of particles and average particle diameter of all HPH modes.

HPH conditions	GFP (g/L)	Particles/mL	⌀ Maximum (nm)
300/30 bar | 1P	3.98	$8{,}08\text{x}10^{11}$	73.5
300/30 bar | 2P	4.13	$3.03\text{x}10^{12}$	77.5
700/70 bar | 1P	4.23	$3.52\text{x}10^{12}$	75.5
700/70 bar | 2P	4.31	$4.47\text{x}10^{12}$	82.5

It can be stated that harsh HPH conditions lead to higher GFP extractions and more particles in suspension, even though the diameter peak is at mildest condition (300/30 bar | 1P) the highest. Lower content of bigger particles that normally disturb the tracking of low-diameter-particles could be the reason for a such measurement artefact. According to GFP extraction, the difference of homogenate's concentration was not tremendous. Due to the use of frozen cell pellets at the beginning of each experiment, the GFP release out of cell was probably improved. Processing frozen cells could also be the reason for such small debris diameters.

Overall, due to the majority of particles under diameters of 100 nm, upcoming particle removal experiments, using depth filters were not expected being effective. To enlarge the average particle diameter in solution, it was tried to use PEI as a particle precipitation aid.

6.2 Treatment of homogenates with PEI of different concentrations

General aim of this approach was to identify the influence of different PEI concentrations combined with heat treatment on the particle distributions of homogenates. Jurjevec (53) recognized that Polyethylenimine (PEI) concentrations of 0.2 – 0.3 % (w/v) would give best results regarding cell debris agglomeration, DNA and endotoxin reduction and GFP conservation. He stated that the most beneficial concentration would be 0.2 % (w/v) PEI with 2 hours of permanent heating at 50°C.

So, homogenates were prepared same as described in chapter 6.1 but extra PEI addition was made. Final homogenates comprised PEI concentrations of 0, 0.10, 0.15, 0.20, 0.25, 0.30 % (w/v). After PEI addition, the homogenates were heated at 50 °C for 2 hours. Afterwards, all prepared homogenates were centrifuged at 2575xg for 10 minutes. Supernatants were analysed via NTU and NTA, receiving information about their particle content.

Table 10 gives an overview about the turbidities of different treated homogenates, regarding to HPH and PEI concentration. All obtained values are given in nephelometric turbidity unit (NTU).

Table 10 Turbidities of PEI treated HPH homogenates. Received values are given in NTU.

	PEI concentration (%) (w/v)					
Homogenisation	0	0.10	0.15	0.20	0.25	0.30
300/30 bar 1 passage	n. m.	178	171	39.1	35.8	37.8
300/30 bar 2 passages	n. m.	132	154	49.3	47.2	43.6
700/70 bar 1 passage	n. m.	126	88.9	58.2	49.7	65.9
700/70 bar 2 passages	n. m.	176	79.3	47.7	50.1	53.0

n. m. = not measurable

Table 10 shows that turbidities of homogenates were in between 40 and 180. Even, homogenates without any PEI treatment revealed such a high turbidity that could not been measured by device. Mild centrifugation conditions are responsible for such high turbidity values.

Interestingly, the homogenisation method with best protein release (700/70 bar | 2 passages) offered the lowest turbidity with 47.7 NTU, which is, luckily, also Jurjevec's (53) concentration of choice in respect to GFP conservation and PEI consumption. A higher turbidity value at higher PEI concentrations can be explained by attachments of PEI molecules on particles at nm range that would lead to a higher particle diameters. Additionally, a higher PEI concentration increases the chance of interconnection of particles between 0 and 100 nm, which probably ends up in slightly bigger colloids that are not able to be removed by centrifugation.

However, due to proper performance of using 0.20% PEI (w/v), particle size distribution of all HPH modes were determined via NTA and visualized in figure 30.

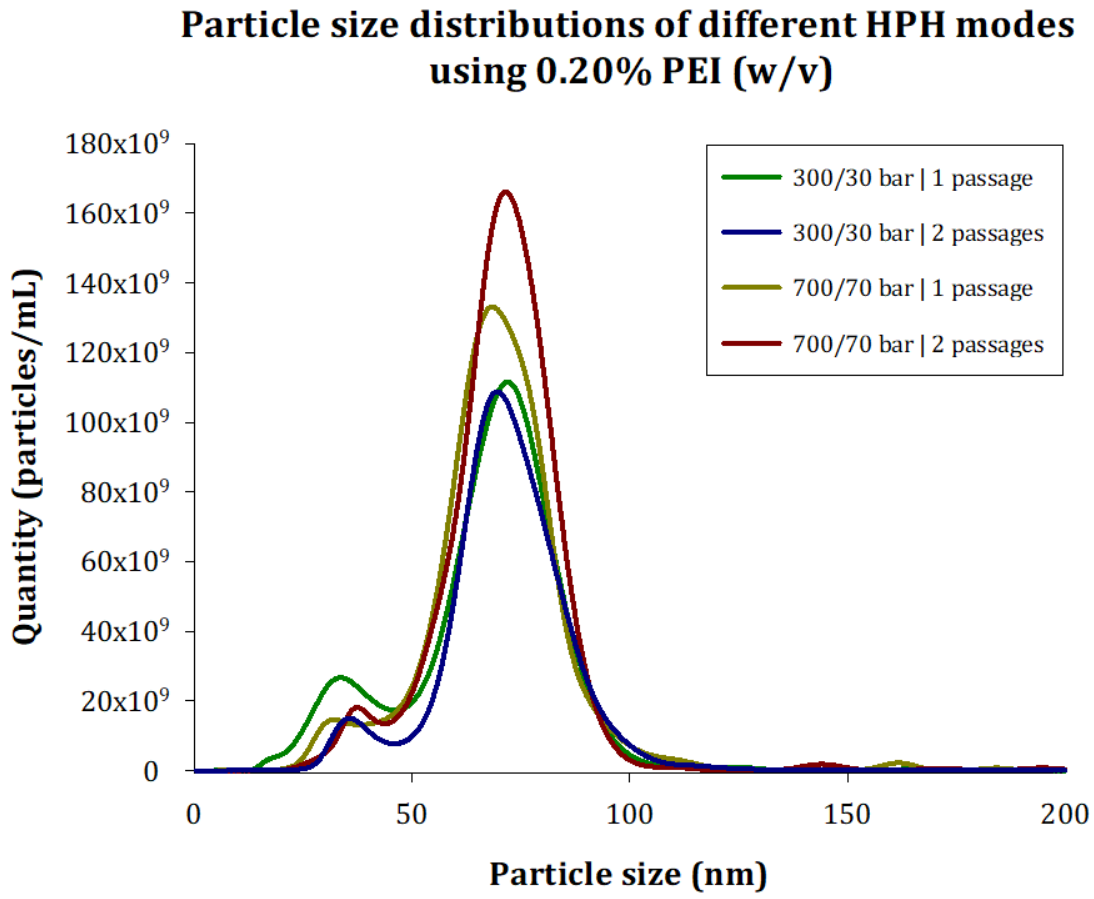

Figure 30 Particle size distribution of different HPH homogenates treated with 0.20% (w/v) PEI. Green, blue, yellow and red lines represent the different HPH modes that are defined in legend.

Figure 30 reveals that a homogenate treatment with 0.20% PEI lead to flocculation of particles with diameters higher than 100 nm. An additional centrifugation step would remove the precipitated particles. Remaining particles were mainly under 100 nm, regardless of applied homogenization pressure. Anyway, a treatment of 700 bar led to slightly higher quantities of particles below 100 nm.

However, next question that has to be answered is if an increase of PEI concentration would reduce the number of particles or enlarge their diameter. It goes without saying that an extension of particle's diameter would improve a later depth filtration step. Therefore, the homogenates, processed by 700/70 bar | 2 passages HPH and treated with different PEI concentrations were analysed by NTA. Figure 31 depicts the particle size distribution of mentioned homogenates.

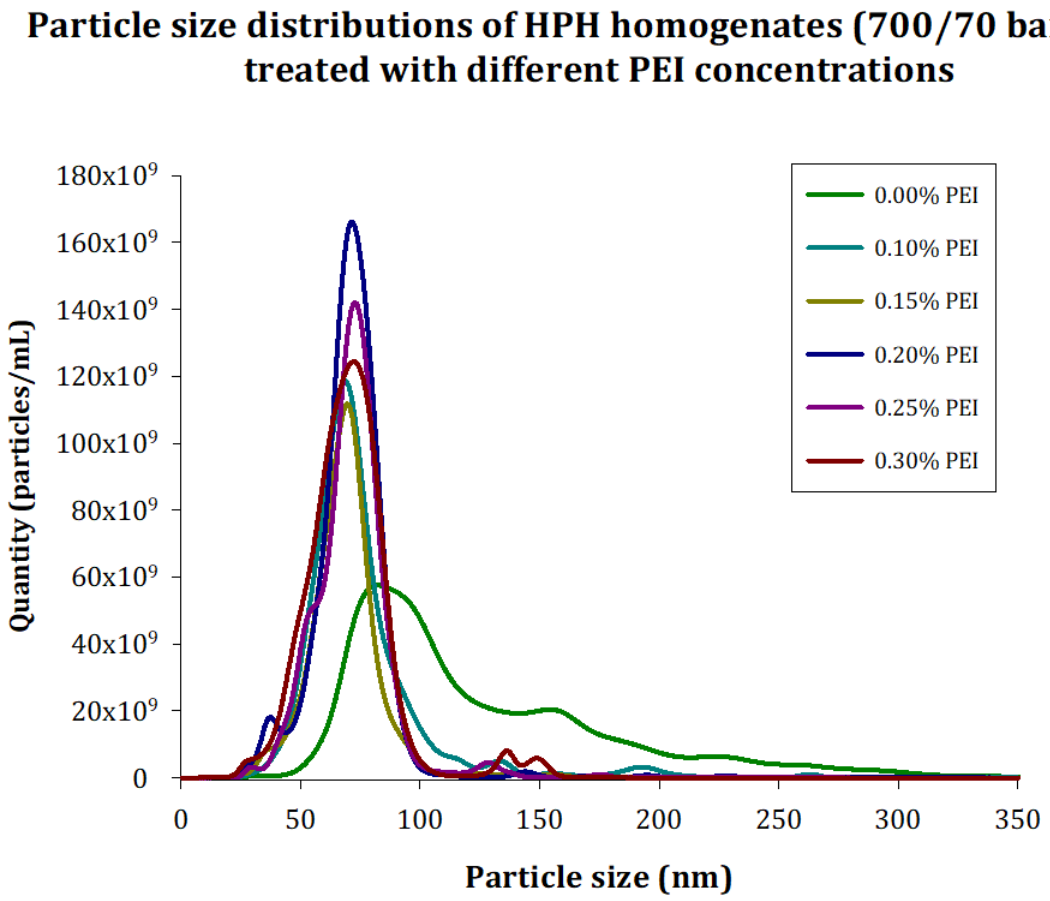

Figure 31 Particle size distributions of HPH homogenates (700/70 bar | 2P) treated with different PEI concentrations. Green, turquoise, yellow, blue, pink and red line represent homogenates of with different PEI content.

As the graph shows, a change in PEI concentration did not give the effect of particle number decrease. Even an increase of PEI to 0.20% is responsible for enlargement of particle quantity below 100 nm. Interestingly, a lack of PEI in homogenate led to a lower content of particles between 0 and 100 nm. Overlaps of big particles on smaller particles during NTA measurement might be the reason for such an artefact.

However, an increase of PEI does not give the expected effect of additional agglomeration, in such way that particles would be removed by a depth filtration step. A reduction of applied pressure during the HPH decreased turbidity and particle content of the homogenate a bit, but could not compensate the potential GFP losses, obtained from milder HPH conditions.

6.3 Centrifugation of homogenates treated with different PEI types.

Main goal of PEI type comparison experiments was to investigate the difference of agglomeration effectiveness, regarding to PEI molecule version. Two PEI molecules of different sizes (1.2 kDa and 10 kDa) were used as supportive agglomeration agents, before a centrifugation step to identify the impact on their flocculation performances. Additionally, a switch from 10 kDa PEI to 1.2 kDa PEI seems to be reasonable, due to a negative influence of 10 kDa PEI on common ultrafilters. During ultra- and diafiltration, the remaining PEI in

homogenate would be rejected and coagulated, due to hydrophobic filter material and conductivity decrease. Consequently, a layer of rejected PEI molecules would be formed above the filter membrane, which could probably lead to a reduced ultra- and diafiltration performance.

The use of 1.2 kDa PEI would be a suitable way to avoid this problem, since smaller molecules would pass the filter pores.

For this reason, homogenates were treated in the same way as described in previous chapters, but with different PEI molecule types and concentrations from 0.1% to 0.3% (w/v) in 0.05% steps. These homogenates were then used for small scale centrifugation experiments. Centrifugal force of 3280xg was applied for 30 minutes. Table 14 (see Appendix) contains all relevant data about the centrifugation efficiency. Data were used to generate graphs that illustrate the decrease of turbidity over centrifugation time. Firstly, the centrifugation experiment of coagulation agent 10 kDa PEI is shown in figure 32.

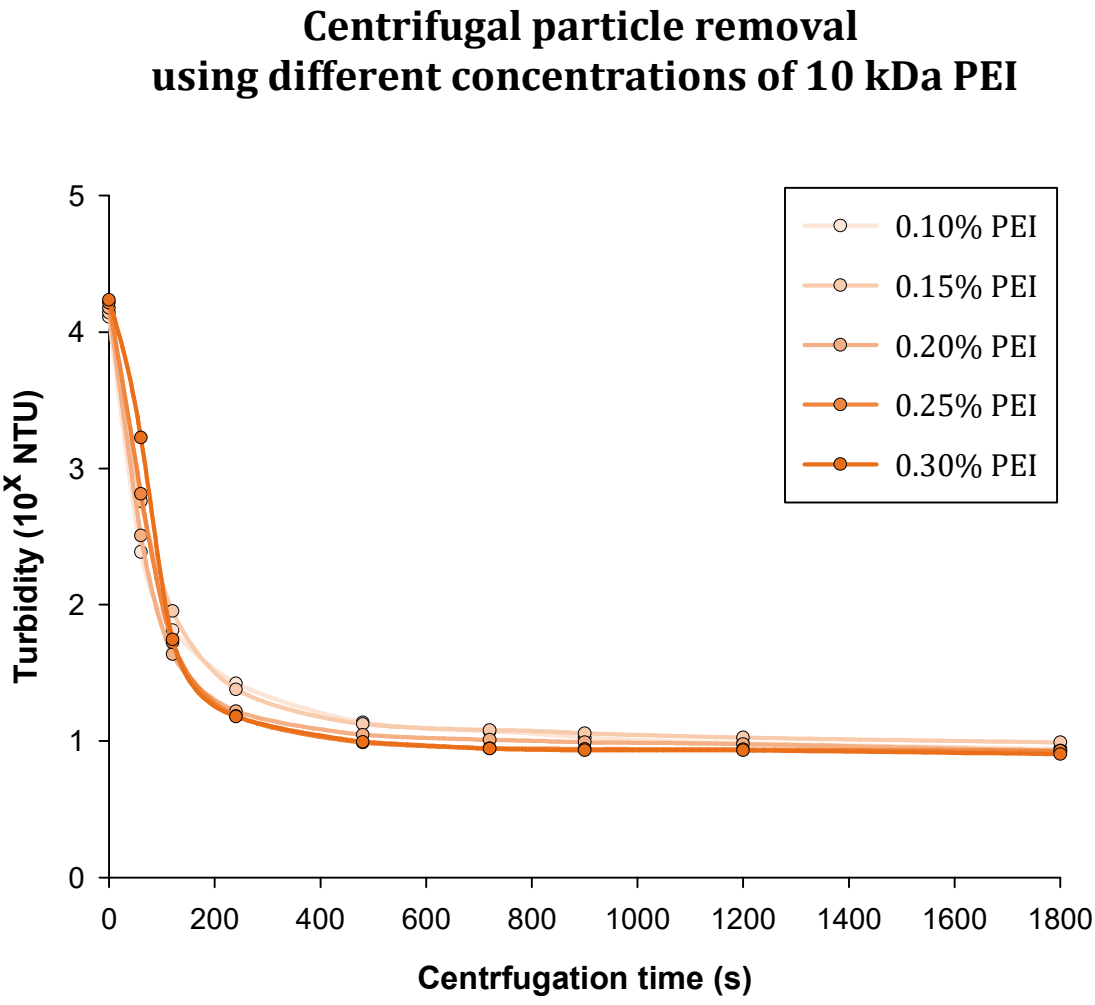

Figure 32 Comparison of different centrifugal samples of different 10 kDa PEI concentrations. The graph illustrates the remaining turbidity of supernatant (log scale) over centrifugation time.

The graph illustrates the trend of cell debris removal, using different concentrations of 10 kDa PEI over centrifugation time. All 5 curves show very similar PEI precipitation effects. At approximately 320 seconds all concentrations reach their minimum, whereas the concentrations 0.25% and 0.30% are responsible for the cleanest supernatants.

However, there are more types of PEI commercially available. 1.2 kDa PEI is approximately 10-fold smaller in size and would also be an ideal choice for upcoming ultra- and diafiltration step. In theory, the 1.2 kDa big molecules would pass through a 10 kDa UF/DF membrane.

Figure 33 shows the outcome of the same centrifugation experiment, when the almost 10-fold smaller version 1.2 kDa was used.

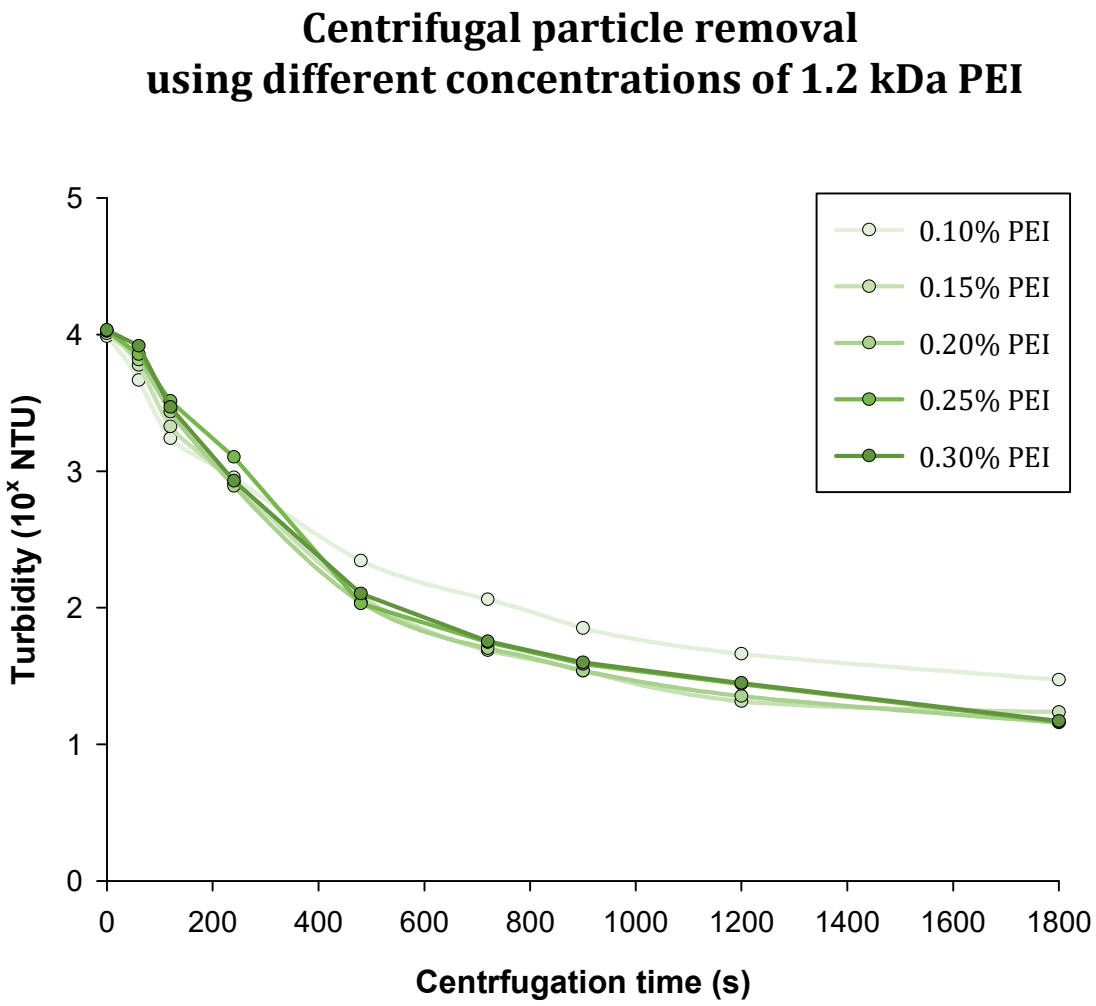

Figure 33 Comparison of different centrifugal probes of different 1.2 kDa PEI concentrations. The graph illustrates the remaining turbidity of supernatant (log scale) over centrifugation time.

It can be stated that the branched 1.2 kDa PEI performs much worse than its 10-fold bigger version. Whereas the turbidity of 10 kDa PEI treated supernatant finds its minimal plateau after 320 seconds, 1.2 kDa PEI needs approximately 4 times longer. Moreover, instead of reaching turbidities of 10 NTU, the treatment of 1.2 kDa PEI results in a final turbidity of 20 NTU. This phenomenon can be explained by a far better crosslinking effect using bigger PEI molecules.

Although 1.2 kDa PEI has about 10 times more molecules in homogenate, its interaction range is much smaller, which leads to weaker agglomeration. Hence, centrifugation requires more time to remove the majority of particles. Figure 34 depicts a schematic drawing about the difference between 1.2 kDa and 10 kDa PEI.

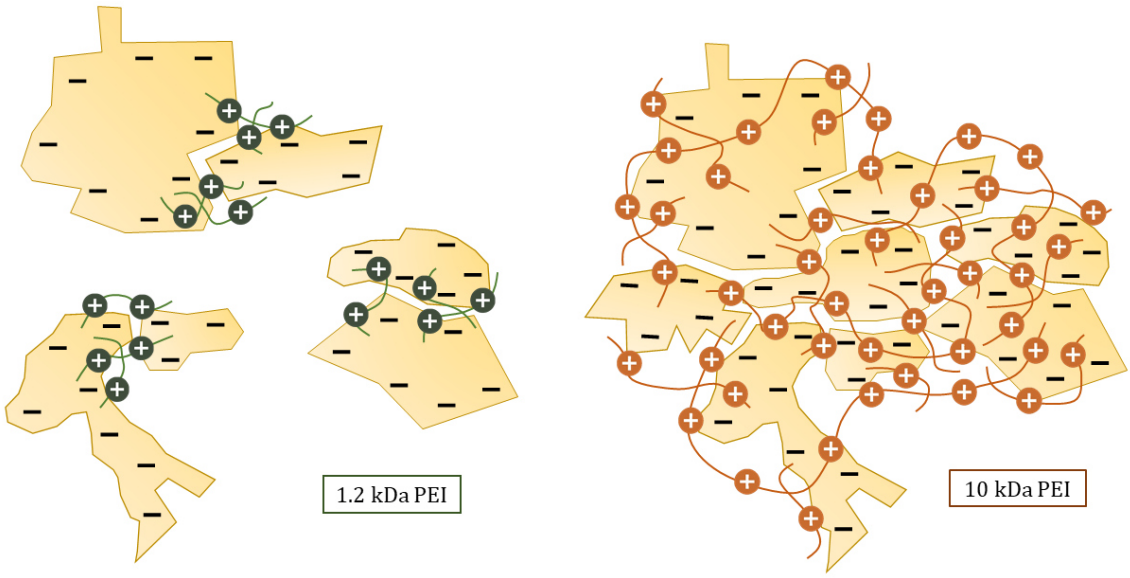

Figure 34 Comparison of agglomeration between 1.2 kDa PEI (left) and 10 kDa PEI (right).

The figure clearly depicts the interaction situation of big and small PEI molecules. The smaller one sticks to the surface of particle assembling to another particle but is not able to grab other particles for proper crosslinking. Literally, on the other side, the bigger version is able to build up a compacted system of numerous crosslinks. Consequently, much more particles flocculate, building bigger agglomerates. On the other hand, 10 kDa may affect ultra- and diafiltration membranes with small pore sizes, negatively, due to pore blocking and surface layer formation.

6.4 Depth and sterile filtration

General aim of depth and sterile filtration experiments was to find an optimal depth filter that removes cell debris particular matter from homogenate broth. There are many depth filters available, all with different properties depending on treatment goal. All in all, they can be distinguished by their pore size and filter material. Pore sizes vary from 0.1 µm to 1 µm, the material of filter ranges from inert substances (e.g. PES) to more adsorptive elements (e.g. glass fiber). However, the density and adsorption effects of depth filters are much smaller than of a sterile filter. As the name indicates, sterile filtration is primarily for the removal of microorganisms from an already manufactured solution, which is normally particle-free. Hence, the filtration capacity is often 10 times less compared to a depth filters. For this reason, some depth filters were tested to find out their grade of turbidity reduction and filter capacity, which is commonly given in L/m^2. Moreover, some solution properties, such as particle content or the

addition of PEI as precipitation aid was varied to understand potential influences on the filter systems. All filters were tested via constant flow method, holding a commonly accepted specific permeate flow (flux) of 200 LMH. To find the maximal filtration capacity, each experiment was compared with curves of different theoretical filtration models and their backpressure development formulas, visualized in figure 35.

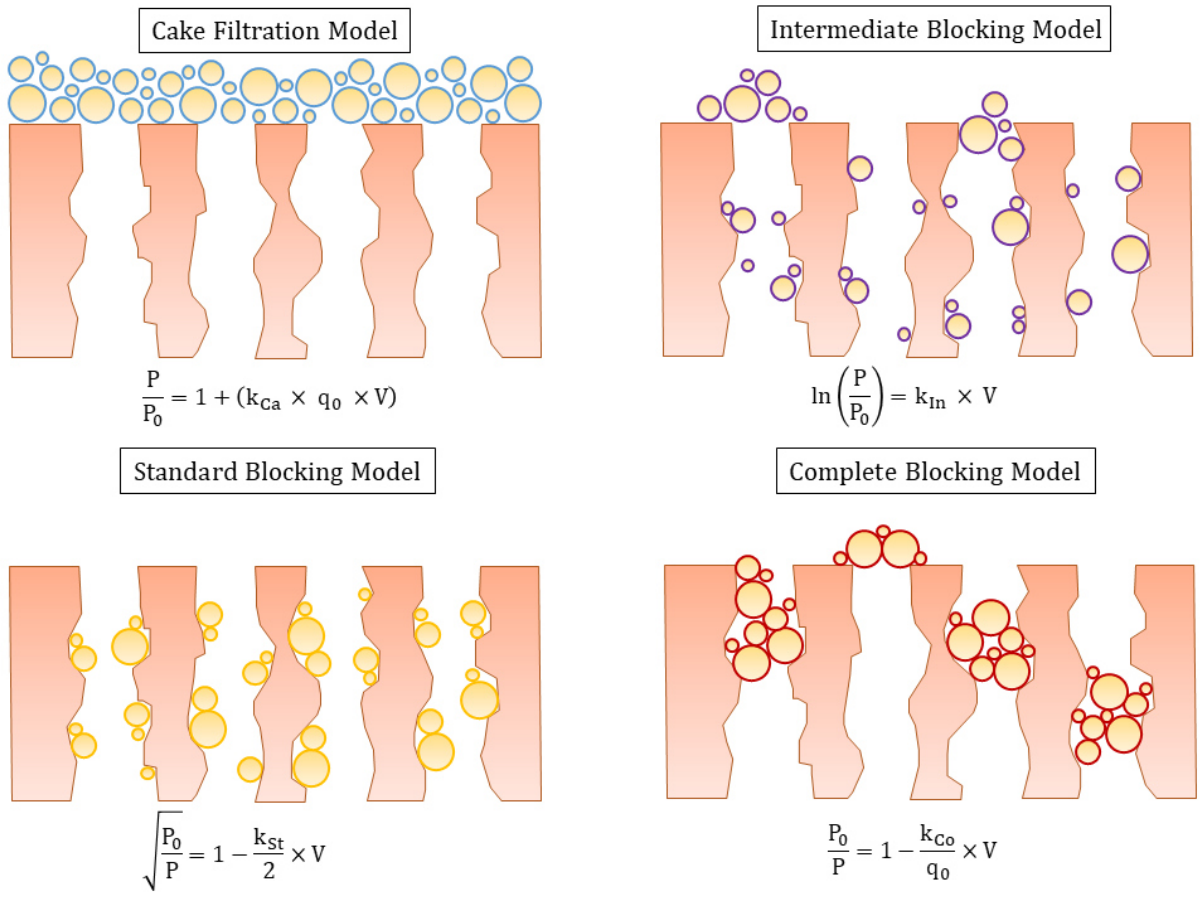

Figure 35 Illustrations of filtration models and their formulas backpressure formation.

P is the backpressure, k_{Ca}, k_{In}, k_{St}, k_{Co} are rate constants for different filtration models, V is the collected filtrate volume and q_0 is the volumetric flow rate. According to Schillinger (54) each constant flow filtration experiment can be compared to its model forms, using following formulas:

$$\Delta P = 1 + V \text{ (Cake filtration)} \quad (41)$$

$$\Delta P = e^t \text{ (Intermediate blocking)} \quad (42)$$

$$\Delta P = \left(1 - \frac{t}{2}\right)^{-2} \text{ (Standard blocking)} \quad (43)$$

$$\Delta P = (1 - t)^{-1} \text{ (Complete blocking)} \quad (44)$$

whereas ΔP is the backpressure difference and V is the normalized collected filtrate over normalized filtration time t. Received backpressure values of each model are then depicted against real filtration time to comparing them with experimental backpressure data.

After empirical determination of the suitable filtration model, equations of figure 35 are used to find the maximal filtrate volume per square meter ($v_{\max}$).

6.4.1 Homogenate properties

All homogenates were prepared by treating 25 g/L cell suspension with high pressure homogenization (700/70 bar | 2 passages). Then homogenates were made that have different properties regarding turbidity. Different centrifugation adjustments were responsible for obtaining homogenates with turbidities of 100 – 480 NTU. Moreover, some homogenates were priorly treated with PEI, whereas others lack flocculation aids. Aim is to identify possible influences of PEI on depth and sterile filtration.

6.4.2 Filtration experiments

For filtration, filters with two different filter areas were used. To guarantee a constant flux of 200 LMH for all filtration experiments, flow rates of 1.5 mL/min and 5.8 mL/min were applied, using filter areas of 4.5 cm^2 and 17.3 cm^2, respectively.

During filtration, backpressure was detected to identify suitable filtration model and determine the maximum filtration volume v_{max}. If no backpressure was detected for 15 minutes, the experiment was stopped and not evaluated. Additionally, to see if filtration works satisfactory, the filtrate was captured for subsequent turbidity measurements.

Graph 36 shows all filtration experiments where backpressure was detected and satisfying particle clarification occurred.

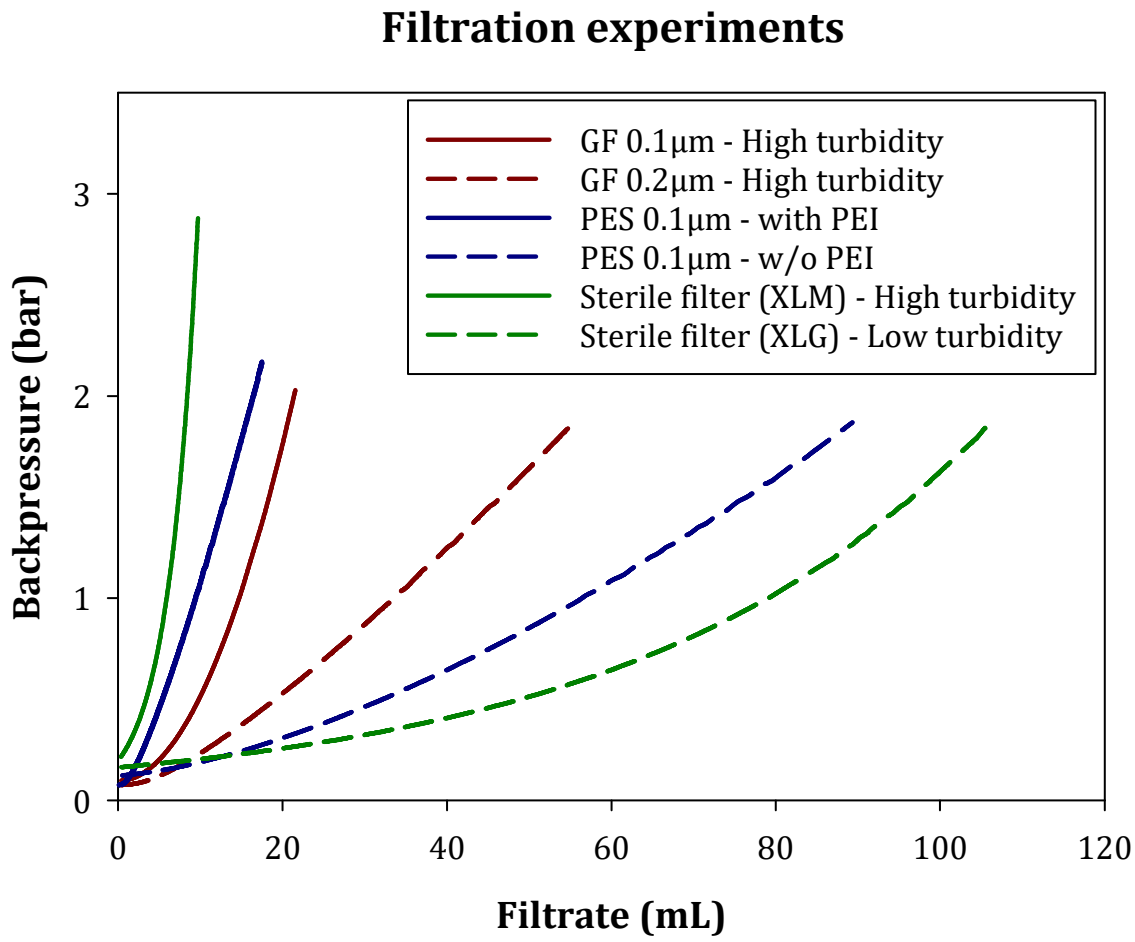

Figure 36 Filtration experiments, testing different properties of filters and homogenates. Depth filters and sterile filters are compared, and the influence of homogenate's properties is depicted.

As the graph shows, there is an influence of filter type as well as properties of homogenate on the rapidness of pore blocking. Red lines show glass fiber depth filters (GF) filtering identical homogenates. It can be seen when using a filter with different pore diameter, it would lead to small differences regarding to backpressure formation. At a backpressure of 2 bar, 3 times more filtrate passed through when using 0.2 µm instead of 0.1 µm pores. Blue lines depict the situation of homogenate treated with PEI. Residuals of 10 kDa PEI led to a much faster pore blocking and backpressure increase than filtering a homogenate without PEI. At last, the difference of homogenate turbidites are illustrated with green lines. A turbidity of 480 NTU led to a rapid backpressure increase, whereas a filtration of low turbid particle solution (107 NTU) produced much more filtrate. Moreover, it can be stated that the initial backpressure of sterile filters is slightly higher than of depth filters. Lower number of pores and more adsorptive effects of filter material are the main reasons.

However, backpressure formation does not give any information about the v_{max} or rest particle content of filtrate. Hence, next two chapters describe the determination of v_{max} for depth filter (GF 0.1 µm) and sterile filter (XLM 0.1 µm)

6.4.2.1 Sartoguard GF, 0.2 µm + 0.1 µm

The *E. coli* suspension was treated with 2 passages HPH at 700/70 bar and was centrifuged to a particle content of 480 NTU.

To maintain a stable flux of 200 LMH during filtration with the 4.5 cm^2 filter, the volumetric flow rate was set to 1.5 mL/min.

After 18 mL of filtrate collection, first backpressure was detected by the sensor and increased until 3 bar at 26 mL filtrate. The nephelometer displayed a turbidity of 199 NTU, 281 NTU less than in feed. Thus, the filtration effect is not very satisfying, using a depth filter device containing glass fiber as membrane material.

However, the pressure data was used to generate in the programme “TableCurve 2D v5.01” a smooth filtration graph. Figure 37 shows the filtration function and its theoretical filtration model versions. For the numerical analysis of models, the equations 41 – 44 were used.

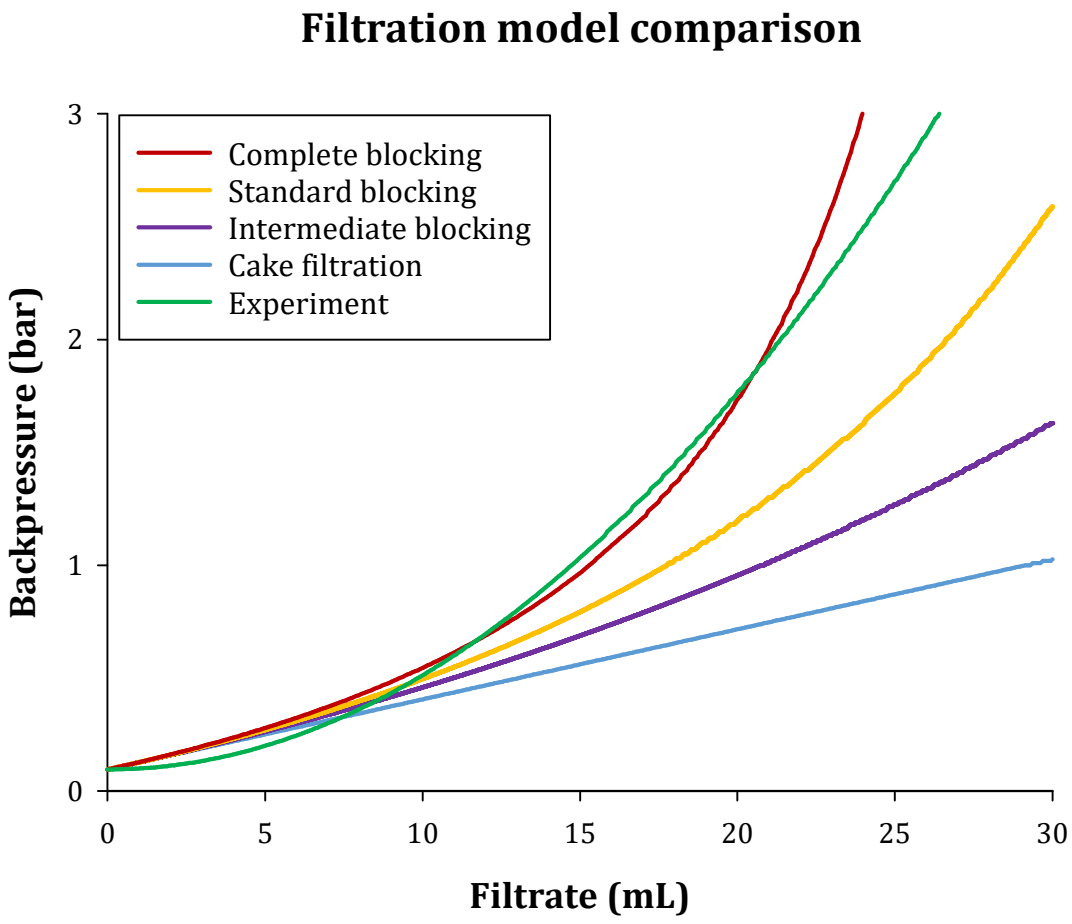

Figure 37 Filtration backkpressure as a function of collected filtrate volume, using the filter system Sartoguard GF 0.1 µm (green). The experimental data are compared with the filtration models cake filtration (blue), intermediate blocking (purple), standard blocking (yellow) and complete blocking (red).

As the graph shows, the experiment has similarities with the complete blocking model, even though it looks like a shifted version of standard blocking model. So, for determination of the

v_{max}, the theory of both were compared. For this reason, the maximal specific area is determined with equation 45 and 46, which are the formulas for complete blocking model and standard blocking model, respectively:

$$\frac{P_0}{P} = 1 - \frac{k_{Co}}{q_0} \times v \tag{45}$$

$$\sqrt{\frac{P_0}{P}} = 1 - \frac{k_{St}}{2} \times v \tag{46}$$

Figure 38 illustrates the linearization fit of complete and standard blocking model.

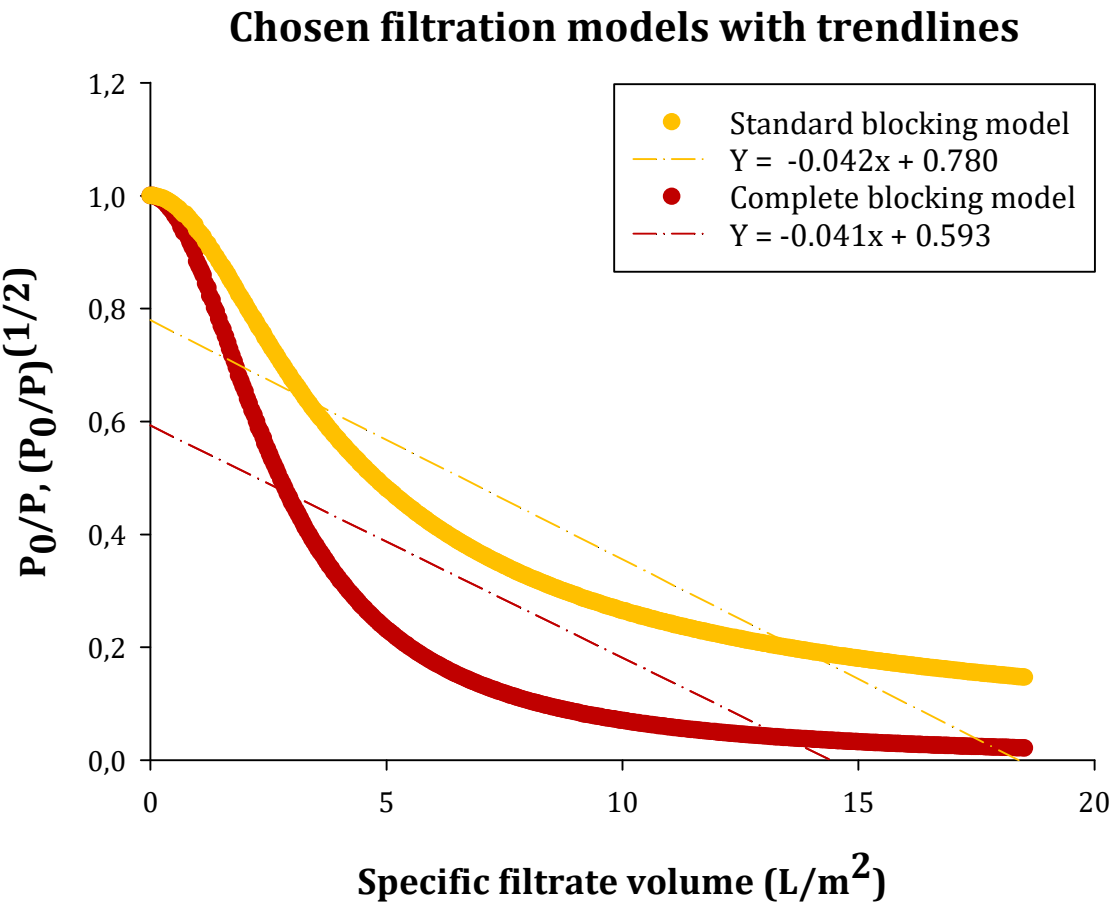

Figure 38 Linearization of complete blocking model (red) and standard blocking model (yellow), performing filtration with Sartoguard GF 0.1 µm filter system. Legend shows the received linear equations.

Obtained trendline seems to be hardly optimal for the determination of v_{max}. However, due to better fit of standard blocking model, equation 46 was used for v_{max} calculation. In theory, when setting backpressure (P) to infinitive ($v \rightarrow v_{max}$) the left side of equation is transformed to zero:

$$0 = 1 - \frac{k_{St}}{2} \times v_{max} \quad (47)$$

In the special case of received linear equation of standard blocking model (legend in figure 38), the terms 1 and $\frac{k_{St}}{2}$ are transformed into 0.780 and 0.042, respectively:

$$0 = 0.780 - 0.042 \times v_{max} \quad (48)$$

Solving equation (48) for $v_{\max}$ results in 18.6 L/m^2.

The accurate particle removal of 281 NTU apparently leads to a relatively low $v_{\max}$. However, residual particles in filtrate (199 NTU) excludes the application of the filter system.

6.4.2.2 Sartopore 2 XLM, 0.2 µm + 0.1 µm

Next experiment is the filtration of high turbid homogenate (480 NTU) with the sterile filter XLM. The homogenised (700/70 bar | 2 passages) homogenate was centrifuged to a final turbidity of 480 NTU. Normally, sterile filters remove microbes and mycoplasma from solution or polish liquid product as a final step. Due to the small pore size and high adsorptive material, particle removal should be much more effective than with depth filters. On the other hand, the smaller membrane area should decrease the particle removal capacity, drastically.

With a filter of 17.3 cm^2 membrane area, a flow rate was hold to 5.8 mL/min, maintaining a stable flux of 200 LMH.

As expected, the turbidity of homogenate was reduced from 480 to 52,9 NTU, which is by far the best result, regarding to other cell debris removal experiments. So, only 11% of particles travels through the membrane. The filtration experiment was stopped after 10 mL of filtrate collection, due to reaching a critical backpressure of 3 bar.

Figure 39 depicts comparison of the filtration experiment with theoretical pore blocking models.

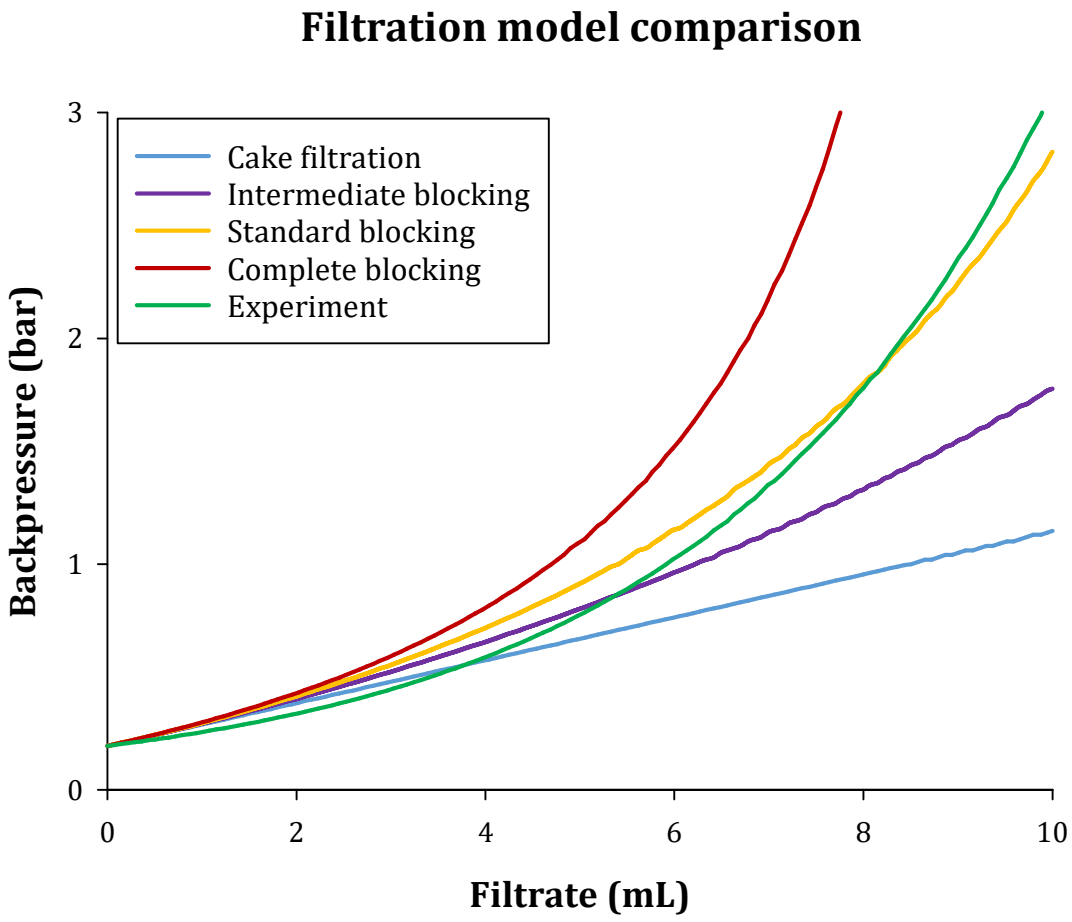

Figure 39 Filtration backkpressure as a function of collected filtrate volume, using the filter system Sartopore XLM, 0.2 + 0.1 µm (green). The experimental data are compared with the filtration models cake filtration (blue), intermediate blocking (purple), standard blocking (yellow) and complete blocking (red).

As the figure shows, first 4 mL of filtrate, the filtration experiment follows a cake filtration principle. However, rest of experiment shows high similarities with standard blocking model. Again, equation 46 was for generating a linear equation, which was then used for the determination of v_{max} (see chapter 6.4.2.1)

Figure 40 illustrates the backpressure function versus specific filtrate volume.

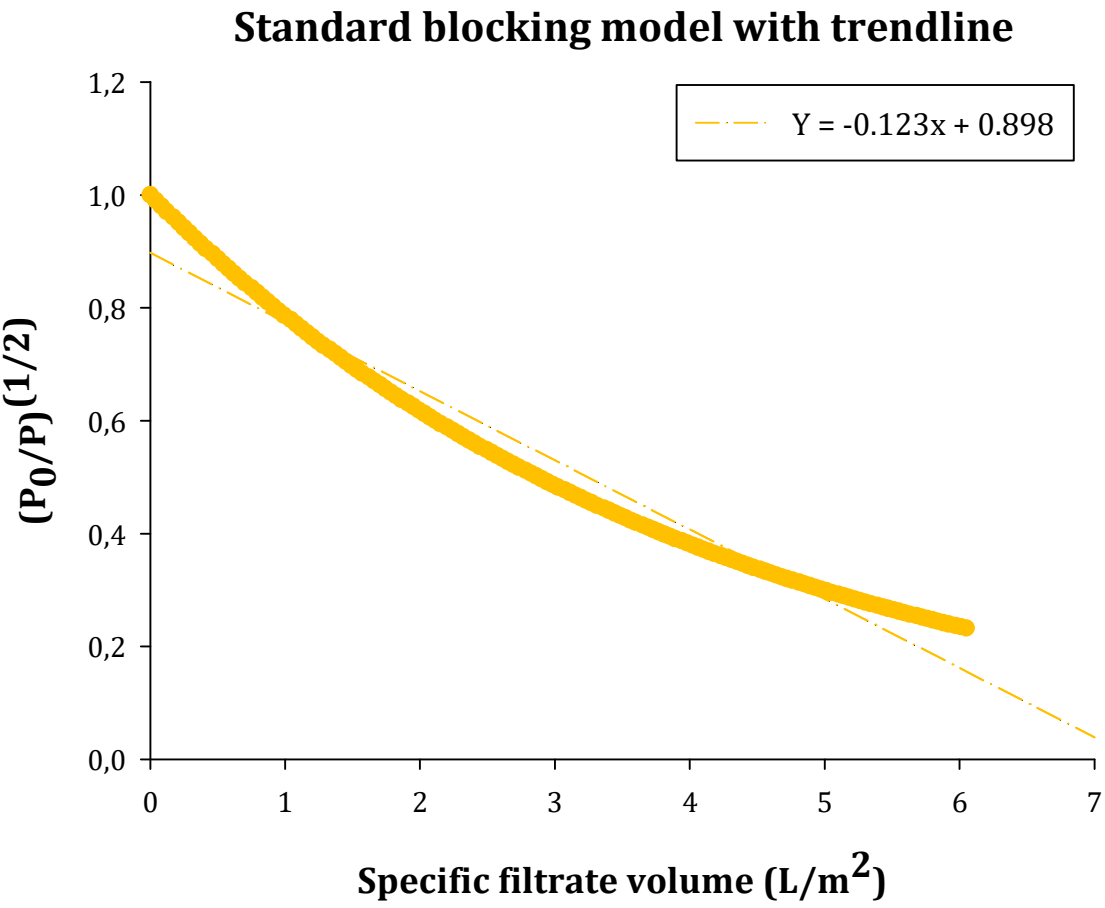

Figure 40 Linearization of standard blocking model, analysing data of filtration with Sartopore XLM, 0.2 + 0.1 µm filter system. Legend shows the received linear equation.

Obtained trendline seems to be optimal for the determination of v_{max}. A high coefficient of determination of 0.97 speaks for a secured model assumption. Following the calculation according to previous chapter, a v_{max} of $7.3\ L/m^2$ was received. In contrast to depth filters, the maximal filtrate volume is much lower. A decreased number of pores and smaller pore area for adsorptive particle capture are the reasons for such filtrate volume reduction. Although a relatively big area would be required, this filter would be a good choice, if particle reduction is the primary goal.

6.4.3 Summary of depth and sterile filtration experiments

A table was prepared that shows all filtration experiments that were made and analysed. Experiments of each filter system is also categorized into different types of used homogenates. Table 11 summarize all investigated filtration experiments.

Table 11 Summary of filtration experiments. The homogenates are categorized into high turbidity, low turbidity and low turbidity with 10 kDa PEI content.

Filter name	Pore diameter (µm)	High turbidity w/o PEI		Low turbidity w/o PEI		Low turbidity with PEI	
		Particle rejection (%)	v_{max} (L/m^2)	Particle rejection (%)	v_{max} (L/m^2)	Particle rejection (%)	v_{max} (L/m^2)
Sartopore GF+	1.2	33	-				
Sartopore GF+	0.65			3	-		
Sartopure PP2	0.65	37	-				
Sartoguard 2 PP3	0.45			2	-		
Sartoguard GF	0.8 + 0.2	41	28.2	4	-		
Sartoguard GF	0.2 + 0.1	59	18.6	7	-	4	-
Sartoguard PES	0.8 + 0.1			7	-	3	-
Sartopore 2 XLG	0.8 + 0.2	29	-				
Sartopore 2 XLM	0.2 + 0.1	89	7.3			65	18

As the table shows, the used prefilters (yellow background) are supportive in clarifying crude fraction of cell debris particles. The treatment of homogenate with high particle content led to approximately 35% rejection. The use of depth filters was more successful regarding particle removal and $v_{\max}$ determination, even though the maximum filtrate volume would be not suitable for an economic bioprocess treatment step. According to experiments where homogenates of low particle content were used, neither prefilters nor depth filters led to adequate clarifications. Also, the presence of 10 kDa PEI did not lead to better result. Otherwise the sterile filter Sartopore 2 XLM clarifies the majority of particles.

All in all, it seems that high pressure homogenisation of *E. coli* cell suspensions leads to such small cell debris diameters that no commercially available depth filter is able to remove particles in an accurate way. Sterile filters may give an adequate option, even though the low maximum filtrate volume would make each filtration process uneconomical.

Therefore, another way of filtration procedure has to be identified. Ultrafilters may give the opportunity to exclude cell debris particles, while letting GFP pass through the membrane pores.

6.5 TFF cell debris particle reduction

Aim of this investigation was to find a filter system that remove all particles from homogenate solutions but keep as much GFP protein as possible in product stream. Due to the failure of commercially available dead-end filters, it was decided to try GE hollow fiber filters of different pore diameters. Main goal was to find the filter with the biggest pore size that is able to remove all particles from solution. Also, the pores should be big enough to let the 26.9 kDa GFP pass through the filter. Two homogenates of different HPH treatments (700/70 bar | 1 passage & 700/70 bar | 2 passages) were treated with PEI and heated (50 °C) for 2 hours. After reducing the particle content to approximately 32 NTU via centrifugation (4780xg for 40 min), the homogenates were filtered with hollow fiber membranes of 500 kDa MWCO, 750 kDa MWCO and 0.1 mikron pore sizes, applying 1 TMP and a tangential flow of 250 mL/min.

Homogenate 1 had an initial turbidity of 32.5 NTU. A filtration treatment with 500 kDa MWCO, 750 kDa MWCO and 0.1 mikron resulted in solution turbidities of 6.79, 6.84 and 23.1 NTU, respectively.

Homogenate 2 was filtered the same way and reveals final turbidities of 7.70, 6.81 and 25.1 NTU.

To find out if the product solutions of low turbidities were particle-free, they were analysed via NTA system. Figure 41 shows an NTA particle intensity analysis of unfiltered and two filtered homogenates. Each filtered homogenate was treated with two different pore sizes (0.1 µm and 750 kDa MWCO)

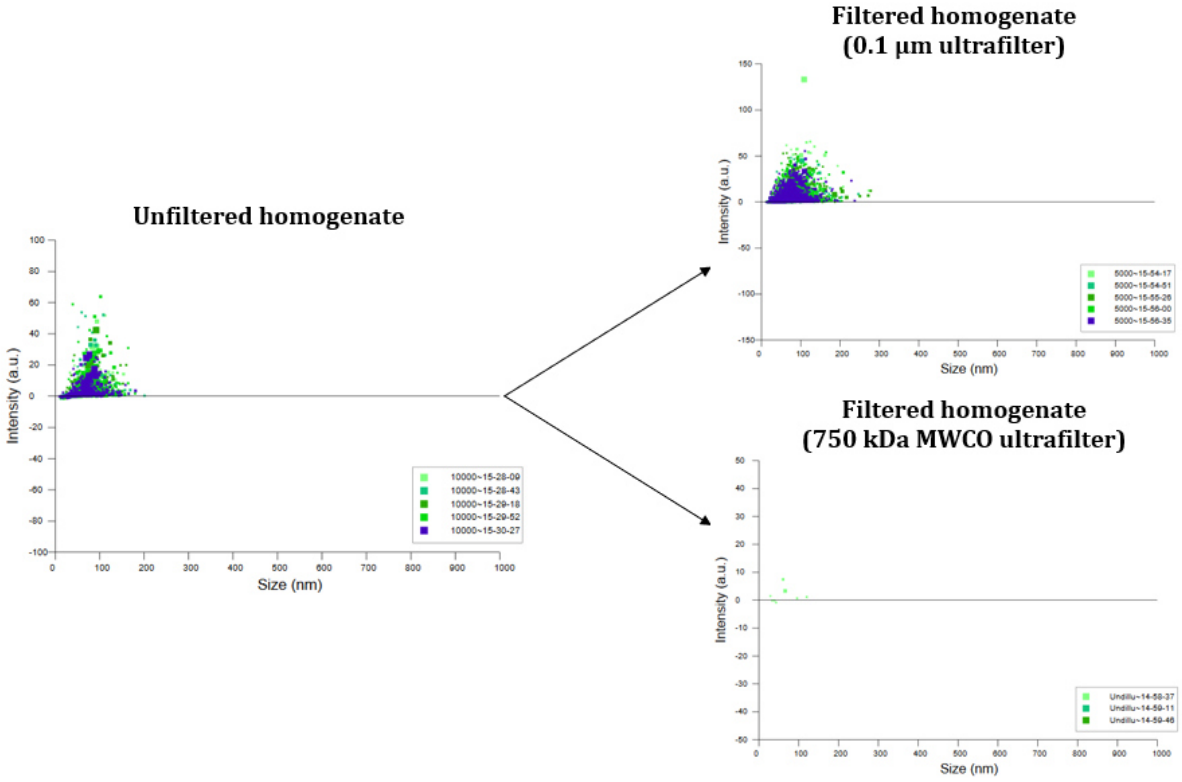

Figure 41 Particle intensity of unfiltered and filtered (0.1 µm & 750 kDa MWCO) homogenates, determined by NTA analysis. The x-axis and y-axis describe the particle diameter and signal intensity, respectively.

The analysis showed no particles in solution except the product solutions filtered with 0.1 mikron hollow fiber. Additionally, turbidity of pure GFP solution was measured to check, if the scattering characteristics are responsible for the small count. As expected, pure GFP solution showed a measurement of 6.51 NTU. So, it can be assumed that GFP solutions under a turbidity of 8 NTU, are free from cell debris particles.

According to received turbidity values, it can be stated that a variation in number of HPH passages does not have any influence on effectiveness of hollow fiber filtration. Hence, a two

passage HPH treatment with a filtration of 750 kDa MWCO was used for upcoming experiments.

6.6 GFP shear stress stability

Before a filtration with hollow fiber filter can be set up, GFP must be tested regarding to its stability. During filtration with hollow fiber membranes, molecules are exposed to a certain shear stress, depending on flow rate and hollow fiber diameter.

GFP itself represents a relatively stable protein. So, the stability was tested with a shear rate of 8000 s^{-1} over a time period of 70 minutes to investigate if GFP would keep biological active, during TFF filtration. For this a pure solution of GFP in PBS buffer was used and diluted to a concentration of 7.5 g/L.

Figure 42 depicts the time dependent GFP concentration of dummy filtration, guiding GFP through fiber lumen the filter system in recirculation mode.

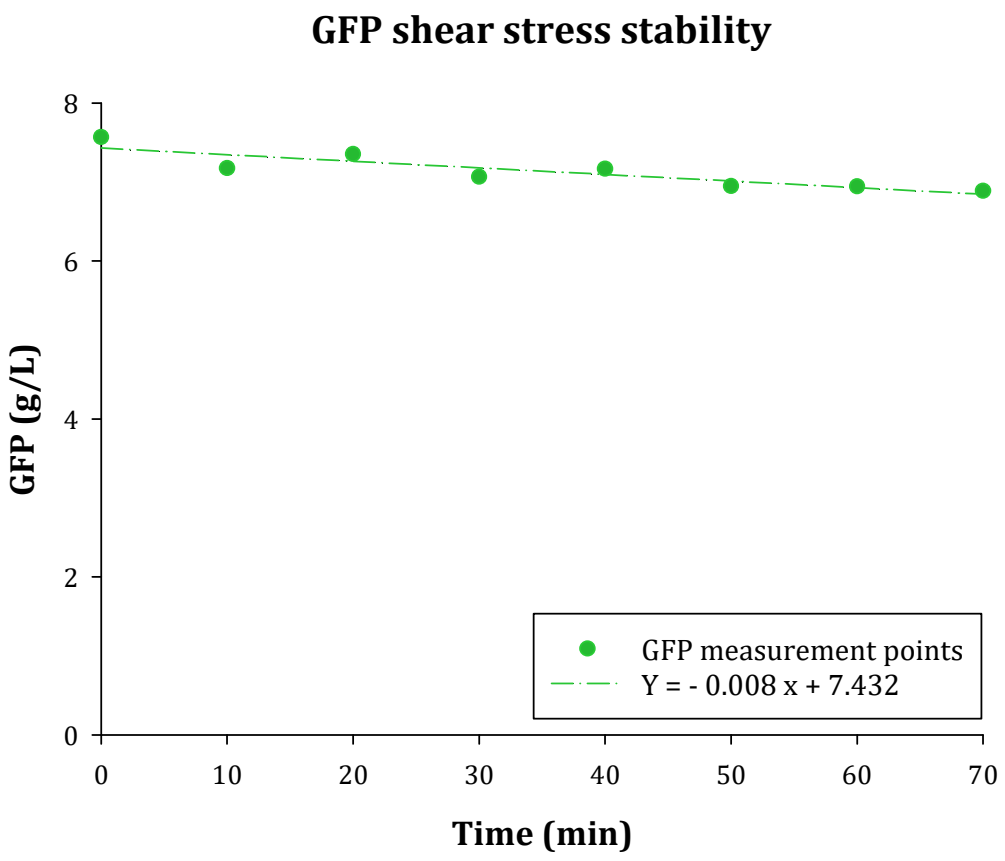

Figure 42 GFP concentration as a function of time, using a GE hollow fiber filter (750 kDa) for 70 minutes with a shear rate of 8000 s^{-1}.

As the graph shows, it came to a low decrease during shear stress. Anyway, for such a high stress level, the reduction of concentration is relatively low. For this reason, GFP seems to hold its stable form for upcoming hollow fiber filtration experiments.

6.7 Flux behaviours of TFF cell debris particle removal

Goal of this experiment series was to find out the optimal filtration parameters for filtration time and GFP permeation through the filter. Hence, for filtration with GE hollow fiber filter (750 kDa), different TMP (0.5, 1.0, 2.0 bar) are combined with different flow rates (400, 500, 600 mL/min) to see the relationship between set up and outcome.

Commonly, the used homogenates were homogenised (700/70 bar | 2 passages), 10 kDa PEI and heat treated for 2 hours and centrifuged (4780xg | 45 min) to reach a final turbidity of 30 NTU. For each filtration experiment, the initial retentate volume was 1000 mL. After concentrating the retentate to 50 mL (C_F = 20), the filtration was stopped and the GFP concentration of retentate and permeate was determined. In principle, the retentate could have been concentrated to higher extent, thereby avoiding GFP losses. The analysis of this problem waits for further investigational experiments.

At first, different TMPs were compared, receiving information about the influence of TMP on flux behaviour. Figure 43 contains 2 graphs that compare different TMPs and the effect of CF rate on filtration times.

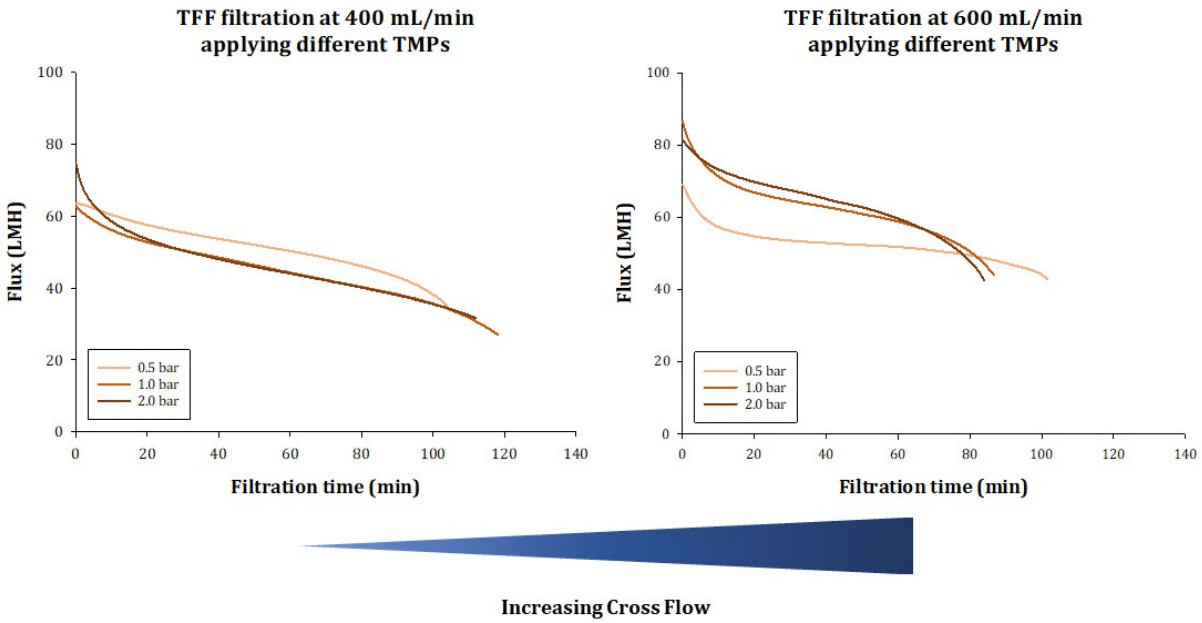

Figure 43 Comparison of filtration flux behaviours, applying different TMPs. Graphs show different cross flow operation modes.

As the figure shows, an increase of TMP does not improve the permeate flux and consequently reduces filtration time. Left graph shows clearly that at low tangential flows, a high TMP would form a compact layer of cell debris particles. As a consequence, liquid or other compounds would be rejected more effectively. Right graph confirms this hypothesis, since higher cross flow rates flush away the formed particle layer before it can act as a second membrane layer. At high tangential flow (600 mL/min), an improvement of TMP can reduce the filtration time

from 100 to 80 minutes. However, the question is if a filtration time increase is able to compensate a possible product loss, due to harder permeation through compacted particles.

For additional interpretation, figure 44 shows 2 graphs that represent comparison between cross flow operation modes.

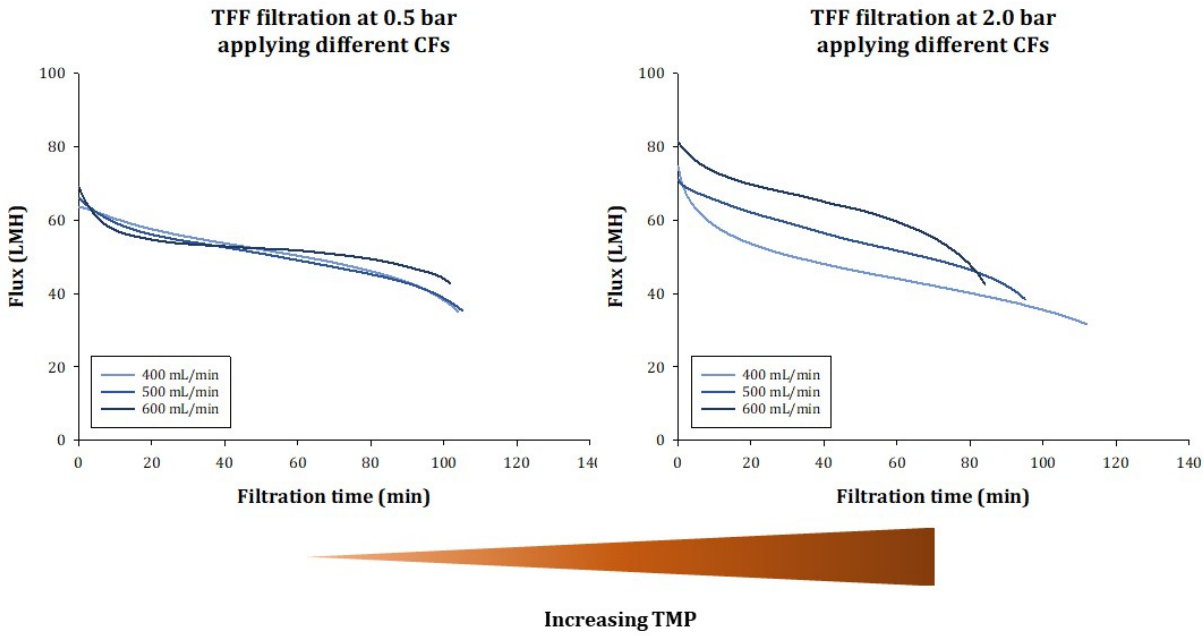

Figure 44 Comparison of filtration flux behaviours, applying different CFs. Graphs show different TMPs.

As the plots show, the flux behaviour of hollow fiber TFF is highly affected by TMP. Whereas a low TMP of 0.5 bar reveals similar filtration trends, at higher pressure levels (>1.0 bar) an increase of CF rate can reduce filtration time drastically.

For a better overview figure 45 illustrates the average fluxes in dependence of TMP and cross flows.

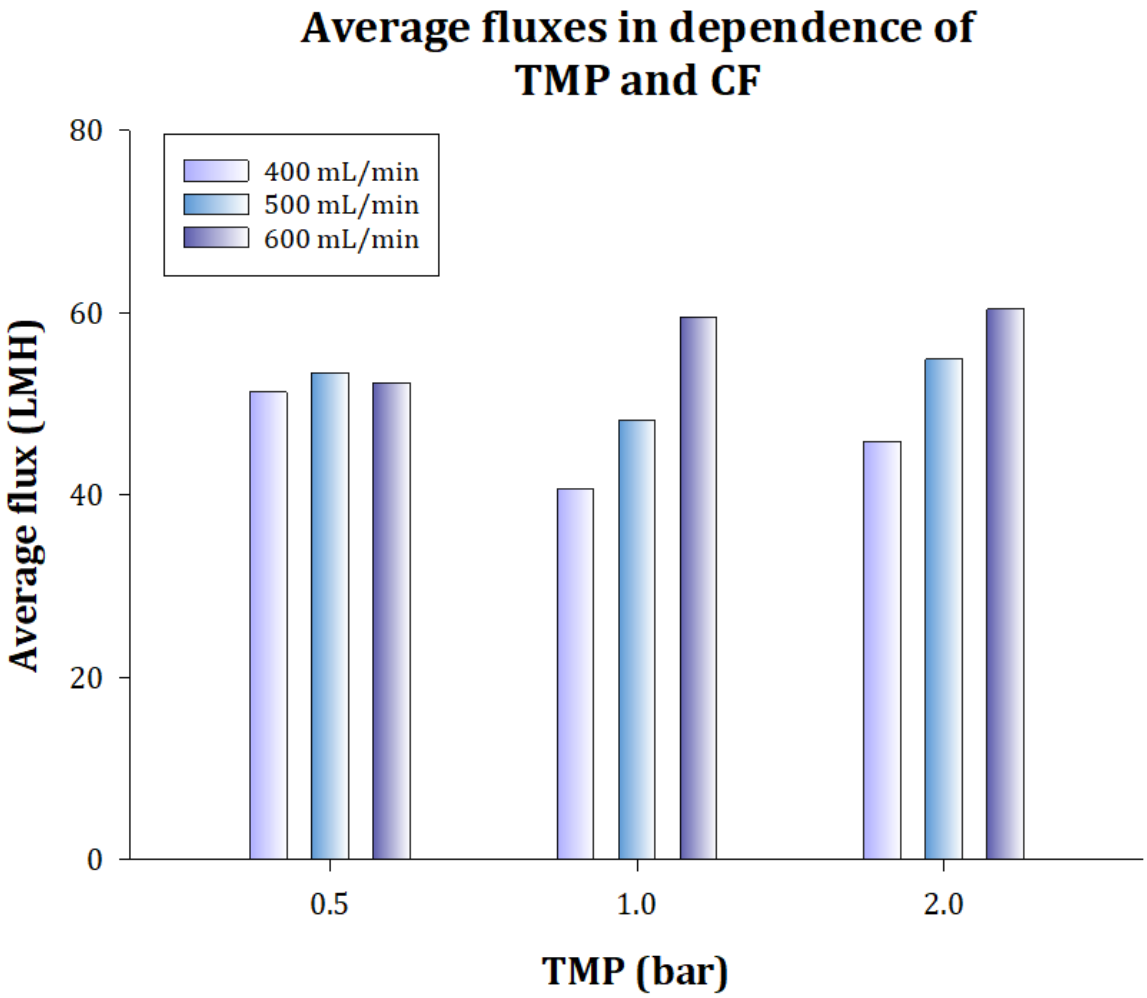

Figure 45 Average permeate fluxes of TFF in dependence of different TMP and CF. TMPs of 0.5, 1.0 and 2.0 are represented as light blue, blue and aquamarine, respectively.

The graph shows clearly that at a low TMP of 0.5 bar, the cross flow does not have an extensive effect on fluxes. At higher pressures, an increase of tangential flow leads to higher flux rates. Table 12 reveals a numerical summary of average fluxes.

Table 12 Average fluxes of different CF operation modes. Received flux values are given in LMH.

	TMP (bar)		
Flow rate	0.5	1.0	2.0
400 mL/min	51.3	40.6	45.9
500 mL/min	53.4	48.1	54.9
600 mL/min	52.3	59.9	60.4

Nevertheless, prior goal is not to safe filtration time. Most critical value is the satisfying transfer of GFP into the permeate. Hence, it has to be investigated, which parameters can improve the product permeation through hollow fiber membrane.

For this reason, during each filtration run, GFP concentration of retentate and permeate was measured, after 950 mL of filtration. This information is essential to gain the percentage of passed protein through membrane.

For proper synopsis, figure 46 depicts a simple bar plot that represents the ratios of rejected protein.

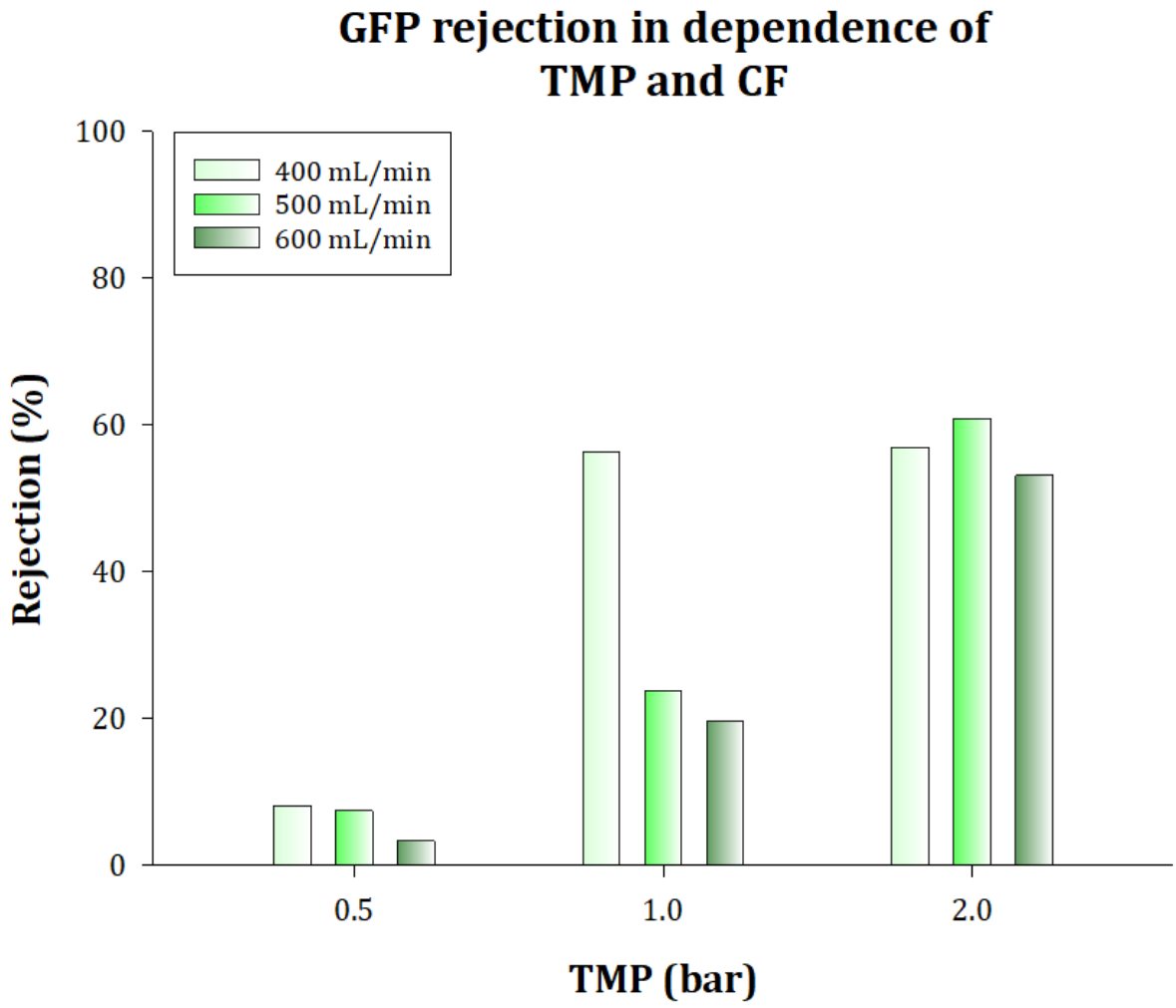

Figure 46 GFP rejection of TFF in dependence of different CF and TMP. TMPs of 0.5, 1.0 and 2.0 are represented as light green, green and dark green, respectively.

As the graph shows, an application of 0.5 bar TMP led to lowest protein rejections. In precise, a TMP of 0.5 bar and a CF of 600 mL/min reveals with only 3.3% the lowest protein rejection, which make it to the optimal filtration operation mode. An applied TMP of 2 result in all 3 CF cases to approximately 55% protein rejection. Interestingly at 1 bar TMP, the CF has to be at least 500 mL/min to obtain acceptable protein permeation.

Table 13 summarises all received GFP rejections in numerical form.

Table 13 GFP rejection comparison, using different filtration parameters. Received rejection values are given in %.

	TMP (bar)		
Flow rate	0.5	1.0	2.0
400 mL/min	8.1	56.4	57.0
500 mL/min	7.5	23.9	60.9
600 mL/min	3.3	19.6	53.1

6.8 Influence of buffer on TFF filtration

Another question is if the homogenate matrix has influence on efficacy of protein permeation through membrane. Therefore, another two TFFs are performed with homogenates, containing higher Tris concentrations (50 mM, 80 mM). To observe a possible effect of buffer increase, an inappropriate filtration mode was chosen (400 mL/min | 2bar).

Figure 47 illustrates the effect of buffer variation during TFF.

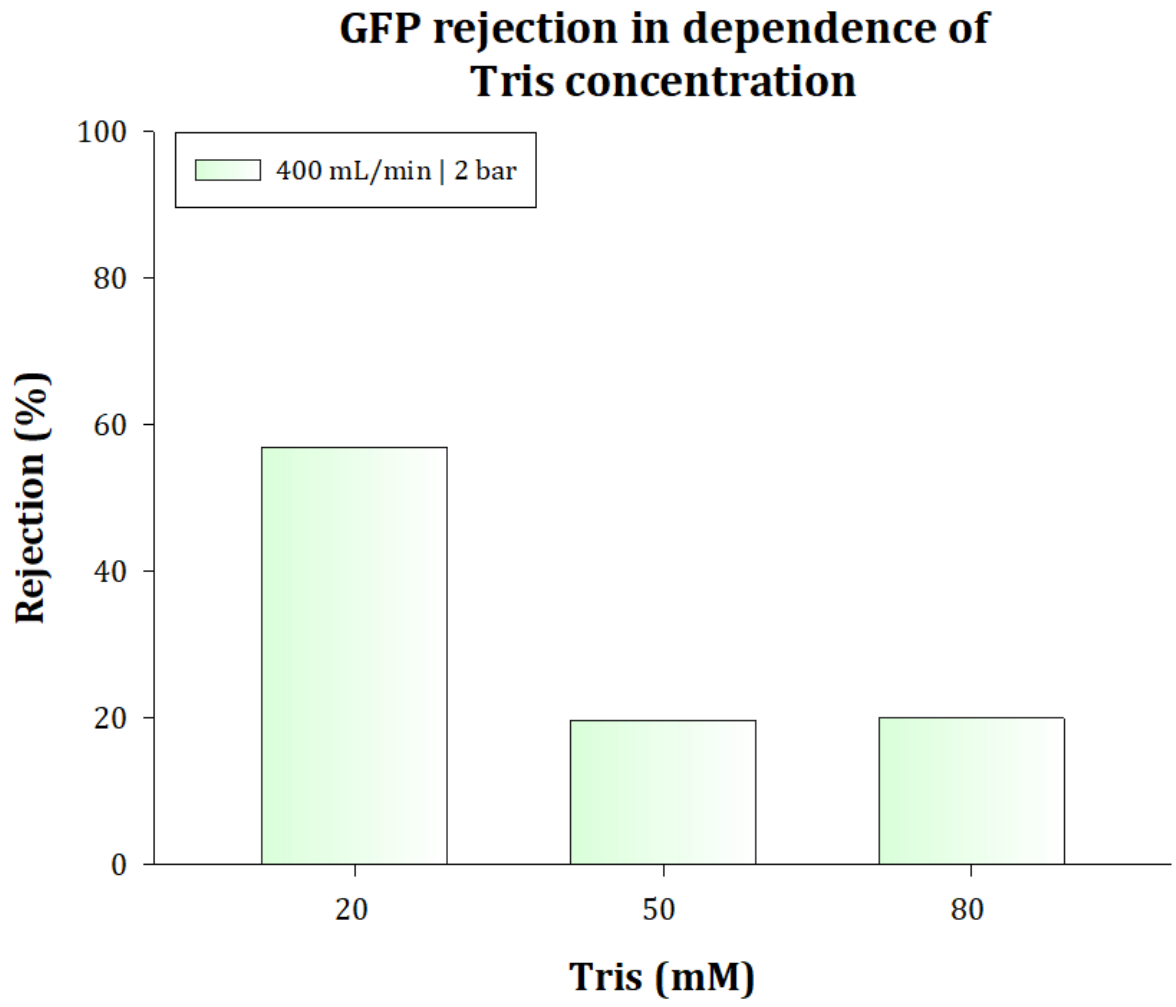

Figure 47 GFP rejection ratios of TFF (400 mL | 2 bar), depending on Tris concentration.

The plot clearly depicts that a concentration higher than 50 mM in homogenate leads to best GFP permeation results. Apparently, a further concentration increase did not have any effect on permeation. A higher Tris concentration seems to shield negatively charged GFP molecule from negatively charged cell debris particle layer and apolar PES membrane. Due to charge shield, GFP molecules probably travel through the pores more effectively. A concentration of 50 mM Tris buffer seems to be the most appropriate choice for permeating GFP through the hollow fiber pores.

6.9 Comparison of flux behaviours under different ultrafiltration conditions

Aim of this study is to describe flux behaviours during ultrafiltration of GFP, using different types of filters. Additionally, the influence of CF, GFP- and PEI concentration has to be investigated. Finally, ideal parameters, such as TMP and CF for an adequate concentration has to be determined, saving filter area and filtration time. Following chapters reveal information about 3 different types of filters. Received flux data are shown in the appendix. Following chapters only contain the most important data for an appropriate comparison. The homogenates for all ultrafiltration experiments were prepared by high pressure homogenization (700/70 bar | 2 passage), heat precipitation (50°C for 2 hours), centrifugation (4780xg | 45 min) and TFF operation (600 mL/min | 0.5 bar). The only variation is the content and type of PEI, which is described in following chapters

6.9.1 Sartocon® Slice PESU Cassette

This filter in cassette form is made of PESU, the most resistant filter medium in biotechnological application that is commercially available. Hence, it is durable and perfect for applying several CIP procedures. On the other hand, the hydrophobic nature rejects salt buffers in a certain extent, which probably leads to a reduced flux during ultrafiltration. Furthermore, next chapters describe the influence of PEI on flux behaviours.

6.9.1.1 10 kDa PEI

PEI is, as already explained, a high molecular molecule that could disturb filtration by blocking pores of filter membrane. Hence, it has to be investigated, if 10 kDa PEI leads to a significant flux reduction during ultrafiltration. Therefore, fluxes of 5 homogenates, each with different GFP concentrations (2, 4, 8, 10 and 14 g/L) are determined. Moreover, flux trends of two different GFP concentration (4 g/L and 14 g/L) are compared in next figures. Additionally, the difference of 3 different CF rates are shown (111 mL/min, 222 mL/min and 333 mL/min).

Figure 48 consists of 2 graphs that illustrate flux behaviours of 4 g/L and 14 g/L GFP homogenates.

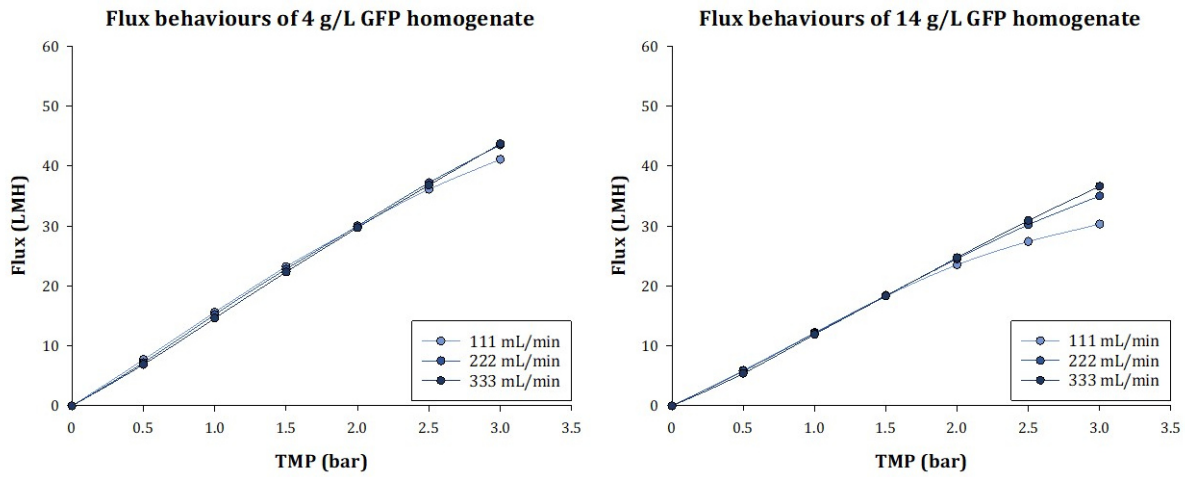

Figure 48 Two graphs of flux behaviours of 10 kDa PEI treated homogenates with two different GFP concentrations (4 and 14 g/L), using 10 kDa PESU filter cartridge. Light blue, blue and dark blue lines depict CF rates of 111 mL/min, 222 mL/min and 333 mL/min, respectively.

As the graph shows, the flux changes in most cases linearly as a function of TMP. According to the 4 g/L homogenate, only at lowest CF, a TMP of 3 bar is responsible for a slight discrepancy. Regarding to 14 g/L GFP homogenate, an approach to a plateau at 111 mL/min and 222 mL/min is visible. Most of the time, especially at 333 mL/min, flux and TMP follow a linear relationship. Additionally, it has to be mentioned that a rise in protein concentration seems to have no significant effect on flux reduction, except for the lowest concentration. It has to be mentioned that for each ultrafiltration measurement, the permeate was recycled back to reservoir to guarantee concentration maintenance.

For proper comparison, figure 49 depicts flux trends of different GFP concentrations at middle CF (222 mL/min).

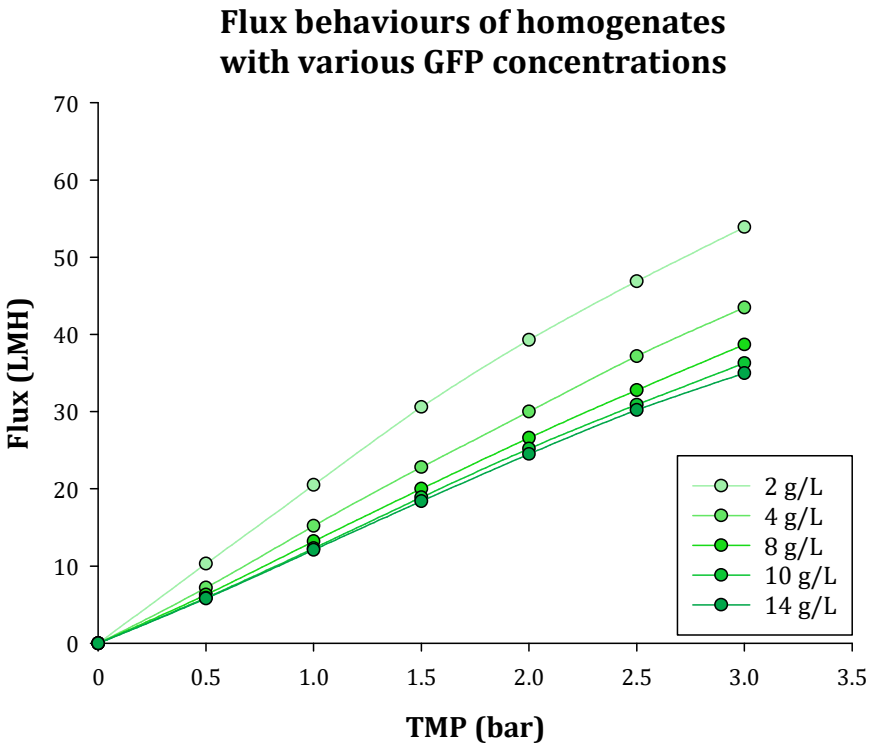

Figure 49 Flux behaviours of 10 kDa PEI treated homogenates with different GFP concentrations, using 10 kDa PESU filter cartridge (CF = 222 mL/min). Tone of colour stands for different GFP concentrations, shown in figure's legend.

The plot reveals that the concentration of GFP has a significant influence on effectiveness of ultrafiltration. At a TMP of 3 bar, the difference of flux is approximately 20 LMH. However, a concentration higher than 8 g/L did not show any critical changes. To see, if the permeate flow is reduced by the GFP concentration itself or concentration and type of PEI, following chapter discusses the same experiment with 1.2 kDa PEI treated homogenate.

6.9.1.2 1.2 kDa PEI

This type of PEI is about 10 times smaller. Hence, the PEI molecules should travel through the 10 kDa filter membrane more easily. Consequently, the phenomenon of second filter layer would be reduced, which should lead to an improved ultrafiltration process. To compare flux behaviours more easily, figure 50 shows permeate flow trends of homogenates with GFP concentrations of 4 and 14 g/L.

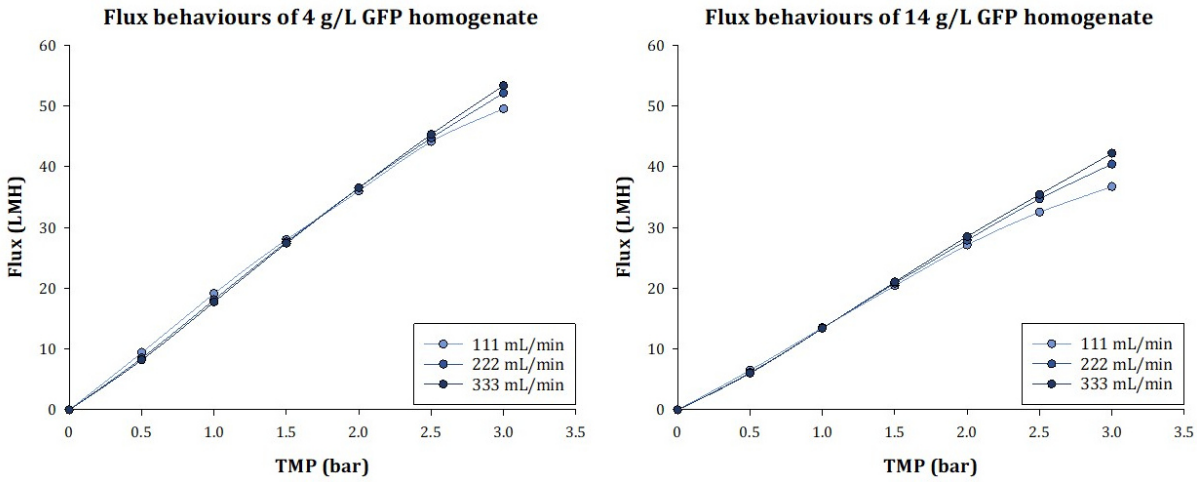

Figure 50 Two graphs of flux behaviours of 1.2 kDa PEI treated homogenates with two different GFP concentrations (4 and 14 g/L), using 10 kDa PESU filter cartridge. Light blue, blue and dark blue lines depict CFs of 111 mL/min, 222 mL/min and 333 mL/min, respectively.

It can be identified that at both GFP concentrations, fluxes could be improved, whereas the form of curves remain the same. According to the homogenate with 4 g/L GFP, at all three CF rates, the fluxes increased about 10 LMH. Right graph shows similar changes, even though the flux improvement seems to be slightly lower. However, the experiment shows clearly that smaller PEI does not built a second rejection layer in an extend 10 kDa PEI does. For further understanding, figure 51 offers information about the impact of various GFP concentrations on flux behaviours at a CF of 222 mL/min.

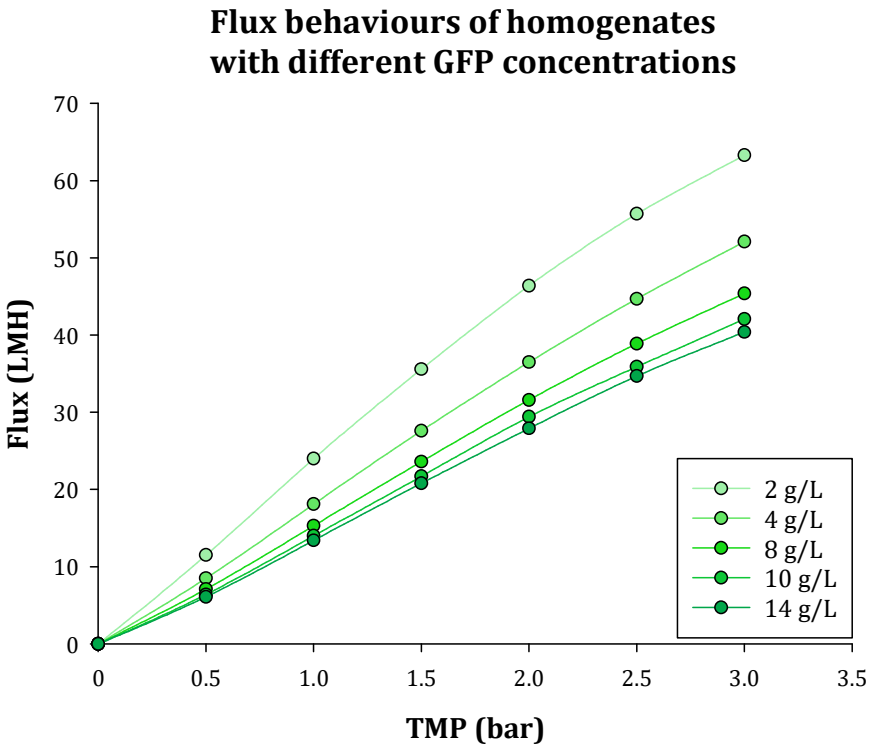

Figure 51 Flux behaviours of 1.2 kDa PEI treated homogenates with different GFP concentrations, using 10 kDa PESU filter cartridge (CF = 222 mL/min). Tone of colour stands for various GFP concentrations as shown in figure's legend.

The figure shows that the pattern of curves looks very similar to the concentration graph in the previous chapter. Nevertheless, all curves illustrate improvements, according to permeate flux. Last but not least, to identify any PEI influences in general, next chapter describe the same experiment processing a homogenate without any PEI application.

6.9.1.3 w/o PEI

Aim of this chapter is to find out, if PEI would compete with GFP during ultrafiltration. Hence, a homogenate without any PEI treatment was prepared by removing the particles with 750 kDa TFF hollow fiber membrane. The method of ultrafiltration experiment remained the same as described in previous chapters. Figure 52 depicts flux behaviours of 4 and 14 g/L GFP homogenates.

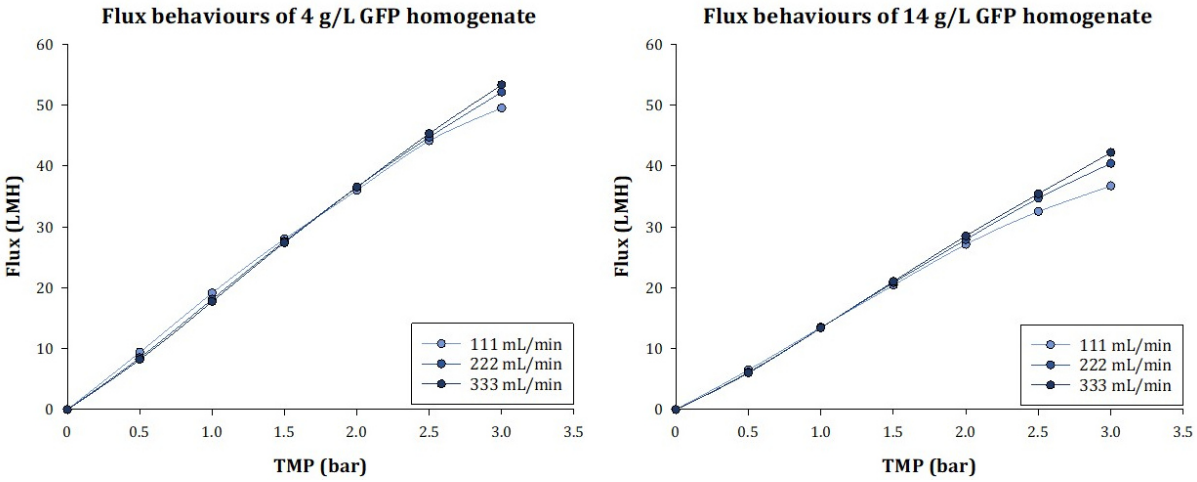

Figure 52 Two graphs of flux behaviours of homogenates (w/o PEI) with two different GFP concentrations (4 and 14 g/L), using 10 kDa PESU filter cartridge. Light blue, blue and dark blue lines depict CFs of 111 mL/min, 222 mL/min and 333 mL/min, respectively.

Both graphs show flux behaviours that reveal mainly linear relationships between TMP and permeate flux. The flux data seem to be nearly identical to data of 1.2 kDa PEI treated homogenate. So, neither second layer formation, nor additional GFP rejection were caused by a 1.2 kDa molecules. For this reason, 1.2 kDa PEI would be an ideal alternative to 10 kDa PEI, even though cell debris flocculation is a bit slower.

Figure 53 illustrates the situation with all GFP concentration at a CF rate of 222 mL/min.

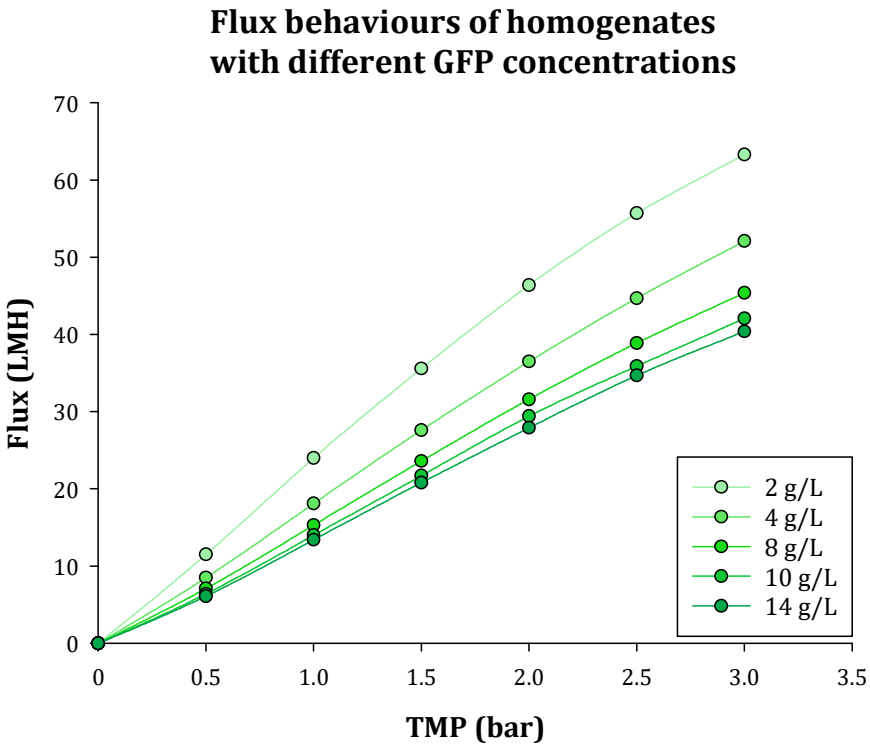

Figure 53 Flux behaviours of PEI untreated homogenates with different GFP concentrations, using 10 kDa PESU filter cartridge (CF = 222 mL/min). Tone of colour stands for various GFP concentrations as shown in figure's legend.

The graph of different GFP concentrations reveals evident similarities to figure 51. It seems that a small PEI molecule does not disturb ultrafiltration process significantly. Next chapter discuss, if the membrane material itself has an essential impact on permeate flux behaviours.

6.9.2 Sartocon® Slice 200 Hydrosart® Cassette

Hydrosart® is according to its manufacturer a cellulose-based membrane, comparable with other regenerated cellulose filter systems. Hence, it can be expected that the more hydrophilic membrane profile would enhance the ultrafiltration process, in contrast to more hydrophobic PES material. However, to see if assumptions can be verified, 10 kDa PEI treated homogenate were used for the ultrafiltration experiment with cellulose membrane.

Figure 54 depicts the flux trend situation of 4 g/L and 14 g/L GFP homogenate.

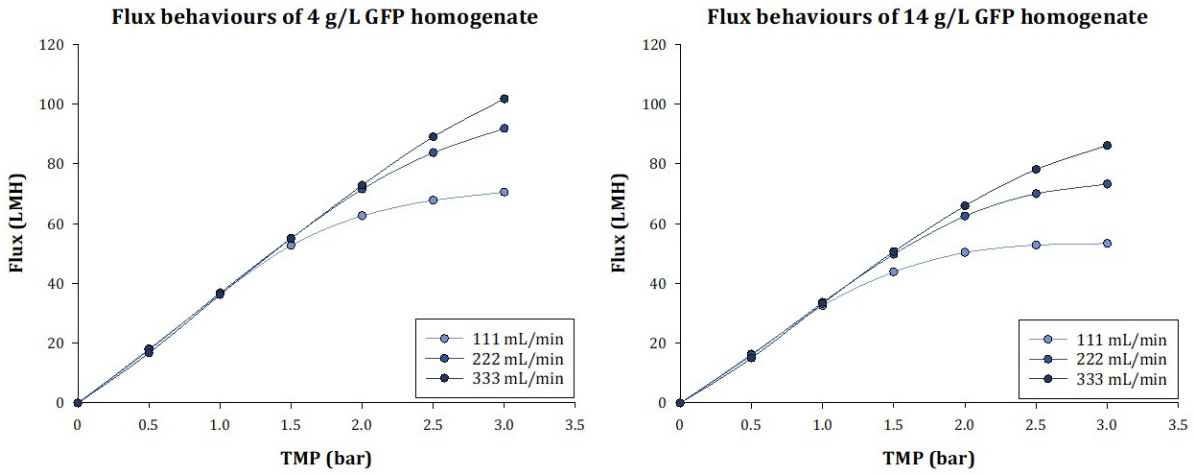

Figure 54 Two graphs of flux behaviours of 10 kDa PEI treated homogenates with two different GFP concentrations (4 and 14 g/L), using 10 kDa Hydrosart® filter cartridge. Light blue, blue and dark blue lines depict CFs of 111 mL/min, 222 mL/min and 333 mL/min, respectively.

As expected, the average permeate fluxes of all determination points are approximately 2 times higher, than using a PES membrane. Both concentrations show mentioned improvements. Additionally, it is the first time, a permeate flux plateau can be recognized, where permeate flow cannot be improved by applying more TMP. However, 333 mL/min is still such a high CF mode, in the way that at 3 TMP, TMP_{opt} could not be reached.

For proper comparison regarding to GFP concentrations, figure 55 shows additional information about protein content, according to permeate flux behaviours.

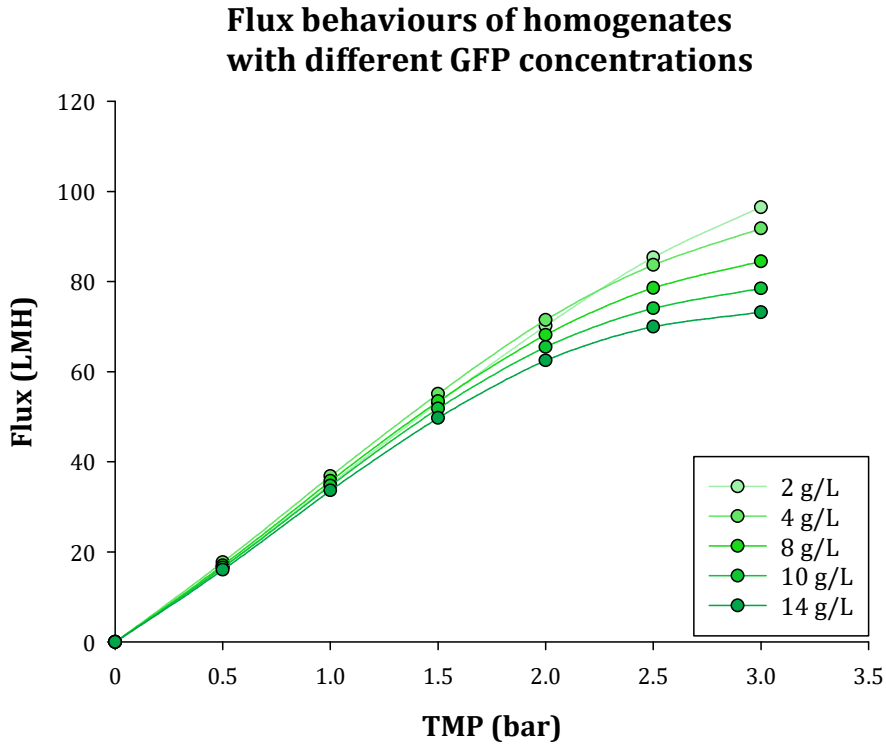

Figure 55 Flux behaviours of 10 kDa PEI treated homogenates with different GFP concentrations, using 10 kDa Hydrosart® filter cartridge (CF = 222 mL/min). Tone of colour stands for various GFP concentrations as shown in figure's legend.

As mentioned, all tested GFP concentrations show improved permeate fluxes. Interestingly, the gap between flux values of GFP concentrations are smaller than using the PES membrane type. Especially, 2 and 4 g/L display minor differences. One reason for such an improvement could be a higher affinity of hydrophilic cellulose membrane to salty buffer matrix. A higher liquid attraction could inhibit a gel layer formation on the membrane surface, which as a consequence reduce the repulsion of liquid.

Next question is, if the design of filter has any influences on the ultrafiltration performance. Therefore, next chapter discuss same ultrafiltration process, using a hollow fiber filter system with identical molecular cut-off of 10 kDa.

6.9.3 Hollow Fiber Cartridge, UFP-10-C-2U

As already explained, it has to be investigated, if the filter design has any impact on flux performance. In contrast to filter cartridges, hollow fiber filter systems contain fibres of specific length and inner diameter, where the retentate passes through. A big advantage of hollow fibers is the easy handling and installation, since no pressure-stable filter housing is required. On the other hand, hollow fiber products are more expensive and are not the first choice for shear sensitive molecules.

To see if type of filter construction would lead to different results, 10 kDa PEI treated homogenate was used to run the experiment. Figure 56 shows two graphs of flux behaviours, processing homogenates with 4 g/L and 14 g/L GFP.

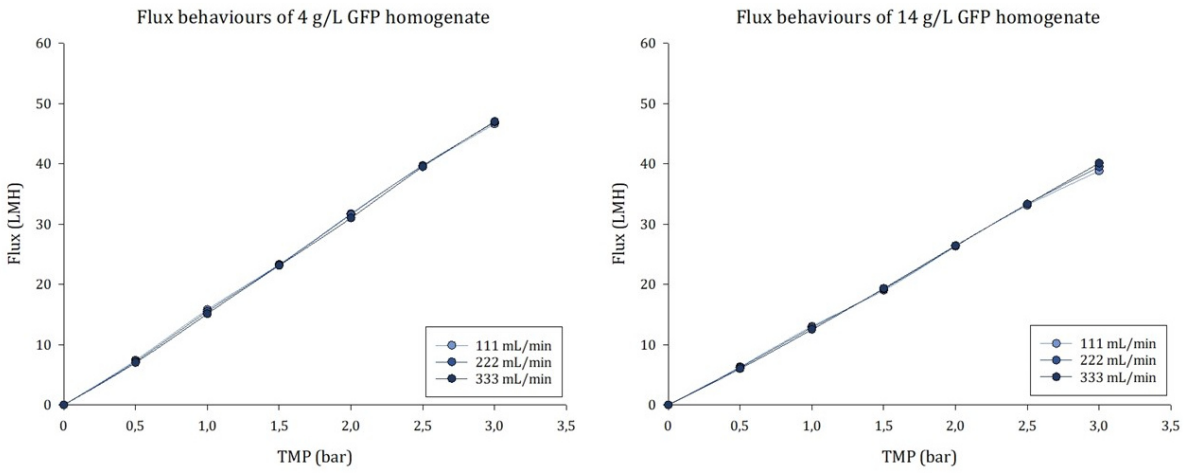

Figure 56 Two graphs of flux behaviours of 10 kDa PEI treated homogenates with two different GFP concentrations (4 and 14 g/L), using 10 kDa hollow fiber filter (PES). Light blue, blue and dark blue lines depict CFs of 111 mL/min, 222 mL/min and 333 mL/min, respectively.

The hollow fiber membrane is made of PES. So, it should be hardly comparable with the first ultrafiltration experiment (chapter 6.9.1). Received values look very similar, even though the permeate fluxes are slightly higher. Furthermore, all received curves follow a strict linear relationship between TMP and flux, even at low CFs (111 mL/min).

This phenomenon can be described by the mentioned shear forces that inhibit formation of protein or PEI gel layer on the membrane's surface. This effect can be seen at stable linear relationship, even at high TMPs. Also, at a relatively high protein concentration of 14 g/L, all 3 CF variants showed linear flux behaviours.

To verify this point of view, figure 57 contains plots of all tested GFP concentrations at a CF rate of 222 mL/min.

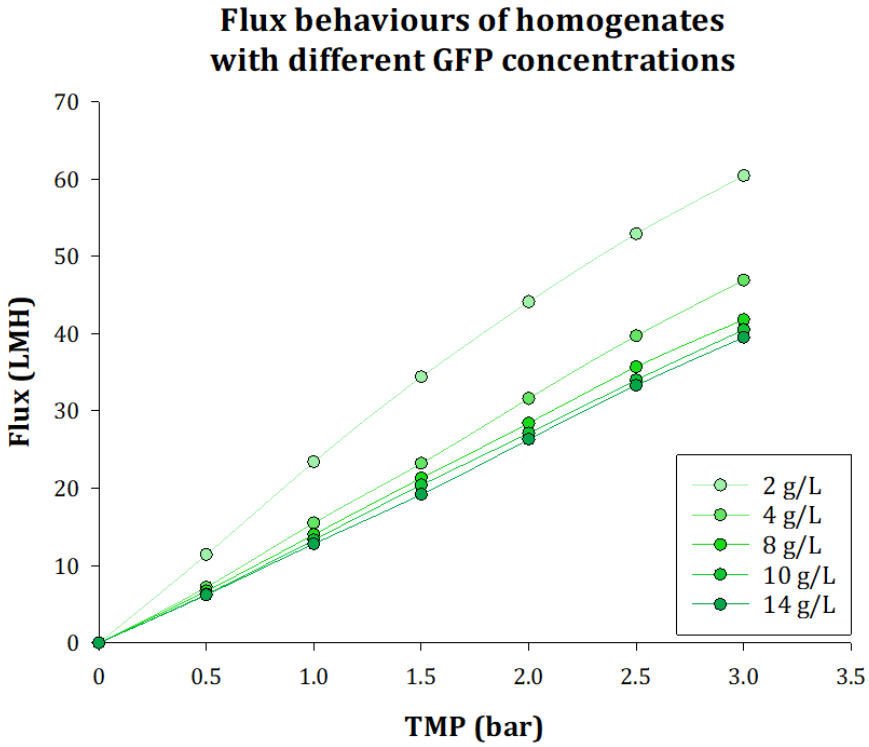

Figure 57 Flux behaviours of 10 kDa PEI treated homogenates with different GFP concentrations, using 10 kDa hollow fiber filter system (CF = 222 mL/min). Tone of colour stands for various GFP concentrations as shown in figure's legend.

The graph shows clearly that almost all GFP concentration types follow linear flux trends. Only, the 2 g/L curve reveals a small deviation. It seems that at lower concentrations, less membrane fouling occurs, which is responsible for higher permeate fluxes, especially in the beginning of pressure-dependent regime.

Nevertheless, the use of hollow fiber filter, would be a suitable option, when working with molecules of low shear sensitive properties. Higher permeate fluxes and a wider linear pressure relationship would enhance the ultrafiltration, regarding to filtration time.

6.10 Comparison of flux behaviours under different diafiltration conditions

Determination of ideal conditions for the ultrafiltration procedure is one argument. To find the best operating parameters for time intensive diafiltration process is the other. Duration of diafiltration is often 5 to 10 times longer than of UF. Hence, the permeate flux trend over a long time period becomes an important factor.

3 different homogenates (4 g/L GFP) with different PEI content were prepared, identifying most influencing PEI factors during diafiltration. For all diafiltration experiments, the initial homogenate buffer (20 mM Tris + 50 NaCl | pH 7.5) was exchanged with diafiltration buffer (20 mM Tris | pH 7.5). The diafiltration runs were stopped after 5 volume changes, due to the fact that the lower conductivity plateau is normally reached after 4 volume exchanges. Figure 58 shows a graph, offering flux behaviours from homogenates containing different PEI activities.

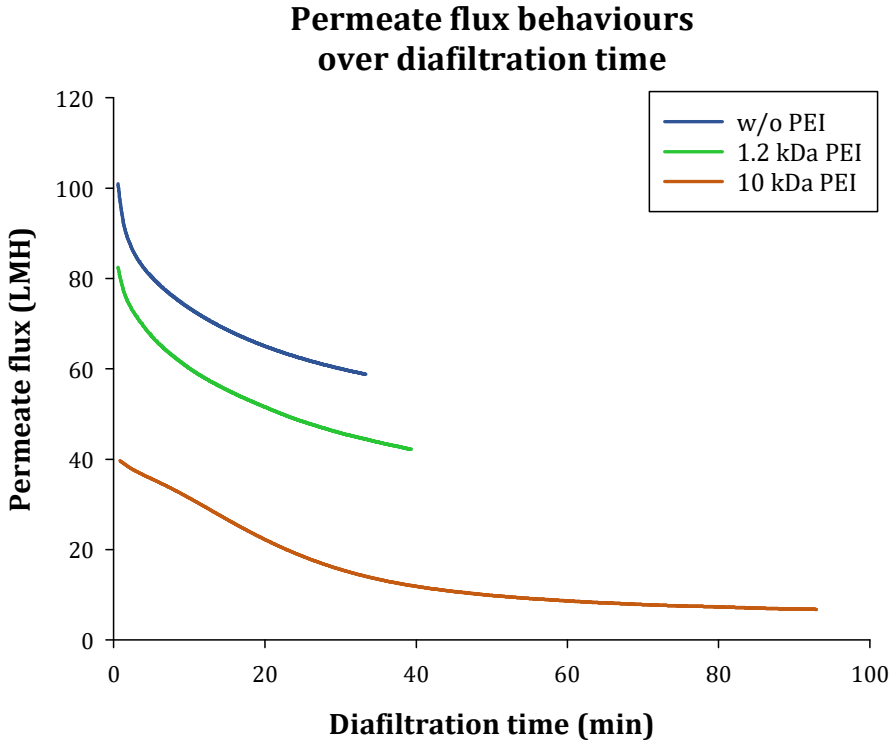

Figure 58 Permeate flux behaviours of GFP homogenates (4 g/L) with different PEI addition, during diafiltration. Blue, green and red lines represent GFP homogenates w/o, 1.2 kDa and 10 kDa PEI, respectively.

According to previous graph, the diafiltration process is highly influenced by the type of PEI that is in use. Whereas, the homogenate with 10 kDa started at an initial permeate flux of 41 LMH, 1.2 kDa PEI treated homogenate began with a flux of about 88 LMH. So, the permeate flow could be more than doubled, using the smaller PEI version. Consequently, the DF process time could be reduced more than a half. However, a homogenate without PEI treatments, revealed the best outcome, but compared to 1.2 kDa homogenate the difference is not excessive. Thus, for long lasting diafiltration processes, the use of 1.2 kDa as flocculant aid would be a suitable option.

To verify this statement, figure 59 depicts the decrease of retentate conductivity over diafiltration time. The conductivity was normalized, due to the circumstance that different PEI molecules give different absolute conductivity values.

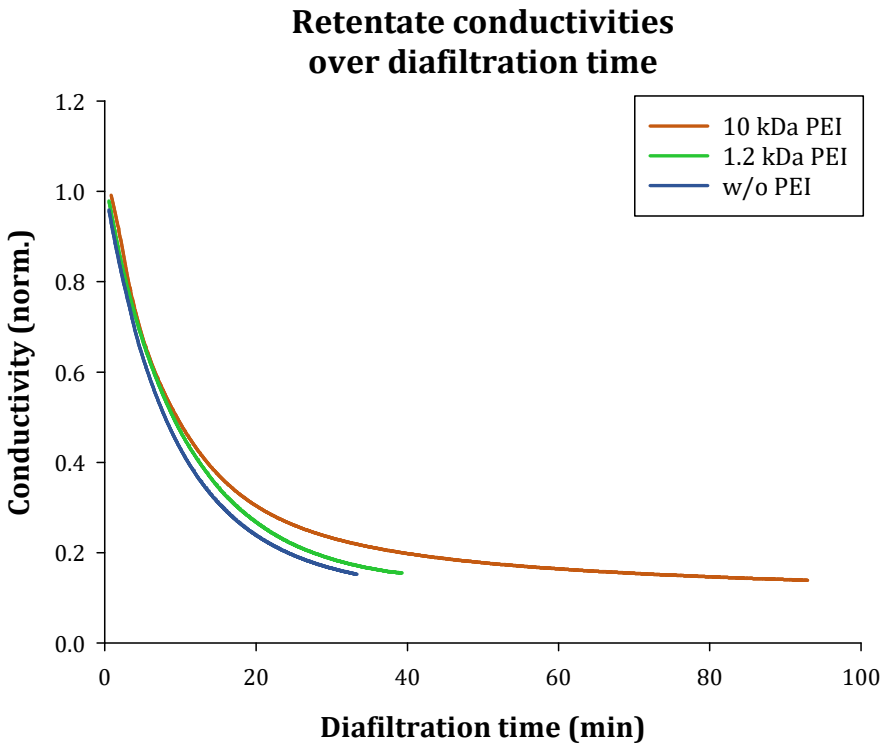

Figure 59 Retentate conductivities over diafiltration time. Red, green and blue line stand for homogenate, treated with 10 kDa, 1.2 kDa and w/o PEI, respectively.

Referring to figure 59, the situation seems as already predicted. Conductivities of blue and green line decreased very rapidly and reached their minimum after 34 and 41 minutes, respectively. Homogenate retentate of 10 kDa PEI attain also an adequate salt level after such time, however it took more than double of time to reach its minimum. Again, latest outcome speaks for the use of 1.2 kDa instead of 10 kDa, when a diafiltration step is required for protein purification.

7 Conclusion

Filtration is a crucial part in every biotechnological purification process. For this reason, the clarification of different high pressure homogenates from *E. coli* was investigated. Cell suspension of *E. coli*, containing the model protein GFP, were treated by high pressure homogenization at different operating conditions. Particle analysis showed that majority of remaining particles after centrifugation have diameters of approximately 100 nm. Interestingly, high pressure operating conditions have only negligible influences on particle diameter distributions. Even, gently pressure conditions (300 bar) leads to smaller particles than applying 700 bar during cell disruption. This phenomenon can be explained by preceding centrifugation that remove bigger particle fractions, predominantly produced by homogenization at 300 bar.

To investigate, if commercially available dead-end filter systems are able to remove cell debris particles out of homogenates, various constant flow filtration experiments were made. As NTA particle analysis and turbidity measurement showed, most of filters failed to clarify homogenates in a satisfactory manner. Only sterile filters could remove majority of cell debris, even though particle fraction under 100 nm in size passed through filter pores. Therefore, the use of filter systems above a pore diameter of 100 nm is not recommended when clarifying *E. coli* high pressure homogenized homogenates.

Ultrafiltration membranes normally have pores smaller than depth filters. Hence, hollow fiber membranes with 500,000 kDa, 750,000 kDa and 0.1 micron cut-offs were tested. It was shown that 500,000 and 750,000 kDa membranes rejected all particles in suspension and let pass GFP through the pores. Thus, 750,000 kDa ultrafiltration membrane was used to identify ideal conditions for transferring most of GFP into the permeate. Experiments revealed that small TMPs and high flow rates resulted in low GFP rejection factors. A flow rate of 600 mL/min and a TMP of 0.5 bar lead to the lowest rejection value (6%). In contrast, using TMP of 2 bar, rejections of about 55% were obtained, regardless of cross flow rate. Additionally, a buffer system of at least 50 mM Tris was required to achieve optimal GFP permeation. During filtration, the flux decline was relatively low and a 20-fold GFP concentration lead to an average flux of 50 LMH.

Further filtrate processing was performed by ultra- and diafiltration. It was shown that a concentration of GFP up to 14 g/L did not lead to losses, even at a high TMPs. Ultrafiltration membranes, made of PES, provided relatively low permeate fluxes and a completely linear relationship of TMP and flux, which remained until 3 bar TMP. Also, the presence of PEI during ultrafiltration did not lead to major differences, even though the use of 10 kDa PEI reduced the average flux, significantly. Ultrafiltration membrane, based on hydrophilic regenerated cellulose, achieved permeate fluxes that were twice as high compared to PES membranes.

Due to such high fluxes, a typical flux decline at lower tangential flows could be detected and the pressure independent region was reached at 2 bar TMP. Anyway, in case of retained GFP, it would be recommended to operate with high tangential flow rate, avoiding potential flux reductions.

Diafiltration experiments showed that the presence of 1.2 kDa in processed solution did not significantly disturb the buffer exchange. Only the use of 10 kDa as a flocculant led to significant flux decreases and therefor to 3 times more diafiltration time.

In the end, all process steps have to be considered as interconnecting unit operations. The choice of one influence another. The use of distinct filtration operation is no exception, since filtration procedures often are core facilities in a biotechnological production processes. Hence, there is no patent remedy and much investigational work still has to be done, developing satisfying filtration procedures.

8 List of figures

9 List of tables

10 List of references

1. **Unzueta, Ugutz, et al.** Strategies for the production of difficult-to-express full-length eukaryotic proteins using microbial cell factories: production of human alpha-galactosidase A. *Applied Microbiology and Biotechnology.* 12. December 2014, S. 1-2.

2. **Baneyx, François.** *Recombinant protein expression in Escherichia coli.* Amsterdam : Elsevier Science Ltd., 1999. 1669(99)00003-8.

3. **Li, Qiang, et al.** An Ultra Scale-Down Approach to Study the Interaction of Fermenation, Homogenization, and Centrifugation for Antibody Fragment Recovery From rec E. coli. *Biotechnology and Bioengineering.* 110, 2013, Bde. 2150-2160.

4. **Kelly, William J. Kelly und Muske, Kenneth R.** Optimal operation of high pressure homogenization for intracellular product recovery. *Bioprocess and Biosystems Engineering.* 2004, 12.

5. **Belafi-Bako, Katalin, Gubicza, Laszlo und Marcel, Mulder.** *Integration of Membrane Processes into Bioconversions.* New York, USA : Kluwer Academic/Plenum Publishers, 2000. 0.306-46437-3.

6. **Nelson, David, Michael, Cox und Held, Andreas.** *Lehninger Biochemie.* Berlin Heidelberg : Springer Verlag, 2001. 3-540-41813-X.

7. **Academy, Khan.** Khan Academy. *Khan Academy.* [Online] Khan Academy. [Zitat vom: 19. März 2020.] https://www.khanacademy.org/science/biology/bacteria-archaea/prokaryote-structure/a/prokaryote-structure.

8. **Nicholas Robert A., Davis Christopher.** *Structural Mechanisms of ß-Lactam Antibiotic Resistence in Penicillin-Binding Proteins.* Boston, USA : Springer, 2012. 978-1-4614-1399-8.

9. **Yoon Low, Lieh, et al.** Role of Net Charge on Catalytic Domain and INfluence of Cell Wall Binding Domain on Bacteriocidal Activity, Specificity and Host Range of Phage Lysins. *The Journal of Biological Chemistry.* 2011, Bd. 286, 39.

10. **Vicennati, Paola, et al.** Polyethylenimine In Medicinal Chemistry. *Current Medicinal Chemistry.* 2008, Bd. 15.

11. **Merck.** Merck. *Merck.* [Online] Merck. [Zitat vom: 20. March 2020.] https://www.sigmaaldrich.com/catalog/search?term=polyethylenimine&interface=All&N=0&mode=match%20partialmax&lang=de&region=AT&focus=product.

12. **Zakeri, Abbas, et al.** Polyethylenimine-based nanocarriers in co-delivery of drug and gene: a developing horizon. *Nano Reviews & Experiments.* 2018, 9.

13. **Inoue, Shinya, et al.** Fluorescence polarization of green fluorescence protein. *Proceedings of the National Academy of Sciences of the United States of America.* 2002, 99.

14. **Eckert, Christoph.** Chromotek. *Chromotek.* [Online] Chromotek, 7. February 2019. [Zitat vom: 20. March 2020.] https://resources.chromotek.com/blog/topic/turbogfp.

15. **Tran, P. T., Paoletti, Anne und Chang, Fred.** Imaging green fluorescent protein fusions in living fission yeast cells. *Elsivier.* 2004, 33.

16. **Cormack, Brendan P., Valdivia, Raphael H. und Falkow, Stanley.** FACS-optimized mutants of the green fluorescent protein (GFP). *Gene.* 1996, 173.

17. **Lambert, TJ.** FPbase: a community-editable fluorescent protein database. *Nature Methods.* 2019, 16.

18. **Ortega-Rivas, Enrique.** *Non-thermal Food Engineering Operations.* New York : Springer Science+Business Media, 2012. 978-1-4614-2038-5.

19. **Doran, Pauline M.** *Bioprocess Engineering Principles.* Amsterdam : Elsevier Academic Press, 2012. 9780122208515.

20. **Wilbey, R. A.** HOMOGENIZATION OF MILK | Principles and Mechanism of Homogenization, Effects and Assessment of Efficiency: Valve Homogenizers. *Encyclopedia of DIary Science (Second Edition).* 2011.

21. **Zartler, Christopher.** *Heatprecipitation of homogenates: scale-up study.* Vienna : BOKU, 2017.

22. *High-Pressure Homogenizers.* **Huppertz, T.** The Netherlands : Elsevier, 2011.

23. *A Novel Technique for Measurement of Disruption in High-Pressure Homogenization: Studies on E. Coli Containing Recombinant Inclusion Bodies.* **Middelberg, Anton P. J., O'Neil, Brian K. und Bogle, Bogle I. David L.** 38, Australia : Biotechnology and Bioengineering, 1991.

24. **Sauer, Thomas, Robinson, Campbell W. und GLick, Bernard R.** Disruption of Native and Recombinant Escherichia coli in a High-Pressure Homogenizer. *Biotechnology and Bioengineering.* 1989, 33.

25. **Trefalt, Gregor und Brokovec, Michal.** Overview of DLVO Theory. *LCSC.* [Online] 29. March 2014. [Zitat vom: 23. March 2020.] www.colloid.ch/dlvo.

26. **Huray, Paul G.** *Maxwell's Equations.* Canada : John Wiley & Sons, 2010. 987-0-470-54276-7.

27. **Mohsen-Nia, M., Amiri, Hamide und Jazi, Bahram.** Dielectric Constants of Water, Methanol, Ethanol Butanol and Acetone. *Journal of Solution CHemistry.* 2010, 39.

28. *Broadband Complex Dielectric Constants of Water and Sodium Chloride Aqueous Solutions with Different DC Conductivities.* **Midi, Shahida, et al.** 9, s.l. : John Wiley & Sons, 2014.

29. **Creighton, Thomas.** *Proteins: structures and molecular principles.* USA : W. H. Freeman and Company, 1984. 0-7167-1566-X.

30. **Hamaker, H. C.** THE LONDON-VAN DER WAALS ATTRACTION BETWEEN SPHERICAL PARTICLES. *Physica IV.* 1937, 10.

31. **Zhang, Hengzhong und Banfield, Julian F.** Interatomic Coulombic interaction as the driving force for oriented attachment. *CrystEngComm.* 2014, 16.

32. **Mukherjee, Soumya.** Isolation and Purification of Industrial Enzymes: Advances in Enzyme Technology. *Biomass, Biofuels, Biochemicals.* 2019.

33. **Kang, Yun (Kenneth), et al.** Development of a Novel and Efficient Cell Culture Flocculation Process Using a Stimulus Responsive Polymer to Streamline Antibody Purification Process. *Biotechnology and Bioengineering.* 2013, 110.

34. **Harrison, Roger G., et al.** *Bioseparation Science and Engineering.* Oxford : Oxford University Press, 2003. 0-19-512340-9.

35. **Lepock, James R.** Meaurement of protein stability and protein denaturation in cells using differential scanning calorimetry. *Methods.* 2004, 35.

36. **Nicholls, Samantha B. und Hardy, Jeanne A.** Strucutral basis of fluorescence quenching in caspase activatable-GFP. *The Protein Society.* 2012, 22.

37. **Fink, Mathias.** *Clarification of E. Coli homogenates by precipitation.* Wien : s.n., 2015.

38. *Extraction of soil solution by drainage centrifugation-effects of centrifugal force and time of centrifugation on soil moisture recovery and solute concentration in soil moisture of loess subsoils.* **Fraters, Dico, et al.** 189, Utrecht : Springer, 2017. 10661-017-5788-7.

39. **Cheryan, Munir.** *ULTRAFILTRATION and MICROFILTRATION Handbook.* Florida, USA : CRC Press, 1998. 1-56676-598-6.

40. **Matteson, Michael J.** *Filtration: Principles and Practices.* New York : Marcel Dekker, Inc., 1986. 0-8247-7582-1.

41. **Wakeman, R.J. und Tarleton, E.S.** *FILTRATION - Equipment Selection Modelling and Process Simulation.* Oxford OX5 1GB, UK : Elsevier Science Ltd., 1999. 1-85617-345-3.

42. **Jiraratananon, R. und Chanachai, A.** Study of fouling in the ultrafiltration of passion fruit juice. *Journal of Membrane Science.* 1996, 111.

43. **Ge, S, Kojio K, Takahara, A und Kajiyama, T.** Bovine serum albumin adsorption onto immobilized organotrichlorosilane surface: influence of the phase separation on protein adsorption patterns. *Journal of Biomaterial Science.* Polymer Edition, 1998, 9.

44. **Jahnson, Monika.** *Gentechnische Methoden.* München : Elsevier, 2007. 3-8274-1537-3.

45. **Hesse, Manfred, Meier, Herbert und Zeeh, Bernd.** *Spektroskopische Methoden in der organischen Chemie.* New York : Georg Thieme Verlag Stuttgard, 1991. 3-13-576104-5.

46. **Marmer, Daniel J. und Hurtubise, Paul E.** Nephelometric and Turbidimetric Immunoassay. *Elsevier.* 1996.

47. **Hach, Company.** *Determination of turbidtiy by 360° nephelometry.* Colorado : Hach Company, 2018.

48. **Filipe, Vasco, Hawe, Andrea und Jiskoot, Wim.** Critical Evaluation of Nanoparticle Tracking Analysis (NTA) by NanoSight for the measurement of Nanoparticles and Protein Aggregates. *Pharmaceutical Research.* 2010, 27.

49. **Feynman, Richard, Leighton, Robert und Sands, Matthew.** *The Feynman LECTURES ON PHYSICS.* New York : Basic Books, 2010. 978-0-465-02562-6.

50. **Atkins, Peter und de Paula, Julia.** *Physical Chemistry .* United Kingdom : Oxford University Press, 2014. 978-0-19-969740-3.

51. **Gasteiger, E., et al.** *ExPASy: the proteomics server for in-depth protein knowledge and analysis.* s.l. : Nucleic Acids Res, 2003. 31:3784-3788.

52. **Gasteiger, E., et al.** Protein Identification and Analysis Tools on the ExPASy Server. [Buchverf.] John M. Walker. *The Proteomics Protocols Handbook.* s.l. : Humana Press, 2055.

53. **Jurjevec, Alexander.** *DNA and endotoxin removal from E. coli homogenate.* Wien : Universität für Bodenkultur, 2018.

54. **Schillinger, Harald.** *Scalle up & Scale down; Scale up with filter laws.* Austria : 3M, 2017.

11 Appendix

Table 14 Raw data set of centrifugation probes. Orange sector represents the 10 kDa PEI type, whereas the green part offers information about the 1.2 kDa version.

10 kDa PEI															
Concentration (%) (w/v)	0.10			0.15			0.20			0.25			0.30		
Centrifugation time (s)	Turbidity (NTU)	Dilution	cor. Turbidity (NTU)	Turbidity (NTU)	Dilution	cor. Turbidity (NTU)	Turbidity (NTU)	Dilution	cor. Turbidity (NTU)	Turbidity (NTU)	Dilution	cor. Turbidity (NTU)	Turbidity (NTU)	Dilution	cor. Turbidity (NTU)
0	129.00	1:100	12900.00	139.00	1:100	13900.00	150.00	1:100	15000.00	164.00	1:100	16400.00	172.00	1:100	17200.00
60	24.40	1:10	244.00	57.30	1:10	573.00	32.10	1:10	321.00	65.10	1:10	651.00	168.00	1:10	1680.00
120	65.00	1:1	65.00	89.50	1:1	89.50	43.30	1:1	43.30	52.70	1:1	52.70	55.40	1:1	55.40
240	26.40	1:1	26.40	23.90	1:1	23.90	16.50	1:1	16.50	15.20	1:1	15.20	15.10	1:1	15.10
480	13.70	1:1	13.70	13.30	1:1	13.30	11.10	1:1	11.10	9.72	1:1	9.72	9.85	1:1	9.85
720	11.80	1:1	11.80	12.00	1:1	12.00	10.20	1:1	10.20	8.83	1:1	8.83	8.77	1:1	8.77
900	10.60	1:1	10.60	11.40	1:1	11.40	9.79	1:1	9.79	8.73	1:1	8.73	8.55	1:1	8.55
1200	9.63	1:1	9.63	10.60	1:1	10.60	9.50	1:1	9.50	8.68	1:1	8.68	8.53	1:1	8.53
1800	8.75	1:1	8.75	9.76	1:1	9.76	8.50	1:1	8.50	8.45	1:1	8.45	8.02	1:1	8.02
1.2 kDa PEI															
Concentration (%) (w/v)	0.10			0.15			0.20			0.25			0.30		
Centrifugation time (s)	Turbidity (NTU)	Dilution	cor. Turbidity (NTU)	Turbidity (NTU)	Dilution	cor. Turbidity (NTU)	Turbidity (NTU)	Dilution	cor. Turbidity (NTU)	Turbidity (NTU)	Dilution	cor. Turbidity (NTU)	Turbidity (NTU)	Dilution	cor. Turbidity (NTU)
0	97.20	1:100	9720.00	102.00	1:100	10200.00	106.00	1:100	10600.00	107.00	1:100	10700.00	108.00	1:100	10800.00
60	464.00	1:10	4640.00	598.00	1:10	59800.00	655.00	1:10	6550.00	720.00	1:10	7200.00	829.00	1:10	8290.00
120	174.00	1:10	1740.00	213.00	1:10	2130.00	273.00	1:10	2730.00	327.00	1:10	3270.00	295.00	1:10	2950.00
240	89.90	1:10	899.00	830.00	1:1	830.00	78.10	1:10	781.00	127.00	1:10	1270.00	85.30	1:10	853.00
480	221.00	1:1	221.00	121.00	1:1	121.00	109.00	1:1	109.00	107.00	1:1	107.00	127.00	1:1	127.00
720	115.00	1:1	115.00	48.60	1:1	48.60	50.50	1:1	50.50	55.90	1:1	55.90	56.70	1:1	56.70
900	70.90	1:1	70.90	34.60	1:1	34.60	34.50	1:1	34.50	38.70	1:1	38.70	39.80	1:1	39.80
1200	45.90	1:1	45.90	20.60	1:1	20.60	22.50	1:1	22.50	27.60	1:1	27.60	28.10	1:1	28.10
1800	29.70	1:1	29.70	17.20	1:1	17.20	14.40	1:1	14.40	14.60	1:1	14.60	14.80	1:1	14.80

Table 15 Flux data of 10 kDa PES ultrafilter cartridge, using a 10 kDa treated GFP homogenate.

	2 g/L			4 g/L			8 g/L			10 g/L			14 g/L		
TMP (bar)	111.11 mL/min	222.22 mL/min	333.33 mL/min	111.11 mL/min	222.22 mL/min	333.33 mL/min	111.11 mL/min	222.22 mL/min	333.33 mL/min	111.11 mL/min	222.22 mL/min	333.33 mL/min	111.11 mL/min	222.22 mL/min	333.33 mL/min
0	0.00	0.00	0.00	0.00	0.00	0.00	0.00	0.00	0.00	0.00	0.00	0.00	0.00	0.00	0.00
0.5	16.30	10.30	8.90	7.70	7.20	6.90	6.70	6.30	5.90	6.10	5.90	5.60	5.90	5.80	5.40
1	28.40	20.50	18.80	15.60	15.20	14.60	13.50	13.20	12.90	12.60	12.30	12.30	12.20	12.10	11.90
1.5	37.20	30.60	28.10	23.20	22.80	22.30	20.10	20.00	19.90	18.80	18.90	18.90	18.30	18.40	18.30
2	44.70	39.30	36.90	29.90	30.10	29.70	26.00	26.60	26.50	24.50	25.20	25.40	23.50	24.50	24.70
2.5	49.70	46.90	44.70	36.10	37.20	36.80	31.30	32.80	33.00	28.90	30.90	31.70	27.40	30.20	30.90
3	54.10	53.90	52.50	41.10	43.50	43.70	35.30	38.70	39.50	32.40	36.30	37.60	30.30	35.00	36.60

Table 16 Flux data of 10 kDa PES ultrafilter cartridge, using a 1.2 kDa treated GFP homogenate.

	2 g/L			4 g/L			8 g/L			10 g/L			14 g/L		
TMP (bar)	111.11 mL/min	222.22 mL/min	333.33 mL/min	111.11 mL/min	222.22 mL/min	333.33 mL/min	111.11 mL/min	222.22 mL/min	333.33 mL/min	111.11 mL/min	222.22 mL/min	333.33 mL/min	111.11 mL/min	222.22 mL/min	333.33 mL/min
0	0.00	0.00	0.00	0.00	0.00	0.00	0.00	0.00	0.00	0.00	0.00	0.00	0.00	0.00	0.00
0.5	13.90	11.50	10.40	9.40	8.50	8.20	7.70	7.10	6.90	6.90	6.40	6.30	6.50	6.10	6.00
1	27.30	24.00	22.40	19.10	18.10	17.70	15.90	15.30	15.10	14.40	14.00	14.00	13.50	13.40	13.40
1.5	38.50	35.60	34.00	28.00	27.60	27.40	23.60	23.60	23.60	21.60	21.70	21.90	20.40	20.80	21.00
2	47.80	46.40	45.20	36.00	36.50	36.50	30.90	31.60	31.70	28.30	29.40	29.60	27.10	27.90	28.50
2.5	55.40	55.70	55.80	44.10	44.70	45.30	37.10	38.90	39.50	34.00	35.90	37.10	32.50	34.70	35.40
3	61.50	63.30	63.60	49.50	52.10	53.30	42.40	45.40	46.50	38.70	42.10	43.70	36.70	40.40	42.20

Table 17 Flux data of 10 kDa PES ultrafilter cartridge, using a PEI untreated GFP homogenate.

	2 g/L			4 g/L			8 g/L			10 g/L			14 g/L		
TMP (bar)	111.11 mL/min	222.22 mL/min	333.33 mL/min	111.11 mL/min	222.22 mL/min	333.33 mL/min	111.11 mL/min	222.22 mL/min	333.33 mL/min	111.11 mL/min	222.22 mL/min	333.33 mL/min	111.11 mL/min	222.22 mL/min	333.33 mL/min
0	0.00	0.00	0.00	0.00	0.00	0.00	0.00	0.00	0.00	0.00	0.00	0.00	0.00	0.00	0.00
0.5	16.00	14.50	12.60	12.30	10.20	9.40	9.40	8.10	7.50	7.80	6.90	6.50	6.80	6.20	5.70
1	33.30	31.30	28.20	24.80	22.40	21.40	19.30	17.80	17.30	16.40	15.30	14.90	14.50	13.80	13.30
1.5	48.10	47.20	43.60	36.60	34.70	33.40	28.80	27.80	27.00	24.70	24.10	23.40	21.90	21.50	21.00
2	62.20	60.90	58.50	46.60	46.00	45.00	37.00	37.10	36.70	31.70	32.10	31.80	28.40	28.90	28.60
2.5	72.60	70.70	71.10	54.70	55.80	55.70	43.80	45.60	45.40	37.90	39.40	39.50	34.00	35.60	35.70
3	76.40	79.20	82.30	59.60	64.20	65.10	47.70	52.60	53.30	41.70	45.70	46.50	38.10	41.10	42.10

Table 18 Flux data of 10 kDa Hydrosart® ultrafilter cartridge, using a 10 kDa PEI treated GFP homogenate.

	2 g/L			4 g/L			8 g/L			10.g/L			14 g/L		
TMP [bar]	111.11 mL/min	222.22 mL/min	333.33 mL/min	111.11 mL/min	222.22 mL/min	333.33 mL/min	111.11 mL/min	222.22 mL/min	333.33 mL/min	111.11 mL/min	222.22 mL/min	333.33 mL/min	111.11 mL/min	222.22 mL/min	333.33 mL/min
0	0.00	0.00	0.00	0.00	0.00	0.00	0.00	0.00	0.00	0.00	0.00	0.00	0.00	0.00	0.00
0.5	16.20	16.60	16.30	18.10	17.70	16.70	17.60	17.00	16.00	16.80	16.50	15.60	16.30	16.00	15.00
1	33.40	35.00	35.20	36.40	36.80	36.20	35.10	35.70	35.20	33.70	34.70	34.40	32.50	33.60	33.20
1.5	50.30	53.10	53.90	52.70	55.10	55.00	49.20	53.40	53.50	46.40	51.80	52.00	43.80	49.70	50.60
2	63.80	70.20	72.10	62.60	71.50	72.80	57.50	68.20	70.70	53.30	65.50	68.10	50.30	62.50	65.90
2.5	72.50	85.40	89.50	67.80	83.70	89.00	61.20	78.60	85.40	56.70	74.10	81.50	52.80	70.00	78.10
3	77.70	96.50	104.40	70.50	91.80	101.70	61.90	84.50	95.60	56.90	78.50	90.50	53.30	73.20	86.10

Table 19 Flux data of 10 kDa hollow fiber ultrafilter, using a 10 kDa PEI treated GFP homogenate.

	2 g/L			4 g/L			8 g/L			10 g/L			14 g/L		
TMP [bar]	111.11 mL/min	222.22 mL/min	333.33 mL/min	111.11 mL/min	222.22 mL/min	333.33 mL/min	111.11 mL/min	222.22 mL/min	333.33 mL/min	111.11 mL/min	222.22 mL/min	333.33 mL/min	111.11 mL/min	222.22 mL/min	333.33 mL/min
0	0.00	0.00	0.00	0.00	0.00	0.00	0.00	0.00	0.00	0.00	0.00	0.00	0.00	0.00	0.00
0.5	12.00	11.40	8.80	7.40	7.20	7.00	6.80	6.70	6.70	6.20	6.30	6.40	6.30	6.20	6.00
1	24.10	23.40	20.50	15.80	15.50	15.10	14.30	14.00	13.50	13.40	13.30	13.00	13.00	12.80	12.50
1.5	35.40	34.40	31.40	23.30	23.20	23.10	21.70	21.30	21.20	20.60	20.40	20.10	19.00	19.20	19.30
2	44.90	44.10	43.40	31.70	31.60	31.00	28.80	28.40	28.20	27.10	27.10	27.00	26.30	26.30	26.40
2.5	53.70	52.90	51.90	39.60	39.70	39.50	35.50	35.70	35.70	34.00	34.00	34.30	33.10	33.30	33.30
3	59.60	60.40	60.50	46.60	46.90	47.00	41.40	41.80	42.00	39.70	40.50	40.90	38.80	39.50	40.10